On photosynthesis parameters for
the A-gs surface scheme for high vegetation

G.J Steeneveld

Wageningen University: Meteorology and Air Quality Group

Supervisor: dr. ir. B.J.J.M. van den Hurk

Royal Netherlands Meteorological Institute

March 2002

Abstract

A review of plant physiological based surface schemes is presented. For forest, it appeared that the so called A-gs scheme assimilated too fast compared to the MOSES scheme used in the Hadley Centre climate model. In addition, the photosynthesis parameter $V_{c,max}$ in the A-gs scheme measured in the field appeared to be a factor 2 lower than derived from laboratory experiments. Field measurements in Scots Pine (C3, *Pinus sylvestris*) were used to calibrate the ratio of intern to extern CO_2 concentration as function of vapour pressure deficit at leaf surface. Also $V_{c,max}$ and the mesophyll conductance has been calibrated, which resulted in $V_{c,max}$ = 2.0 mg/m^2/s and g_m = 3.2 mm/s. This is a factor 2 lower than the standard values in the A-gs scheme, but in agreement with literature values based on field experiments. Eventually a new parameter set is proposed for high vegetation for both C3 and C4 plants.

One dimensional model simulation using a tiled representation of the surface resulted in a quite good simulation of both seasonal and monthly averaged diurnal cycles of latent and sensible heat flux for Scots pine. CO_2 flux density calculations showed proper amplitudes, but some phase shift due to the time lag introduced by CO_2 storage change.

The robustness of the parameter values across three different forests field data sets was tested in a Monte Carlo approach. A unique parameter combination could not be found within the forest. Contrary, an area of acceptable parameter sets was present. It appeared that the considered forests did not have a parameter set in common. Especially boreal forests tend to have a dissent parameter set. This may be due to nutrient deficiency.

Table of contents

1. Introduction.

The description of the land to atmosphere processes plays an essential role in numerical weather prediction and climate modelling. The interaction of the vegetation with the environment defines the transport of moisture and carbon dioxide to the atmosphere and so the partition of available energy (net radiation minus soil heat flux) over latent and sensible heat fluxes. So the vegetation plays a vital role in climate modelling of the soil-water-atmosphere system. It forms an essential part of the hydrological cycle. Figure 1.1 illustrates the interactions of vegetation with its environment. Photosynthesis, and thus transpiration, not only depends on atmospheric quantities and soil moisture, but also on an extensive biochemical cycle.
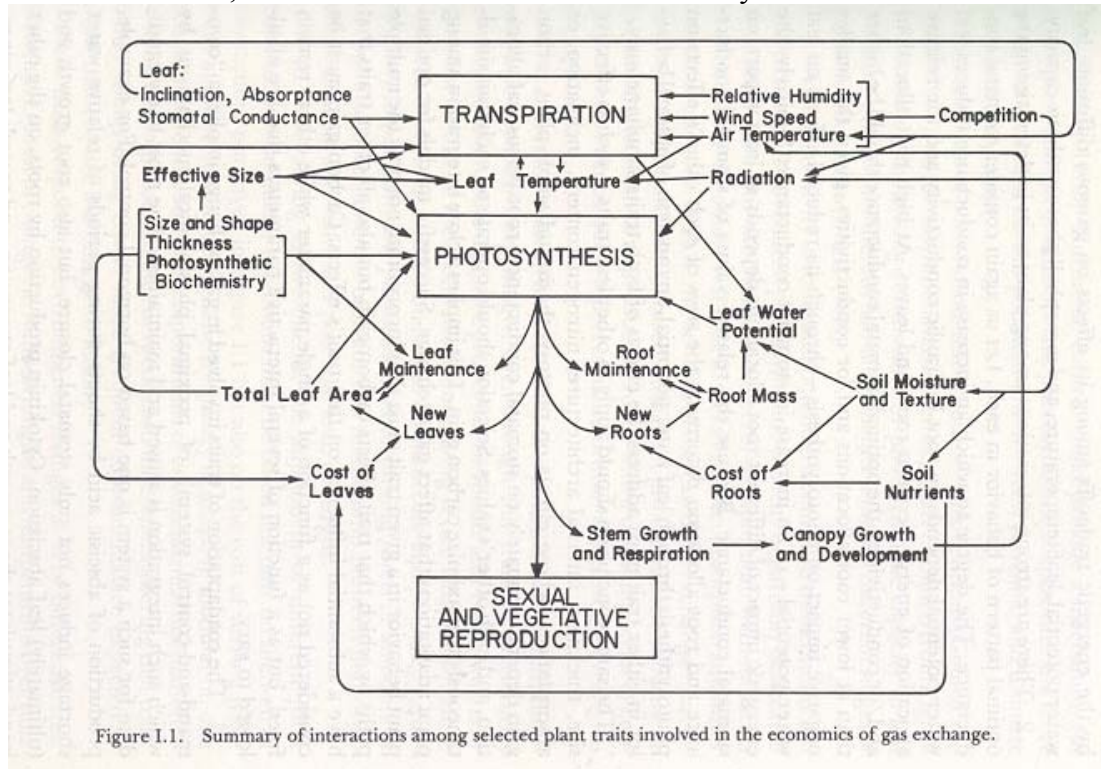
Figure I.1.   Summary of interactions among selected plant traits involved in the economics of gas exchange.

Figure 1.1: Schematic overview of soil-plant-atmosphere interaction, illustrating the complex processes photosynthesis and transpiration (Givnish, 1983).

In a soil-vegetation-atmosphere transfer model (SVAT) water is extracted from the topsoil by plant roots, and is transported to the leaves where it has to overcome the stomatal and boundary layer resistances before it reaches 'free' air. In the meantime carbon dioxide is transported through the same stomata inwards to be used in photosynthesis. These transport processes can be written in analogy with Ohm's Law, so that a resistance can be defined as the ratio of a gradient and a flux density.

Many formulations have been presented in the past describing these resistances and fluxes. Commonly used is the idea of Jarvis and Stewart (Jarvis, 1976; Stewart, 1988) who presented empirical relationships for the stomatal conductance (i.e. reciprocal of resistance) as stress functions. Nowadays there is a movement to use physiological processes as basis for the calculation of the stomatal conductance (Jacobs, 1994; Cox *et al.*, 1998,1999; Ronda *et al.*, 2001). This results in proper simulation of latent heat fluxes for low vegetations. Analysis using

5

observations from the BOREAS and Garderen experiments revealed that additional mechanisms regulate the canopy conductance of trees. The model overestimated evapotranspiration. This additional mechanism is considered to control water loss in dry air because tall vegetation is quite sensitive to atmospheric conditions due to the strong aerodynamical coupling (Van den Hurk, 2001).

The aim of this study is to get insight in the photosynthesis model, the latent heat flux and the carbon dioxide flux of high vegetations. This will be done with the surface model of the regional climate model RACMO. Eventually it is the purpose to implement the results in RACMO on a European scale.
Section 2 deals with theory about modelling the canopy resistances in a physiological way. In section 3 the calibration and off line validation of Scots pine forest is considered. A statistical approach to evaluate the robustness of the parameter values is described in section 4. In section 5 recommendations for further research are proposed.

2. A review of modelling canopy conductance and plant assimilation

2.1 Introduction

Plant assimilation plays an important role in the interaction of the atmosphere with the vegetated land surface. During daytime CO_2 diffuses via the stomata (see figure 2.1) into the leaf, where it is used in the photosynthesis process. In the meantime water vapour transpires from the leaf into the atmosphere. The stomatal opening that depends on the ambient environmental conditions influences both diffusion processes. The stomatal opening can be seen as a resistance for the diffusion process.
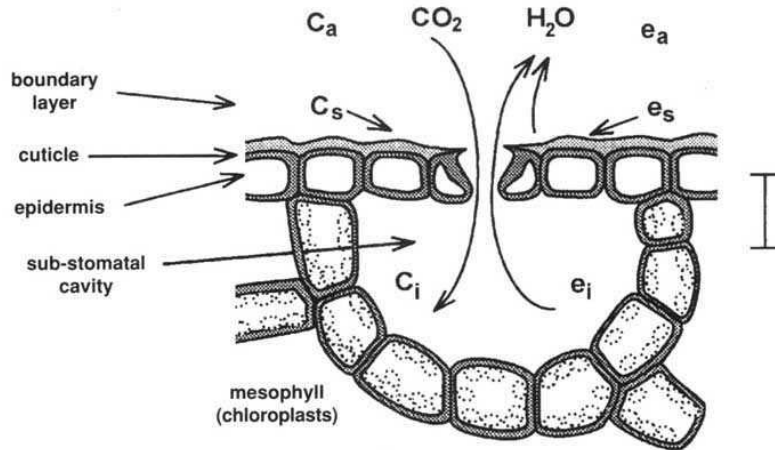
Figure 2.1: Cross section of a leaf stoma and CO_2 and water vapour fluxes. C stands for CO_2 concentration, e for water vapour pressure. Subscripts denote concentrations in free atmosphere (a), at leaf surface (s) and in the stomata (i).

This plant stomatal resistance has a major impact in the energy partitioning at the earth's surface:

$$Q^* - G = H + L_v E \tag{2.1}$$

in which Q^* is the net radiation, G the soil heat flux density and H and $L_v E$ denote the sensible and latent heat flux respectively, all expressed in Wm^{-2}. The latter is the sum of evaporation and transpiration, which depends on stomatal opening of the vegetation.
Here a review of proposed stomatal and canopy conductance models is presented. The first one by Jarvis (1976) is an empirical approach, the others are based on a plant physiological approach. This means that the effect of all environmental conditions is taken into account as a whole.

2.2 The empirical approach.

Jarvis (1976) and Stewart (1988) (JS) proposed the following scheme for the determination of the stomatal conductance:

$$g_s = g_{s,max} \prod_i f_i(x_i) \tag{2.2}$$

where g_s is the stomatal conductance (m/s), $g_{s,max}$ the maximal value of g_s. This parameter has to be calibrated for each vegetation type. Functions $f_i(x_i)$ are stress functions within a range between

0 and 1, due to vapour pressure deficit, vegetation cover quantified by the Leaf Area Index (LAI), soil moisture content, temperature and global radiation. These empirical functions reduce the stomatal conductance from its maximum value depending on the environmental conditions. It is important to note that they act independent of each other. Empirical formulations for $f_i(x_i)$ can be found in Niyogi and Raman (1997), henceforth NR97, Shuttleworth (1989) and Van den Hurk *et al.* (2000).

2.3 The plant physiological approach

2.3.1 C3 & C4 pathways

With the knowledge that plant transpiration and plant photosynthesis use the same way through the stomata to transport water vapour and carbon dioxide respectively, it's obvious that a physiological description of the canopy conductance provides a conceptually more realistic model. This was confirmed by NR97 in a comparison study. The basis of these models is plant physiology. It describes the plant photosynthesis and transpiration and so the surface conductance in a vegetated area. Major advantages of this kind of models is that (1) they react on CO_2, (2) a description of synergistic interactions is an implicit characteristic, (3) the applicability is wider, because they rely on plant nature and less on statistics (Jacobs, 1994). In this approach distinction must be made between the biological pathways, such as C3 or C4.

a) The C3 pathway
In this process, which is the most common one, CO_2 is fixed in the Calvin cycle into a three-carbon acid by the enzyme RUBISCO that is present in massive amounts in the leaves (25% of the total leaf nitrogen). This enzyme can also act as an oxygenase and under present atmospheric conditions this activity results in a wasteful release of CO_2 reducing by about one-third of the net amount of CO_2 that is fixed. This is known as photorespiration. Photorespiration increases with temperature, with the consequence that the overall efficiency of carbon fixation declines with temperature.
The net photosynthesis of C3 plants increases with increasing radiation, but reaches a maximum. For many species this maximum is reached under radiation intensities far below maximum solar radiation. Plants with the C3 mechanism have a low water use efficiency, compared to C4 and CAM plants, mainly because RUBISCO cannot maintain a steep gradient of CO_2 between the leaf mesophyll and the outside atmosphere. Therefore in a C3 plant the CO_2 diffuses rather slowly into the leaf and so allows time for a lot of water to diffuse out. Typical C3 species are temperate deciduous and coniferous forests and most grasses.

b) The C4 pathway
In this pathway the Calvin cycle is present but only in cells lying deep in the leaf. CO_2 that diffuses into the leaf via the stomata meets mesophyll cells that lie in its path and that contain the enzyme PEP-carboxylase. This enzyme combines atmospheric CO_2 with PEP to produce a four-carbon acid. This diffuses and releases CO_2 to the inner cells where it enters the C3 pathway. PEP-carboxylase has a much greater affinity to CO_2 than RUBISCO. Consequences are:
- C4 plants can absorb CO_2 much more effectively than C3 plants, so the CO_2 gradient into the cell is much steeper in C4 plants than in C3 plants, whilst the water gradient has not changed.
- As a result C4 plants have a higher water use efficiency.

- Losses by photorespiration are almost completely prevented.
- The efficiency of carbon fixation does not change with temperature in C4 plants.
- The RUBISCO concentration is a third to a sixth of that in C3 plants, and the leaf nitrogen content is correspondingly lower.

Typical C4 species are maize, mangrove and tropical species such as prairie grass. Ecologically, it is interesting to ask why C4 plants have not used their high water use efficiency to dominate the vegetation at world scale. The C4 metabolism has a high light compensation point and is inefficient at low light levels. C4 plants seem to use their high water use efficiency to invest in a greater fraction of the plant body in the root system than in the shoot. This indicates that they are more sensitive to water shortage and lack of nutrients and that growth is not limited by carbon assimilation (Begon *et al.*, 1998).

In following sections attention will be paid to these physiological models, especially to the so-called A-gs scheme and the MOSES scheme. Plants with a CAM metabolism, which means that CO_2 is taken up at night so water losses are minimised, are excluded in this study.

2.3.2 General design of physiological models

The set up of these models consists of three relationships. The first describes leaf conductance as function of net assimilation (A_n) and CO_2 concentration outside (C_s) and inside (C_i) the stomata:

$$g_s = f_1(A_n, C_s, C_i) \tag{2.3}$$

The second is for assimilation as function of the environmental variables (X):

$$A_n = f_2(X, C_i) \tag{2.4}$$

Two major schools are present for (2.4). Farquhar *et al.* (1980) proposed a biochemical relationship with a maximum photosynthesis rate, which was levelled off by limiting environmental conditions. See also Collatz *et al.* (1991). Goudriaan *et al.* (1985) directly connect conductance to CO_2 assimilation to describe the CO_2 diffusion between air and chloroplasts (Jacobs 1994). In this study Goudriaans results will be used.

Because (2.3) and (2.4) are a set of two equations with three unknown variables (C_i, g_s, A_n), a third equation is necessary as closure:

$$C_i = f_3(X) \tag{2.5}$$

In physiological models C_i is always related to air humidity. Two approaches can be recognised, the one using relative humidity, and the other using vapour pressure deficit. In the next section four closely related models are presented.

2.3.3 Ball-Berry model

The Ball-Berry model (Ball and Berry, 1987) is one of the earliest models of a physiological based canopy conductance. This model is characterised by the coupling of stomatal conductance to relative humidity:

$$g_s = m \frac{A_n RH}{C_s} + g_{min,c}$$
(2.6)

Herein RH (-) denotes the relative humidity at the leaf surface, A_n the net photosynthesis rate, gross assimilation minus dark respiration. Parameter $m = 1.6$ accounts for the difference in diffusivity of carbon dioxide and water in air. $g_{min,c}$ is the cuticular conductance for CO_2, which is small, 0.25 mm/s observed over different vegetation types (Jacobs (1994), Calvet *et al.* (1998) and Ronda *et al.* (2001)). See also Collatz *et al.* (1991). This model has caused concern because it is known that stomata respond to humidity deficit rather than to surface relative humidity (Leuning, 1995).

2.3.4 Kim-Verma scheme

Instead of the relative humidity, the Kim and Verma (1991) scheme uses the vapour pressure deficit at leaf surface (D_s):

$$g_s = g_{min,c} + m \left(1 - \frac{D_s}{D_0}\right) \frac{A_n}{C_s - C_i}$$
(2.7)

with D_0 set to 45 g kg^{-1}.

2.3.5 A-g_s model

Jacobs (1994) set up the A-g$_s$ scheme and Ronda *et al.* (2001) derived a simplified version. No vegetation dependent parameters as $g_{s,max}$ in the Jarvis approach are necessary but only the biological pathway (C3 or C4) followed in the assimilation process is needed as input information. The model set up is as follows.
The transport of carbon dioxide into the leaf is the result of gross assimilation (A_g) and dark respiration (R_d):

$$A_n = g_{l,c}(C_s - C_i) = A_g - R_d$$
(2.8)

in which A_n denotes the net photosynthesis, $g_{l,c}$ the leaf conductance for CO_2. Note that the conductance for water vapour and CO_2 are related as follows: $g_{l,c}=g_{l,w}/1.6$. Jacobs (1994) found that the ratio of C_i and C_s can be expressed as a closure:

$$f = \frac{C_i - \Gamma}{C_s - \Gamma} = f_0 \left(1 - \frac{D_s}{D_0}\right) + f_{min} \frac{D_s}{D_0}$$
(2.9)

Here Γ is the CO_2 compensation point. This is the equilibrium CO_2 concentration, which is

reached under experimental conditions in a leaf chamber where CO_2 becomes depleted till net photosynthesis is zero. D_s the vapour pressure deficit at leaf level, D_0 the value of D_s at which the stomata close fully, given by:

$$D_0 = \frac{f_0 - f_{min}}{a_d}$$
(2.10)

Parameter f_0 is the maximum value of $(C_i - \Gamma)/(C_s - \Gamma)$ while f_{min} represents its minimum value when $D_s = D_0$. a_d is an empirical coefficient and is different for C3 and C4 plants. This results in a smoother response of C_i to vapour pressure deficit than (2.7). Alternative proposals for (2.9) are summarised in NR97. Zhang and Nobel (1996) rewrote equation (2.9) to

$$f = \frac{C_i - \Gamma}{C_s - \Gamma} = f_0 - a_d D_s$$
(2.11)

with D_s in kPa here.
Combining (2.8) and (2.9) results in the leaf conductance for CO_2:

$$g_{l,c} = g_{min,c} + \frac{a_1 A_g}{(C_s - \Gamma)\left(1 + \dfrac{D_s}{D_*}\right)}$$
(2.12)

where a_1 is defined as $1/(1-f_0)$ and $D_* = D_0/(a_1-1)$. Ronda *et al.* (2001) have scaled up (2.12) from leaf to canopy, applying a big leaf approach taking into account an exponential decay of photosynthetic active radiation (PAR). PAR is defined as the part of the spectrum between 400 and 700 nm. This can be estimated as half of the global radiation (Lövenstein *et al.*, 1995). Integrating (2.12) over the leaf area index (LAI) results in an expression for the canopy conductance for CO_2:

$$g_{c,c} = g_{min,c} LAI + \frac{a_1 (A_m + R_d)}{(C_s - \Gamma)\left(1 + \dfrac{D_s}{D_*}\right)} \times \left\{ LAI - \frac{1}{K_x}\left[E_1\left(\frac{\alpha K_x PAR_t}{A_m + R_d} e^{-K_x LAI}\right) - E_1\left(\frac{\alpha K_x PAR_t}{A_m + R_d}\right)\right]\right\}$$
(2.13)

Here $E_1(x)$ denotes the exponential integral, K_x the decay coefficient for *PAR*. α is the initial light-use efficiency and A_m the maximum gross assimilation under high *PAR* and CO_2 conditions. PAR_t is photosynthetic active radiation at the top of the canopy. In appendix A the leaf photosynthesis model is described. Parameters to be known to find $g_{c,c}$ are α_0 (maximum initial light use efficiency), Γ, g_m, $A_{m,max}$, f_0, a_d, and $g_{min,c}$. The three first are temperature dependent. $A_{m,max}$ provides a limitation to A_m because at high CO_2 and *PAR* conditions photosynthesis is hampered by the regeneration of RUBISCO.

Soil moisture stress is described by a linear stress function (Calvet *et al.*, 1998; Cox *et al.*, 1998,

henceforth C98, Cox *et al.*, 1999, henceforth C99; Soet *et al.*, 2001)

$$\beta(\theta) = \begin{cases} 0 & \theta < \theta_w \\ \dfrac{\theta - \theta_w}{\theta_c - \theta_w} & \theta_w < \theta < \theta_c \\ 1 & \theta > \theta_c \end{cases} \tag{2.14}$$

where θ is the root zone averaged moisture content on volume basis expressed in ($m^3\ m^{-3}$). θ_c is the soil moisture content at field capacity (pF=2.0) and θ_w at permanent wilting point (pF= 4.2). Ronda *et al.* (2001) adopt a quadratic equation in $\beta(\theta)$

$$f_2(\theta) = 2\beta(\theta) - \beta^2(\theta) \tag{2.15}$$

There are a number of options applying soil moisture stress. Ronda *et al.* (2001) implemented soil moisture stress by multiplying the unstressed gross assimilation with (2.15), while Calvet *et al.* (1998) multiplied the unstressed mesophyll conductance with (2.14). C99 multiplied (2.14) with unstressed net leaf photosynthesis.

2.3.6 MOSES scheme.

The Hadley Centre uses the land surface model MOSES (MetOffice Surface Energy Scheme) in climate modelling. It consists of a canopy with 4 soil layers. See C99 and Pope *et al.* (2000) and figure 2.2. The net assimilation of CO_2 is calculated with

$$A_n = g_{l,c}(C_s - C_i) = \frac{g_{l,w}}{m}(C_s - C_i) \tag{2.16}$$

$g_{l,c}$ and $g_{l,w}$ are the leaf conductances for CO_2 and water vapour respectively. The photosynthesis model was adopted from Collatz *et al.* (1991). A_n can be written as function of environmental variables and the internal CO_2 concentration. The closure MOSES uses is:

$$f = \frac{C_i - \Gamma}{C_s - \Gamma} = F_0 \left\{ 1 - \frac{D_s}{D_c} \right\} \tag{2.17}$$

F_0 and D_c are parameters that are different for C3 and C4 plants (C98). See table 2.1. Equalising equations (2.11) using the calibration of Ronda (2001) and (2.17) yields $F_0 = f_0$. This is because when D_s =0, both F_0 and f_0 values should be the same. When $F_0 = f_0$ then it follows that $D_c = F_0/a_d$. These values are summarised in table 2.1. These values will be used further.

Table 2.1: Parameter values in MOSES and derived from Ronda *et al.* (2001).

	C3 (C99)	C3 Ronda *et al.* (2001)	Forest (C99)	C4 Ronda *et al.* (2001)
F_0 (-)	0.925	0.89	0.875	0.85
D_c (kPa)	24.5	12.7	14.6	5.5
D_c (kg/kg)	0.150	0.078	0.09	0.034

The scaling up to canopy level is essentially different for MOSES as compared to (2.13). The authors explain that extinction in the canopy of PAR, $A_{m,max}$ and R_d is the same for all mentioned parameters. So it's tenable to assume that assimilation and stomatal conductance also decays exponentially (because of the fixed ratio of $A_n/g_{s,c}$ (see Wong *et al.*, 1979)). This results in

$$g_{c,c} = g_{s,c} \frac{1 - \exp(-K_x LAI)}{K_x}$$ (2.18)

$g_{s,c}$ and $g_{c,c}$ are the leaf conductance and canopy conductance for CO_2 respectively. In literature parameter K_x ranges from 0.5 (C98) to 0.7 (Van de Kassteele, 2001).
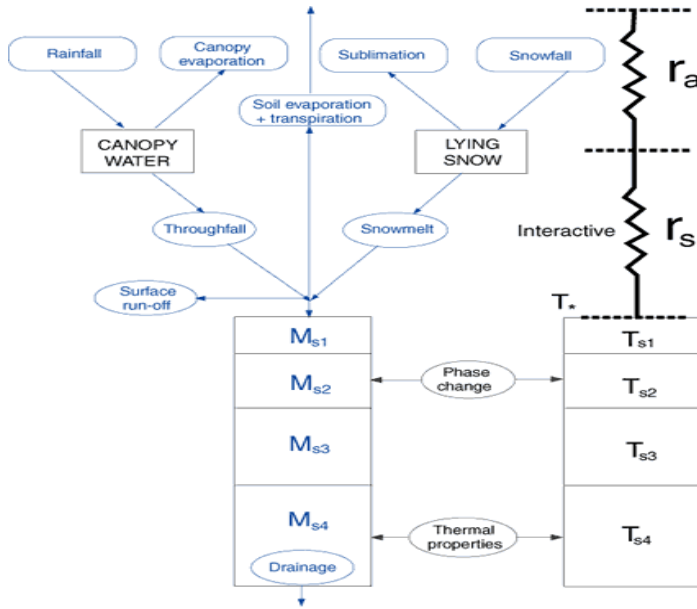
Figure 2.2: The MOSES scheme, from: C99.

Another difference between MOSES and the A-g_s scheme is the implementation of soil moisture stress. A-gs in the form of Ronda *et al.* (2001) uses (2.15) were C98 and C99 took (2.14). They both apply the soil moisture stress on gross assimilation.

2.3.7 Influence of leaf nitrogen content on the carboxylation of RUBISCO.

An essential difference between MOSES and A-gs is the parameterisation of the maximum rate of RUBISCO carboxylation $V_{c,max}$. The MOSES scheme uses a relationship to include the dependence on leaf nitrogen while A-gs uses a constant value. C99 used a study of Schulze *et al.*

(1994) to relate the maximum rate of carboxylation of rubisco $V_{c,max}$ ($\approx 2\ A_{m,max}$ for C3 plants) to leaf nitrogen content n_l (kg N (kg C)$^{-1}$). The maximal RUBISCO photosynthetic capacity is linearly dependent on leaf nitrogen content. A linear relationship between maximal stomatal conductance and leaf nitrogen content leads to a linear relationship between $V_{c,max}$ and n_l. C99 used a constant value of n_l =0.05, although the nitrogen content differs among species (Schulze *et al.*, 1994) and in time (Wilson *et al.*, 2000) but overall n_l =0.05 is a proper value (Van Hove, pers. comm., 2001). Figure 2.3 presents the sensitivity of the canopy conductance in the MOSES scheme to canopy conductance for C3 and C4 grassland. It is obvious that there is a strong influence due to nitrogen content, but it is stronger for C3 than for C4.

Dependence of stomatal conductance on leaf nitrogen content
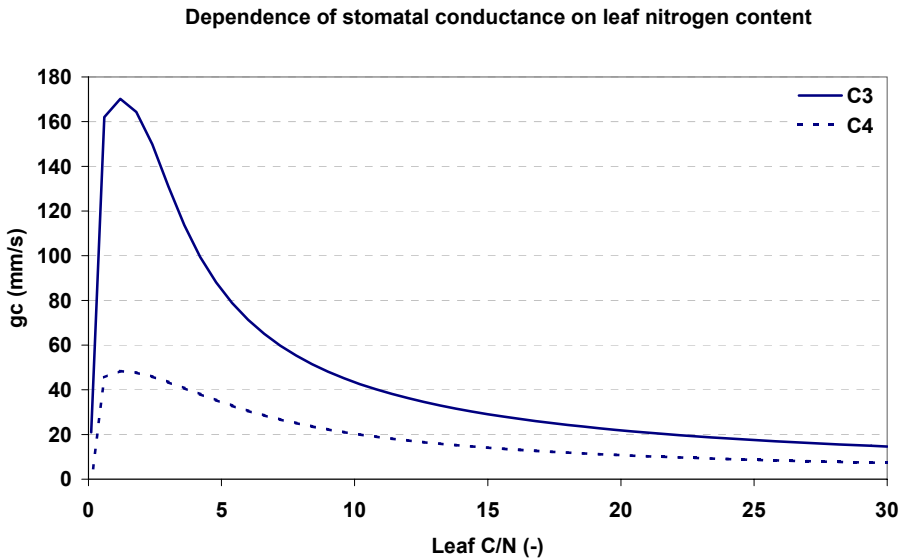
Figure 2.3: The influence of nitrogen content on canopy conductance in MOSES. PAR =400 Wm^{-2}, T_{sk} = 293 K, LAI = 4 and D_s= 0 g/kg.

Table 2.2 summarizes the averaged values of N contents for vegetation communities according to Schulze *et al.* (1994). These data can be used in combination with a vegetation chart when the model will be used at a European scale.

Table 2.2 Leaf nitrogen content on mass basis for some plant communities.

Species	Mean (mg N/g dry weight leaf)	Standard Error (mg N/g dry weight leaf)	n_l (kg N/ kg C)	Standard Error n_l (kg N/ kg C)
Broadleaved crops	38.4	1.8	0.096	0.005
Cereals	33.6	1.9	0.084	0.005
Deciduous conifers	20.7	1.7	0.052	0.004
Evergreen conifers	11.0	0.6	0.028	0.002
Monsoonal forest	11.4	0.9	0.029	0.002
Sclerophyllous scrub	11.4	0.6	0.029	0.002
Temperate deciduous forest	19.6	2.7	0.049	0.007
Temperate deciduous fruit trees	23.8	2.4	0.060	0.006
Temperate grassland	25.5	1.6	0.064	0.004
Temperate evergreen broadleaf tree	13.5	1	0.034	0.003
Temperate evergreen crop	25.2	-	0.063	-
Tropical deciduous forest	27.1	1	0.068	0.003
Tropical fruit plantations	13.6	4.6	0.034	0.012
Tropical grassland	10.7	4	0.027	0.010
Sugarcane	12.0	-	0.030	-
Tropical rainforest	16.5	1.6	0.041	0.004
Tundra	20.5	1.1	0.051	0.003

Parameter n_l was found from this table by assuming that 40% of the dry mass is carbon (C99).

To examine to the influence of nitrogen nutrition on plant photosynthesis on both long and short time scales a short literature review is presented.

Nitrogen on short time scales...
At first we should recognize that a constant value of the RUBISCO carboxylase capacity ($V_{c,max}$) is not quite realistic. Wilson *et al.* (2000) clearly show that in oak and maple an annual cycle in $V_{c,max}$ is present. This may be due to the effect of leaf age (De Jong *et al.* (1985), Field and Mooney (1983), Reich *et al.* (1997) and Lambers *et al.* (1998), p. 57) or nitrogen allocation (Wilson, 2000). Takeuchi *et al.* (2001) found that the N concentration decreases during summer and increases with height in the canopy. So using the equations proposed by Jacobs (1994) and Ronda *et al.* (2001) on a seasonal time scale, e.g. in climate modelling may lead to a bias in latent and sensible heat fluxes when a constant carboxylase capacity is assumed.
Field and Mooney (1983) show that a strong linear correlation between nitrogen content and maximum net photosynthesis is present. This is confirmed by Wong (1979), Wong *et al.* (1985), Schulze *et al.* (1994), Reich *et al.* (1997), Hikosaka and Hirose (1998) and it was used by C99 in climate modelling. The relationships used in C99 are:

$$V_{c,max} = 35.2n_l \text{ mg } CO_2/m^2/s \text{ for C3 and}$$
$$V_{c,max} = 17.6n_l \text{ mg } CO_2/m^2/s \text{ for C4 plants.}$$

Most authors use a linear relationship between nitrogen and photosynthesis, but Reich *et al.* (1997) show a log linear plot. In addition a strong correlation between nitrogen and RUBISCO is present following Field and Mooney (1983). On the other hand not only the amount of RUBISCO and its capacity, but also its regeneration and allocation of N to chlorophyll seem to be important factors (Hikosaka and Hirose, 1998). Evans (1989) shows that a variation appears between

species in the relationship between photosynthesis and nitrogen content when both assimilation and leaf nitrogen are based on leaf area. Making this difference between nitrogen on mass and area basis, Wilson *et al.* (2000) and Wilson (pers. comm., 2001) present that the relationship between nitrogen and $V_{c,max}$ (and thus $A_{m,max}$) is much weaker on mass basis (N_m, R^2 typically 0.25) than on area basis (N_a, R^2 typically 0.6).

It is known that other nutrients have also impact on photosynthesis rate. According to Lövenstein *et al.* (1995) the ratio of phosphorus to nitrogen must be in a range between 0.05 and 0.14 for good plant functioning.

In the long run…

It should be mentioned that it is unknown how the relationships between nitrogen and $A_{m,\ max}$ will hold under conditions of enhanced CO_2 concentrations. Several researchers indicated that photosynthetic acclimatisation, i.e. changes in nitrogen partitioning can improve photosynthesis at enhanced CO_2 levels. However, this has not been confirmed in experiments (Hikosaka and Hirose, 1998). Takeuchi *et al.* (2001) report that this acclimatisation means a decrease of N concentration and carboxylation capacity. So this acclimatisation is poorly understood. Since climate modelling is on a long time scale, we don't know the effects of climate change e.g. according to enhanced CO_2 on carbon and nitrogen assimilation. Wong (1979) and Kunz *et al.* (1995) report the possibility of changing patterns of competition between species and thus the effects of forage and herbivory on vegetation can change. This may result in changing vegetations, meaning that a fixed vegetation characterization like USGS or PELCOM does not hold in the long run.

We conclude that maximum assimilation rate is related to leaf nitrogen content. This dependence may increase model performance when implemented. How this relation must be implemented, on area or mass basis, is not quite clear. On the other hand the relationships seem to be affected by climate change, thus they cannot be used in climate prediction studies.

2.3.8 Comparison of A-gs and MOSES scheme.

a) Theoretical

Figure 2.4 shows the gross assimilation for both models and for C3 and C4 plants. A very pronounced disagreement is seen: the A-g_s scheme assimilates twice as fast as the MOSES scheme does. This holds both for C3 and C4 plants. An explanation for this difference can be found in Calvet (2001). He summarizes unstressed values for the mesophyll conductance for a variety of species. Comparing these values with the a priori value of $g_m(@25)= 7.0$ mm/s in the A-g_s scheme, it appeared that the latter is a high estimate. The average values in Calvet (2000) for $g_m(@25ºC)$ are 0.8 mm/s, 0.53 mm/s and 6.37 mm/s for C3 plants, C3 woody plants and C4 plants respectively. Goudriaan (pers. comm., 2001) argues that this 0.8 mm/s is a too low value for a proper photosynthesis. It appeared that both models' photosynthesis can be compared quite well when the mesophyll conductance was chosen as 1.8 mm/s for C3 and 2.5 mm/s for C4 plants. This is in agreement which was found by Jacobs (1994) for a vineyard, $g_m = 2.0$ mm/s. On the other hand g_m is related to the maximum rate of carboxylation of rubisco $V_{c,max}$, where for C3 plants $A_{m,max}= 0.5V_{cmax}$, (Jacobs, 1994):

$$g_m = \frac{\partial A_n}{\partial C_i} = \frac{V_{c\,max}}{\Gamma + K_c \left(1 + \dfrac{O_a}{K_O}\right)} \qquad (2.19)$$

K_C and K_O are the Michaelis constants for CO_2 and O_2 respectively. These are constants, based on enzyme kinetics. O_a is the atmospheric O_2 concentration. This equation implies that lowering g_m cannot be done without lowering $V_{c,max}$. Table 2.3 shows a literature review of $V_{c,max}$ values of both laboratory and field measurements. It is seen that values derived in the laboratory are a factor of 2 larger than those obtained in the field. This was confirmed by Dang *et al.* (1998) who reported a variety in $V_{c,max}$ values. They also stated that poor results for the upper part of the canopy were obtained when model simulations used laboratory values of $V_{c,max}$. Beyond the field and laboratory difference, spatial variability within the field is found because of leaf age (Porte and Loustau, 1998) and leaf level (Carswell *et al.* 2000). Another cause of the difference is that the standard value of $V_{c,max}$ ($V_{c,max}$ =4.3 mg/m^2/s, Jacobs, 1994) was derived for agricultural crops only. These are monocultures. In nature species live mixed and compete with each other for resources. So in nature plants live sub optimally, investing energy in the competition, leading to sub optimal values of the assimilation parameters.

Wullschleger (1993) reports $V_{c,max}$ values for 109 species, although not all of them are corrected to 25ºC. A summary of his results is presented in table 2.4. Note that the values in tables 2.3 and 2.4 are not all obtained with the same measuring methods.

With the knowledge that the A-gs scheme, using $V_{c,max} = 4.3$ mg/m^2/s, shows overestimation of evapotranspiration in forests, $V_{c,max}$ and so $A_{m,max}$ should be brought down by a factor 2. In the following we use $A_{m,max}$(@25)= 1.1 mg/m^2/s for C3 and 0.85 mg/m^2/s of C4. As a consequence g$_m$ was adjusted to g$_m$(@25)=3.5 mm/s for C3 and 8.8 mm/s for C4 plants. The parameter value of $V_{c,max}$ is not affected significantly by changing climate conditions (Takeuchi *et al.*, 2001; Wang *et al.*, 1996). On the other hand we know that N decreases under elevated CO_2 (Takeuchi *et al.*, 2001), so coupling of $V_{c,max}$ and N as done by C99 may result in biased surface fluxes when their parameterisation is used under enhanced CO_2 concentrations.
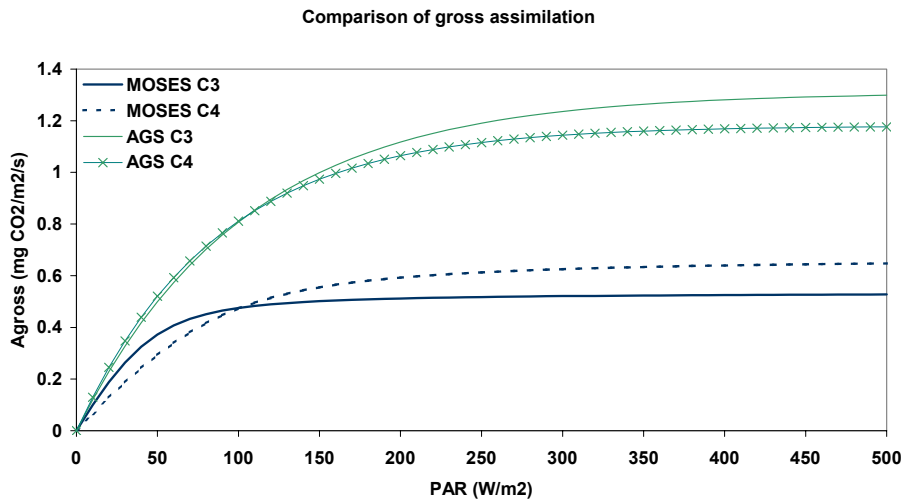
Figure 2.4: Comparison of gross assimilation in both models using parameter values as in literature.

17

A sensitivity analysis is presented that explores the behaviour of the MOSES and A-gs model (with the adapted value for $g_m(@25)$). Here reference values are used for of PAR = 400 Wm^{-2}, LAI = 2, D_s = 0 kg kg^{-1} and T_{sk}= 20 °C, leaf C/N ratio = 20. In these cases no soil moisture stress was included. Variables have been normalised with their maximum value.

Table 2.3: Overview of $V_{c,max}$ values in literature before and after correction to 25ºC. Uncertainties are given in standard errors. The last column indicates whether the data are field (F) or laboratory (L) based.

Publication	Species	V_{cmax} (μmol/m2/s)	$V_{cmax}(@25)$ (μmol/m2/s)	Field (F)/ Lab (L)
Farquhar *et al.* 1980	-	98	98	L
Calvet 1998	-	200	200	L
Calvet 2000	-	98	98	L
Jacobs 1994	-	98	98	L
Dang *et al.* 1998	Black spruce	13.4	20.8	F
Dang *et al.* 1998	Jack Pine	18.7	28.6	F
Baldocchi *et al.* 1999	Temperate forest	45.7	45.7	F
Baldocchi *et al.* 1999	Aspen Hazel Stand	34	34	F
Cox *et al.* 1998	Prairie C4 grass	43.0	41.5	F
Dekker 2000	Douglas fir stand	50	48.2	F
Carswell *et al.* 2000	*Cedrela odorata*	27	27	F
Kellomäki and Wang 1997	*Pinus sylvestris*	39.7-61.6*	41.0-63.6*	F
Porte and Loustau 1998	*Pinus pinaster* 1 yr. old	53.1±6.7	53.1±6.7	F
Porte and Loustau 1998	*Pinus pinaster* 2 yr. old	37.1±9.3	37.1±9.3	F
Carswell *et al.* 2000	Amazonian rain forest (gr. level)	20.5±1.3	20.5±1.3	F
Carswell *et al.* 2000	Amazonian rain forest (crown)	42.8±5.9	42.8±5.9	F
Dreyer *et al.* 2001	*A. Pseudo.*	77.8±5.9	77.8±5.9	F
Dreyer *et al.* 2001	*B. pendula*	70.5±6.6	70.5±6.6	F
Dreyer *et al.* 2001	*F. silvatica*	66.3±2.2	66.3±2.2	F
Dreyer *et al.* 2001	*F. excelsior*	84.6±4.3	84.6±4.3	F
Dreyer *et al* 2001	*J. regia*	63.6±5.4	63.6±5.4	F
Dreyer *et al.* 2001	*Q. petraea*	87.7±3.1	87.7±3.1	F
Dreyer *et al.* 2001	*Q. robur*	90.5±6.3	90.5±6.3	F
Harding *et al.* 2000	C3 grassland			F
	Standard case	40	38.5	
	Multvar regr	146	141	
	Optim. Vmax	28.6	27.6	

*depending on nitrogen nutrition

Table 2.4. Averaged V_{cmax} values divided into vegetation classes (after Wullschleger, 1993). The given uncertainty is one standard deviation.

Plant categories	Mean (mg/m²/s)	Range (mg/m²/s)
Agricultural crops		
• Dicots[1]	4.0±1.8	1.3-8.5
• Monocots[1]	3.0±0.9	1.5-4.8
Horticultural crops		
• Fruit trees	1.6±1.0	0.5-3.0
• Vegetables	2.6±1.3	0.7-4.3
Temperate forests		
• Hardwood	2.1±1.5	0.5-5.2
• Conifers	1.1±0.5	0.3-2.0
Tropical forest	2.2±1.4	0.4-5.5
Understorey herbs and forbs	2.9±2.2	0.5-6.5
Desert annuals and perennials	6.7±2.4	4.0-8.2
Sclerophyllous shrubs	2.3±0.7	1.5-3.1

[1] Dicots and monocots differ in the way of flowering. More information is available in Monocots (2002).
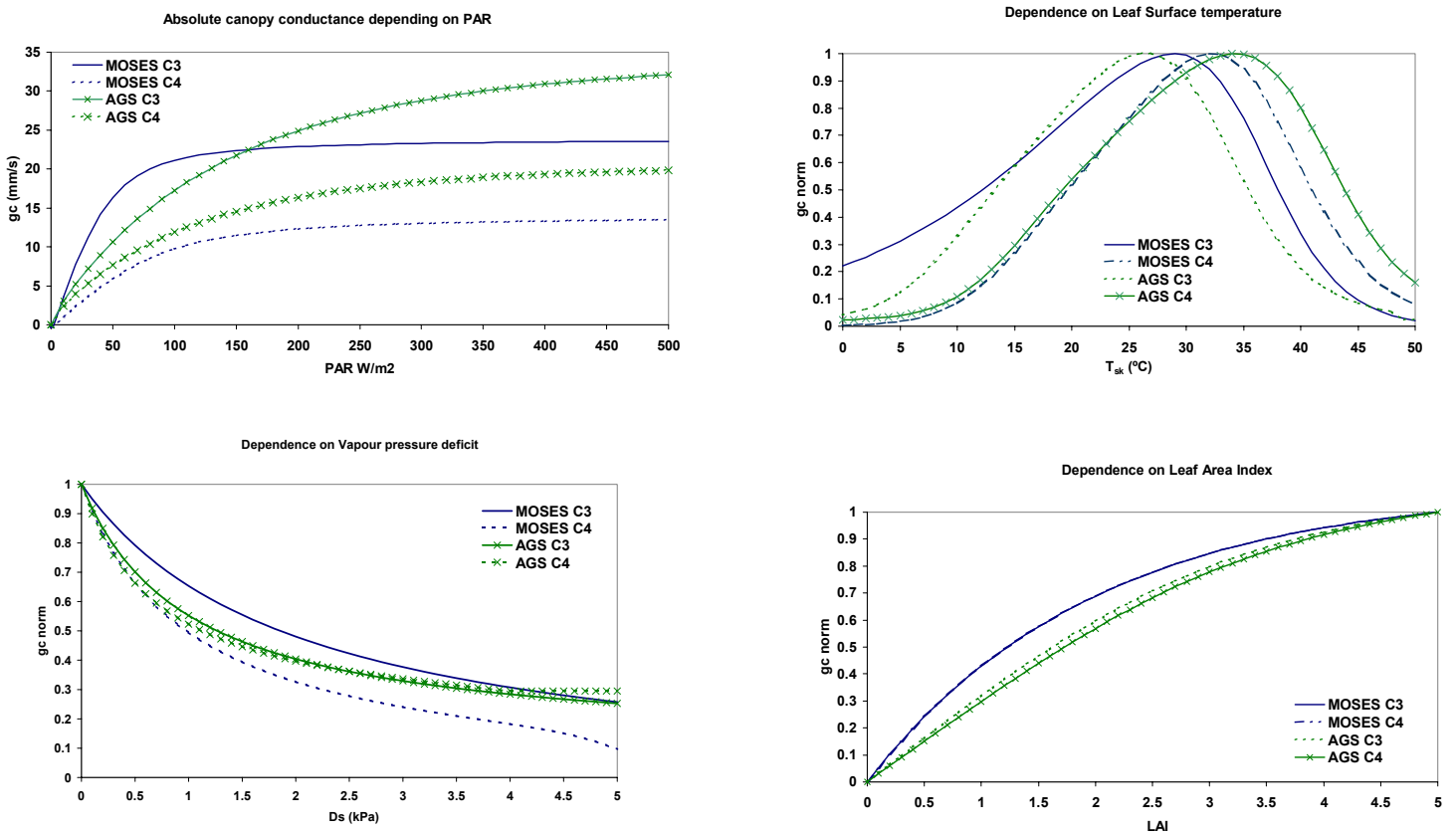
Figure 2.5: The sensitivity of canopy conductance to the environmental variables PAR, LAI, T_{sk} and D_s.

Figure 2.5 shows that MOSES and A-gs show a similar response to PAR: increasing PAR leads to larger conductance values. C4 plants have lower values of the stomatal conductance at the same value of PAR than C3 plants. For LAI the models behave nearly the same for C3 and C4. A-gs realises lower conductances. A higher optimum temperature value for C4 is seen. This is a common feature. Also the dependence on vapour pressure deficit does not vary much between the models, except that MOSES C3 exhibits smaller stress at lower deficit values.

Table 2.5 gives a sensitivity analysis for MOSES C3 calculation with ceterus paribus values of the environmental variables as above. No soil moisture stress is applied. For high and low values of PAR and D_s, the parameters C/N, F_0 and D_c have been increased with ten percent and the relative change has been summarized in table 2.5. For the A-g_s scheme a similar analysis can be found in Van de Kassteele (2001). His results are summarized in table 2.6. The sensitivity for a_d and D_c are quite the same in both models. At very low vapour pressure deficit MOSES is more sensitive to F_0 than A-gs.

Table 2.5. Relative changes (%) of canopy conductance for water in C3 grassland in MOSES with a 10% increase of parameter for different values of environmental variables.

Parameter	PAR =400 W m^{-2} Ds= 0 kPa	PAR =400 W m^{-2} Ds= 5 kPa	PAR =50 W m^{-2} Ds= 0 kPa	PAR =50 W m^{-2} Ds= 5 kPa
C/N	-8.6	-8.6	1.2	1.3
F_0	57.4	26.9	56.6	26.1
D_c	0.0	8.4	0.0	7.8

Table 2.6. Relative changes (%) of canopy conductance for water in a C3 grassland in A-gs with a 10% increase of parameter for different values of environmental variables. Van de Kassteele (2001).

Parameter	PAR =400 W m^{-2} Ds= 0 kPa	PAR =400 W m^{-2} Ds= 5 kPa	PAR =50 W m^{-2} Ds= 0 kPa	PAR =50 W m^{-2} Ds= 5 kPa
F_0	428.6	25.9	397.2	16.4
a_d	0.0	-9.2	0.0	-5.5

It appears again that C/N ratio is an important variable, especially in high PAR conditions. It is clear that F_0 affects canopy conductance mostly, with a more than 50% change in $g_{c,w}$ with a ten percent change in F_0. Parameter D_c has impact only at high values of vapour pressure deficit.

In figure 2.6 the ratio of internal to external CO_2 concentration for C3 vegetation, f, is depicted as function of vapour pressure deficit for both models. A-gs shows a steeper line at low values of D_s while at higher values of D_s a constant value, f_{min}, is obtained. This means that the A-gs scheme realizes a smaller stomatal opening at the same vapour pressure deficit, and so a smaller latent heat flux than MOSES.
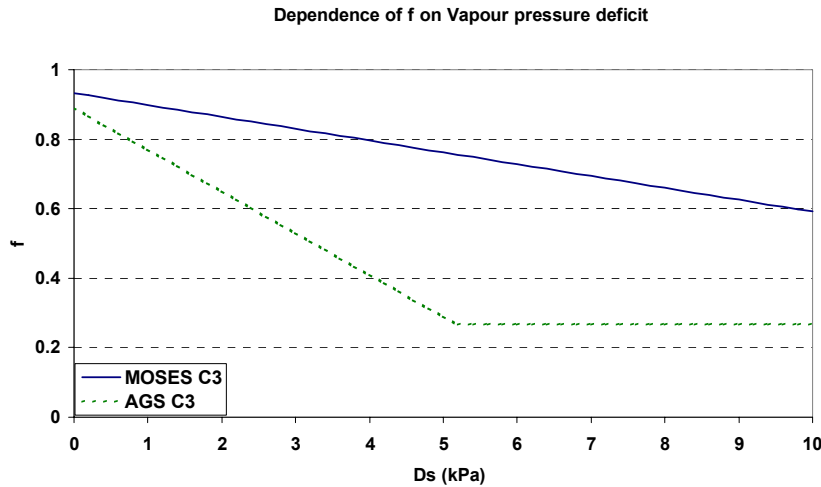
Figure 2.6: f as function of vapour pressure deficit for a C3 grassland modelled with MOSES and A-g$_s$ scheme with ceterus paribus values as in figure 2.5.

b) Practical experiences
Climate studies are sensitive to the vegetation classification that is used. Van de Kassteele (2001) studied the latent heat flux on European scale using the A-gs model with the USGS vegetation classification. Due to problems with excessive high transpiration values in high vegetation Van de Kassteele (2001) developed specific parameter values for needle leaf forest beside that for C3 and C4 plants.
C98 and Harding (2000) employed the land use classification of Wilson and Henderson-Sellers (1985). Cox (pers. comm.) is not aware of overestimation of transpiration in high vegetation with MOSES, but it was tested above a C3 grassland (Harding, 2000) and a C4 grassland (FIFE) (C98) and only rudimentary for other biomes. Note that in MOSES a much lower value of g$_m$ is used than in Van de Kassteele (2001).

2.4 Conclusion.

It is clear that a physiological model calculates canopy conductance parameter values that do not appear robust across all biomes. Because the A-gs scheme seems to work quite well for low vegetation (Ronda *et al.*, 2001) parameters will not be explored for this vegetation type. We propose to examine the parameters $A_{m,max}$, f_0, a_d and g_m at 25ºC for high vegetation in the A-g$_s$ scheme.
Another message is that leaf nitrogen content can have an important impact in the photosynthesis mechanism, and so in the canopy conductance. At the end of the next section a table of proposed parameter values will be presented.

3 Calibration and validation of model parameters for a Scots pine forest.

In this section the A-g_s model will be evaluated against field data from the Loobos site. At first a site description will be presented, followed by calibration of some parameters. Eventually the model will be validated.

3.1 Loobos site description
(pers. comm. Moors *et al.*, 2001)

The Loobos site is located near Kootwijk in the Netherlands (52°10′00″ N - 5°44′38″ O). The main tree species is Scots pine (*Pinus silvestris*). In all directions the forest extends for more than 1.5 km. The trees were planted around 1909 on sand dunes and are widely spaced with some open spots. In a radius of 500 m around the flux tower 89% of the area is covered with Scots pine, 3.3% with Corsican or black pine, 2.3% with birch, 1.3% with Douglas fir, 0.6% with oak and 3.5% of the area is open and mostly covered with heather and grass. The average tree height is 15.1 m. The undergrowth of the forest is a closed cover of mainly grass (*Deschampsia*). Because of the local topography caused by the sand dunes the distance to the ground water table depends on the location. At the base of the tower the ground water table is at a depth of ± 6.5 m below the surface. In the valleys the ground water table reaches ± 3.5 m.

LAI measurements were done on an irregular basis using the LAI 2000 (Li-Cor). To obtain the true one side projected LAI, it was estimated that the measurements of the LAI 2000 should be multiplied by 1.2. This accounts for needle clumping and area of stem and twigs seen by the instrument. In table 1 the vegetation characteristics of the site are summarised. Here the corrected LAI is given.

Table 3.1 Vegetation characteristics of the Loobos site.

Quantity	
Tree density (Treeha^{-1})	360
Tree height (m)	15.1
Displacement height (m)	8.1
Roughness length for momentum (m)	1.5
LAI trees (-) max./min.	2.2/1.9
LAI grass (-)max./min	1.1/0.0

To obtain the turbulent fluxes eddy-correlation technique is used. The measurements system is based on a 3D ultrasonic anemometer (Solent, Gill) in combination with a fast infrared gas analyser (Li-Cor 6262) placed on the top of a 26 m tower. Additionally profiles (five levels) of CO_2 and H_2O concentrations (CIRAS-SC, PP systems) as well as wind speed and temperature were measured. To determine net radiation, the four components of the radiation balance were measured separately. Incoming and reflected short wave radiation were measured with two pyranometers (CM21, Kipp). The long wave components were measured by pyrgeometers (CG1, Kipp), with the sensor for the incoming long wave radiation being ventilated. At the top of the scaffolding tower (23 m) standard meteorological measurements of precipitation, horizontal wind speed, wind direction, relative humidity and air temperature were made. The soil heat flux was measured using

four heat flux sensors (TPD-TNO) under the litter layer at a depth of 3 cm in the mineral soil. Soil moisture and temperature was measured in two profiles at five depths until 200 cm. deep.

3.2 Calibration of internal to external CO_2 concentration versus vapour pressure deficit.

3.2.1 Introduction.

Because the difference in behaviour of the A-gs model and the model by C99 may be due to the difference in adopted closures (2.9) and (2.17), we decided to perform a calibration of the ratio of internal to external CO_2 concentrations and vapour pressure deficit (D_s) closure used in these models. The Loobos data include all necessary quantities to do that.

3.2.2 Soil respiration

Calibration is only possible when the contribution of canopy and soil respiration rate to the total CO_2 flux is known. An expression of respiration as function of soil temperature and soil moisture content must be found. Because photosynthesis is absent at night, the whole CO_2 flux can be attributed to respiration processes. Therefore night time data of the net CO_2 flux, soil temperature and volumetric soil moisture content θ at 5 cm below surface were selected between 0:00 and 5:00 local time. Days with precipitation were neglected in the analysis. Measured CO_2 fluxes have been corrected for changes in CO_2 concentrations between the mast and the canopy. See figure 3.1. To examine the influence of soil moisture in this case, the data set has been split in wet episodes ($\theta \geq 0.08$) and dry episodes ($\theta < 0.08$). This threshold value has been chosen because 0.08 is the average value in the data. To reduce the scatter in the data, the data were also divided in classes according to soil temperature. Between 0 and 20ºC eight classes of 2.5ºC width were constructed. So eventually 16 classes were obtained.

Figure 3.2 shows the data including error bars, representing the standard deviation within each class. A first remark is that no distinction between the soil moisture regimes can be made from this data set. In contrast to e.g. Davidson *et al.* (1998) who found a relationship between soil moisture and soil respiration. The two points marked with triangles deviate a lot from the other points. Their large standard deviations indicate that a few extreme members of that class affect the class average. These data were not used in the exponential regression curve shown. It shows an explained variance (R^2) of 0.83, which is quite acceptable. For illustration two other models are shown. They have been obtained from Foster and Hadley (1998) and Davidson *et al.* (1998). The found curve agrees well with these models. Note that these two models represent soil respiration, and the proposed curve represents soil respiration and dark respiration from the vegetation.

Figure 3.1: Illustration of CO_2 budgets.

Determination of respiration rate

$y = 0,037e^{0,094x}$

$R^2 = 0,8297$

FCO2 (mg CO2/m2/s)

Tsoil -5cm (ºC)

| ♦ DATA | – – – FH98 | – – DT98 | △ DATA2 | —— Fit |
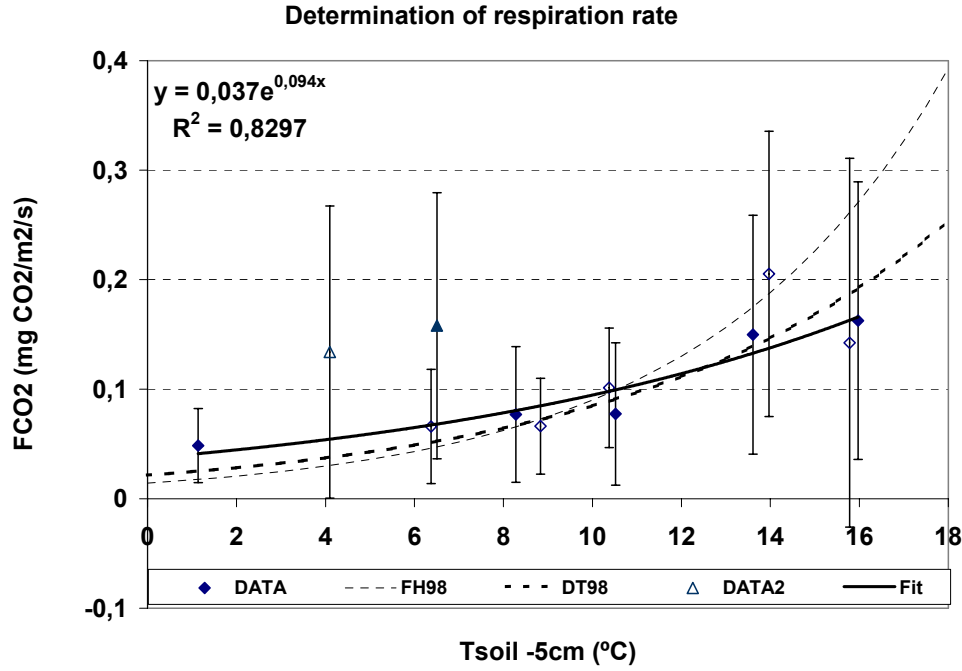
Figure 3.2: Determination of respiration processes as function of temperature. Open point indicators are 'wet' points, where solid indicators are the 'dry' points. An exponential curve is commonly used in literature. See e.g. Foster and Hadley (1998) and Davidson et al. (1998).

Figure 3.3 displays a sketch of the resistance scheme for the transport process of CO_2 and water vapour. Assuming no flux divergence, it follows that (see Appendix C):

$$L_v E = g_c \left(q_{sat}(T_{sk}) - q_{leaf} \right) \rho_a L_v$$
$$L_v E = g_a \left(q_{leaf} - q_a \right) \rho_a L_v$$
$$L_v E = \left(\frac{g_a g_c}{g_a + g_c} \left(q_{sat}(T_{sk}) - q_a \right) - q_a g_a \right) \rho_a L_v$$

(3.1)

in which $L_v E$ is the measured latent heat flux, q_s and q_a the specific humidity at stomatal and measurement level respectively (kg/kg). $q_{sat}(T_{sk})$ is the saturated specific humidity at skin temperature. g_a and g_c are the aerodynamic and canopy conductances respectively (m/s). In this exercise the vapour pressure deficit has been determined at stomatal level by scaling down g_c with (2.18).

What also holds is:
$$F_{CO_2} = g_c \left(C_{in} - C_{out} \right)$$
$$F_{CO_2} = g_a \left(C_{out} - C_{ext} \right)$$

with the ambient CO_2 concentration C_{ext} was chosen as 640 mg/m^3 (350 ppm) and C_{out} the CO_2 concentration at leaf level. See figure 3.3.

C_{ext}, T_a, q_a Air

                    ⇧ L_vE, F_CO_2 g_a

C_{out}, T_{sk}, q_{leaf} Leaf Surface

                    ⇧ L_vE, F_CO_2 g_c

C_i, T_{sk}, q_s=$q_{sat}(T_{sk})$ Stomata
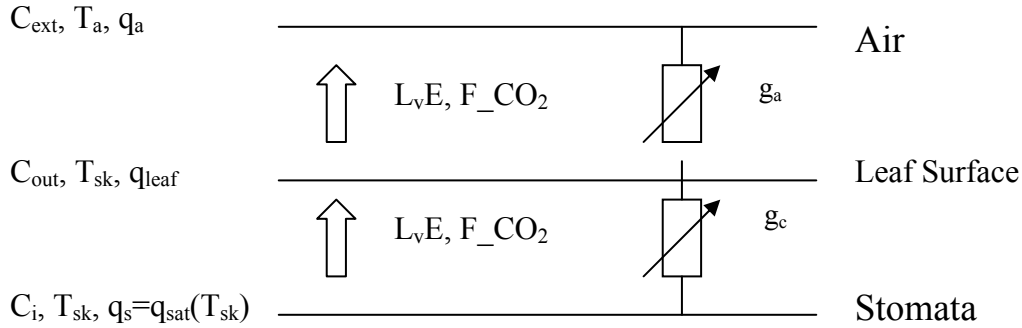
Figure 3.3: Resistance scheme for water vapour and CO_2.

3.2.3 Calibration

From the measured CO_2 flux and a parameterisation for soil respiration the assimilation at canopy level can be estimated.

Data selection is necessary to perform an optimal calibration. Because of the optimal functioning of photosynthesis, only data around noon (10:00 – 14:00 local time) were selected. Measurements on days with precipitation have been neglected, because rain causes a large amount of interception and the following interception evaporation is not representative for the photosynthesis model. In addition the data points with a latent heat flux of less than 100 W/m^2 have been ignored, because calibration during a low evaporative fraction is not optimal. This is also true for time slots with a low net CO_2 influx into the leaf. When this was less than 0.5 mg CO_2/m^2/s data were skipped. Because of the danger of large uncertainties in measured absolute low CO_2 fluxes, values larger than −1.0 μmol CO_2/m^2/s have also been skipped. Uncoupling between above forest air and within forest air can be a problem at low wind speeds, resulting in non-representative measurements. Therefore data with wind speeds lower than 2 m/s has been ignored. Surface temperature has been determined from measured outgoing radiation and an emissivity of ε=0.98. The assimilation rate has been determined by:

CO_2 assimilation (A_n) = Measured flux - Respiration + Storage change.

Calibration of the ratio $f = \dfrac{C_i - \Gamma}{C_a - \Gamma}$ needs a model for the CO_2 compensation point Γ. This was chosen as: $\Gamma = 68.5\rho_a$, where Γ is expressed in mg/m^3 and the air density ρ_a in kg/m^3 (Ronda *et al.*, 2001). We used equation (2.18) to obtain f at stomatal level, thus corrected for LAI. The used FORTRAN program can be found in Appendix B.

At first figure 3.4 shows a plot of the stomatal conductance versus the vapour pressure deficit. At low D_s, g_s is large and it decreases exponentially at higher D_s.
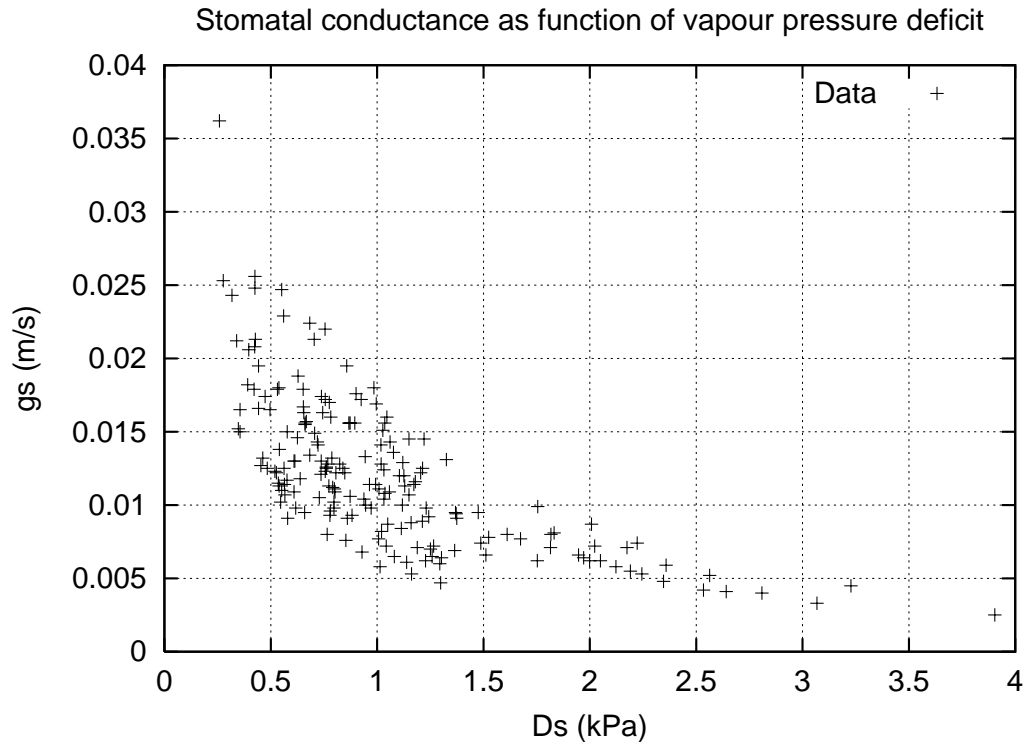
Figure 3.4: Dependence of stomatal conductance on vapour pressure deficit for Loobos

Eventually, this procedure results in a calibration shown in figure 3.5, where the 187 remaining data points are depicted. A non-linear curve fitting procedure by the Marquardt-Levenberg algorithm, minimising the weighted sum of squares of residuals was performed. This resulted in:

$$f = f_0 + a_d.D_s \qquad\qquad (3.2)$$

with $f_0 = 0.903$ (± 0.008) and $a_d = -0.124$ (± 0.007) kPa^{-1}. The given uncertainties are standard errors. Statistical properties of this calibration are $\chi^2 = 0.60$ and root mean square error (RMSE) = 0.057. Appendix D gives a summary of statistical quantities and their properties. Equation (3.1) can be rewritten in the form used by C99:

$$f = F_0(1-D_s/D_c) \qquad\qquad (3.3)$$

leading to $D_c = 7.3$ (± 0.4) kPa. and $F_0 = 0.903$ (± 0.008). The values of C99 used for forest are $F_0 = 0.875$ and $D_c = 14.6$ kPa.
Figure 3.5 also shows the relationships found by Zhang and Nobel (1996) and the one used by C99. See also table 3.2. Zhang and Nobel (1996) performed the same calibration for a wide range of plant species (both C3 and C4), but only for low vegetation, i.e. no forest species. Their work is partly based on laboratory experiments, resulting in more conditioned circumstances. Van de Kassteele (2001) did a calibration for needle leaf forest with BOREAS data, where a much lower f_0 value was obtained ($f_0 = 0.4$) The current found value for $a_d = -0.124$ is quite consistent with what was found by Van de Kassteele (2001) ($a_d = -0.12$).

26

Table 3.2. Overview calibration results for parameters f_0 and a_d.

Study	f_0 (-)	a_d (kPa^{-1})	Vegetation type
Current study	0.903	-0.12	Loobos
Zhang and Nobel (1996)	0.89	-0.07	Low vegetation
C99	0.875	-0.06	Forest
Morison and Gifford (1983)	0.89	-0.18	Rice and phalaris grass
Van de Kassteele (2001)	0.4	-0.12	Boreal forest
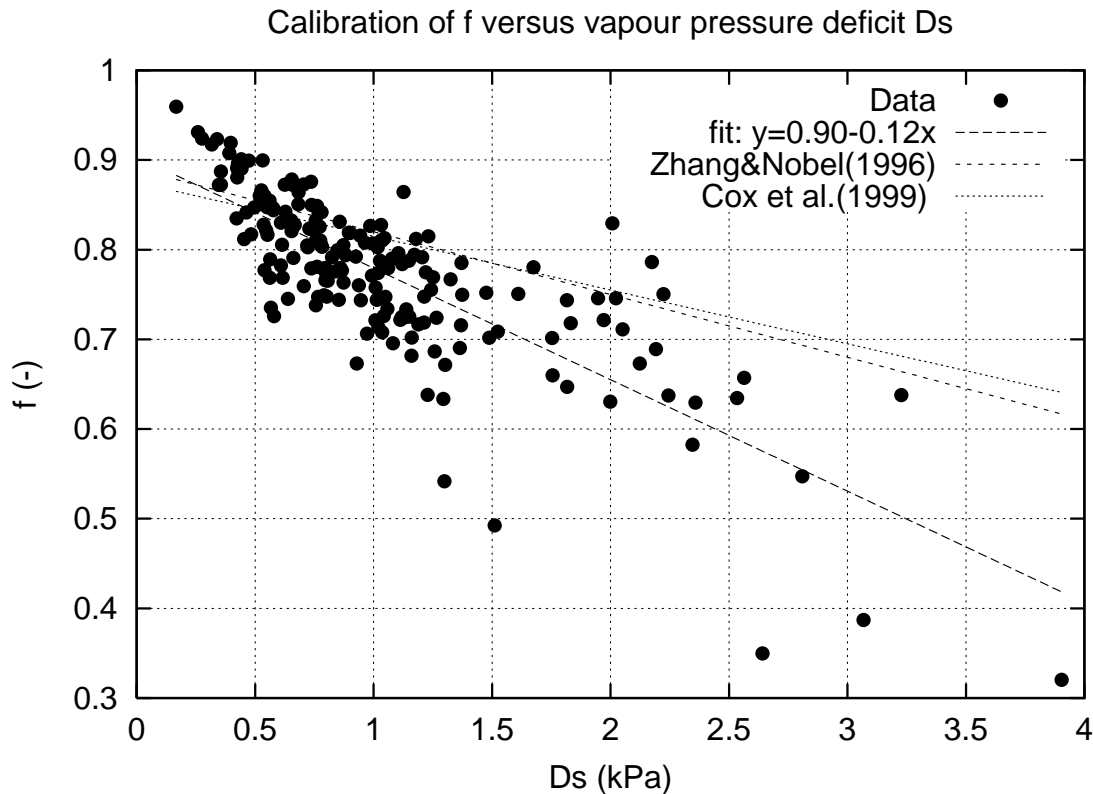
Figure 3.5: Results of the calibration of f versus the vapour pressure deficit. Also shown are functions by Zhang and Nobel (1996) and C99.

3.2.4 Discussion.

Due to the fact this calibration needs a lot of input measurements it is worth to examine the influence of measurement accuracy on the calibration result. Table 3.3 shows the accuracy assumptions that were made including its source. All procentual accuracies are percentages of the measured value. Figure 3.6 shows the data and the fits when these uncertainties are applied in such a direction that extreme values are obtained. Note that nearly all points between 0 and 1.5 kPa. lies between the two fits. This give confidence to the uncertainty estimates in table 3.3. Applying the accuracies in table 3.3 results in the following upper and lower boundary values:

Upper:　　　$f_0 = 0.955 \pm 0.004$
　　　　　　$a_d = -0.125 \pm 0.005$ kPa^{-1}
Lower:　　　$f_0 = 0.821 \pm 0.009$
　　　　　　$a_d = -0.130 \pm 0.016$ kPa^{-1}

It was found that this upper and the lower limits are mainly introduced by uncertainties in the outgoing long wave radiation, thus in the surface temperature.

It seems that f_0 is the parameter that is affected mostly by measurement uncertainties. So f_0 seems not so easy to calibrate, and that agrees with the range of f_0 found in literature. This is important because in the A-g_s scheme $\partial g_s / \partial f_0$ is a quadratic function of f_0 (Appendix E). The scatter shown in the data could give some variation in a_d, which is seen in table 3.2, but the decreasing scatter at low vapour pressure deficits would suggest that f_0 is more easy to find.

Summarizing the results of sections 3.2.2 and 3.2.3 the calibration for f as function of vapour pressure deficit is:

$$f = 0.90 \ (\pm 0.06) - 0.12 \ (\pm 0.01).D_s$$

Table 3.3: Estimated measurement uncertainties for the quantities necessary for the calibration.

Quantity	Accuracy	Source
Latent heat flux	5%	Berger *et al* 2001
Sensible heat flux	5%	Berger *et al* 2001
CO_2 flux	10%	Own assumption
Air Temperature	0.1 K	Jacobs and Heusinkveld (1999)
Relative humidity	5%	Jacobs and Heusinkveld (1999)
Outgoing long wave radiation	5%	Measurement (2001)
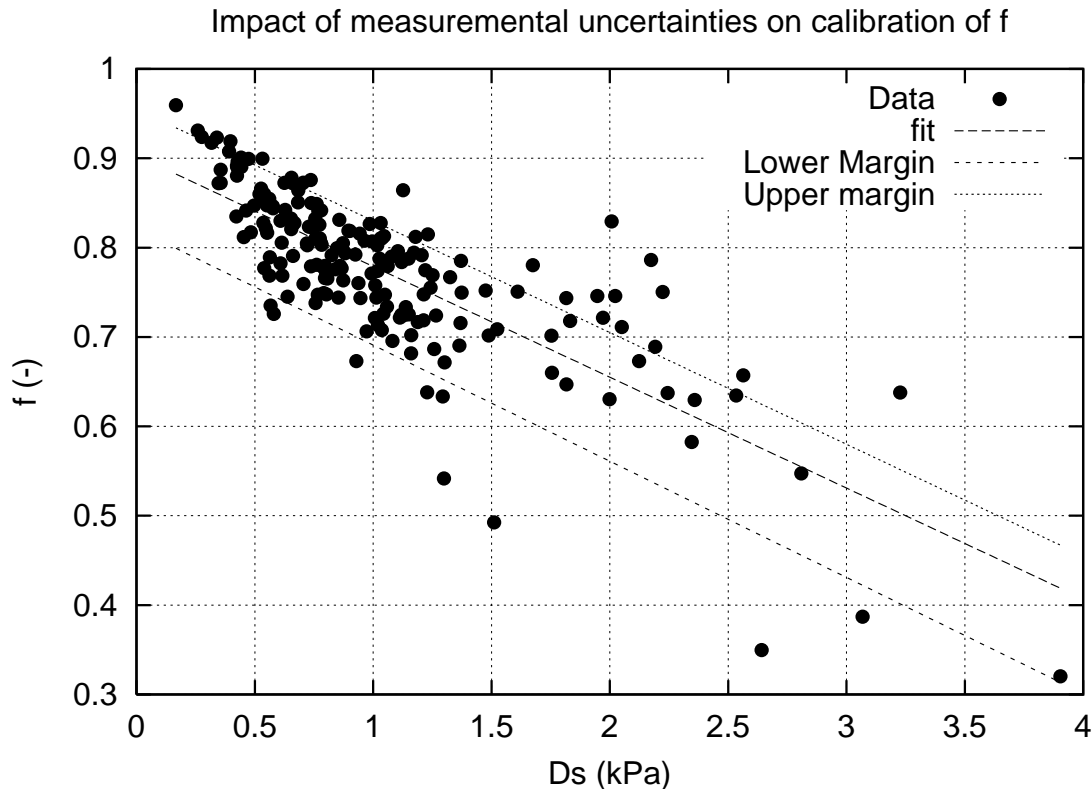
Figure 3.6. Effect of assuming measurement uncertainties on the calibration. Especially the intercept f_0 seems to be affected.

Figure 3.7 shows the value of the atmospheric decoupling coefficient according to Jarvis and McNaughton (1986):

$$\Omega = \left[1 + \frac{\gamma}{s+\gamma} \frac{g_a}{g_s} \right]^{-1}$$ (3.4)

This Ω represents how much the air in the forest is decoupled from the atmosphere. For a proper calibration a low Ω should be found, so the coupling between the atmosphere and the surface is quite well. If not, then processes in the forest have bad correlation with what is measured at atmospheric level, and calibration will be bad. In the present study Ω ranges between 0.1 and 0.6, with most of the points having an Ω of 0.3. This is quite acceptable. Notice that at larger f values the decoupling is stronger, which may affect the determination of f_0.
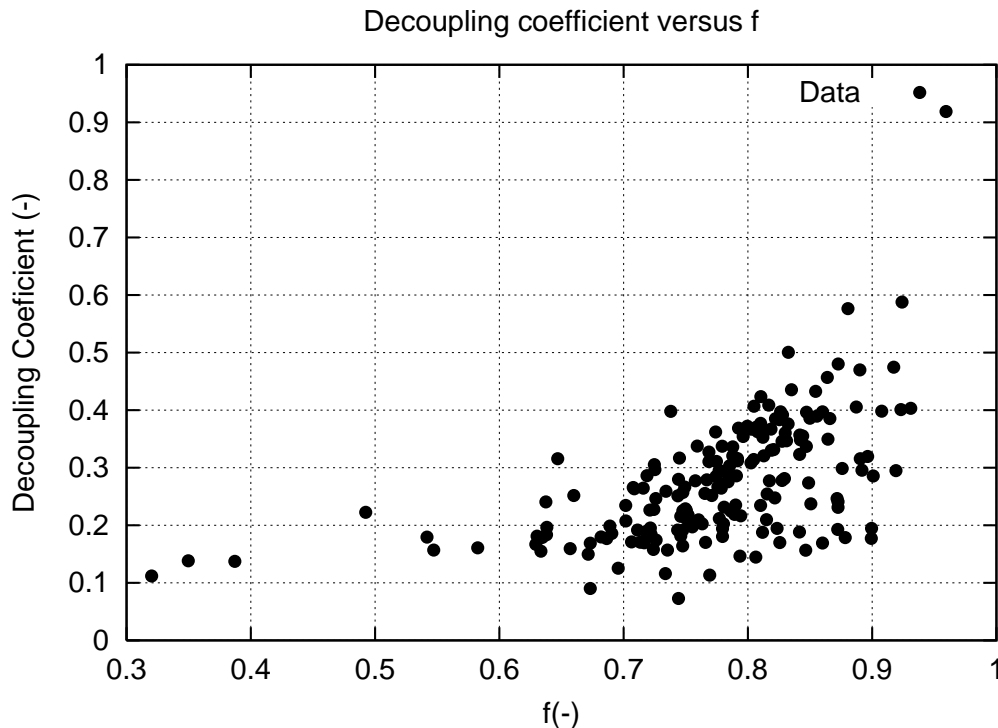
Figure 3.7: Decoupling between the forest and the atmosphere.

Because field data were used to calibrate the found relationship, it is clear that we must be more aware of sensitivities than in laboratory experiments. Not all factors can be controlled in this case. At first note that the range of calibration is quite large. This range occurred due to the strong constraints applied. In the case of large vapour pressure deficits ($D_s > 4$ kPa), the proposed function should not be used. Also Zhang and Nobel (1996) limited their experiment over a range of 4 kPa.

Second, the relationships in the field may be affected by unknown factors like air pollution. For instance, it is known that ozone has a considerable impact on plant behaviour. Although, comparing the obtained fit with the ones from literature, this effect seems of minor importance. On the other hand, Morison and Gifford (1983) concluded that f is independent of irradiance, leaf

age and nutrient status. We must also be aware of the fact that with measuring fluxes above the forest, the internal forest processes are not explicitly accounted for. For instance during day time a stable stratification is often present in a forest. This is because warming of the forest interior air is slow due to low insolent radiation. At night, due to cooling at the top the forest, convection may occur (Bosveld *et al.*, 1999). This may be one of the reasons for the scatter in the diagrams, besides all measurement uncertainties.

Feddes *et al.* (2001) and Reyl *et al.* (2002) suggest that hydraulic lift can influence forest transpiration. Hydraulic lift is a process where plant roots redistributes water from the deeper soil layers towards to upper layers at night. During daytime this redistributed soil water is used for transpiration. For example sugar maple trees can lift 100 litre water each night (Feddes, *et al* 2001). Reyl *et al.* (2002) found this process may increase transpiration with 20% during some days. This redistribution is overseen in the current model. At last we need to be aware of the empirical approach. The obtained results were found for the Loobos site, but need not be valid for other forests. This certainly applies when broad-leaved vegetation is concerned.

Taking into account the limitations mentioned before, including the quality of the data set and strong constraints we applied, it can be concluded that the found relationship is acceptable and valuable.

3.3 Calibration of $A_{m,max}(@25)$ and $g_m(@25)$.

Section 3.2 dealt with the humidity part of the model, which resulted in an acceptable calibration. In this section the photosynthesis part is examined. As mentioned in table 2.3, the maximum rate of carboxylation of rubisco V_{cmax} is not the same under laboratory and field conditions. Approximately a factor 2 difference can be recognised, i.e.: higher estimates in the laboratory. Because of relationship (2.19) the mesophyll conductance is coupled to $A_{m,max}$. There are three ways to find $V_{c,max}$ and g_m. At first V_{cmax} and g_m can be found with the initial slope of an A_n-C_i diagram, taking the denominator of (2.19) as a constant. The main problem with this method is that there are not enough points at low internal CO_2 concentrations to derive a slope. This method appeared to be unuseful. The second way is to do a multi-variable regression procedure, minimising the root mean square error (RMSE), as was done by C99 and Harding *et al.* (2000). This method has the disadvantage that many relative minima in RMSE can be found depending on the domain and the starting points of the regression. Also the number of parameters to be fit can result in large variability. For example Harding *et al.* (2000) found a difference of a factor 5 in V_{cmax} when V_{cmax} was optimised alone or together with F_0 and D_c. Because of these disadvantages we did not use this method. The third method is to run a 1D surface model (see Van de Kassteele, 2001) with varying parameters both $V_{c,max}(@25)$ and $g_m(@25)$ with the same ratio and then compare model results with measurements. To ensure that the soil moisture and soil temperature is in equilibrium with the fluxes of latent and sensible heat, the model has been run several times for the same period. At the end of this period the soil moisture content and soil temperature were used as initial conditions in the next run. After five iterations the soil variables converged. With the Loobos data we determined both $V_{c,max}(@25)$ and $g_m(@25)$, minimizing the bias in the latent heat flux. This has been done for the same data points and with the calibration of f in paragraph 3.2.3.

This approach resulted in $A_{m,max}(@25) = 1.0$ mg CO_2 m^{-2} s^{-1} and $g_m(@25)= 3.2$ mm s^{-1}. Figure 3.8 shows the results, comparison of model output with data for these calibration points for the latent- and sensible heat flux and the CO_2 flux at leaf level.

Half hourly values of latent heatflux

y = 1.01x
R^2 = 0.65

Half hourly values of sensible heatflux

y = 0.73x
R^2 = 0.56

Half hourly values of CO2 flux

y = 0.82x
R^2 = -0.27
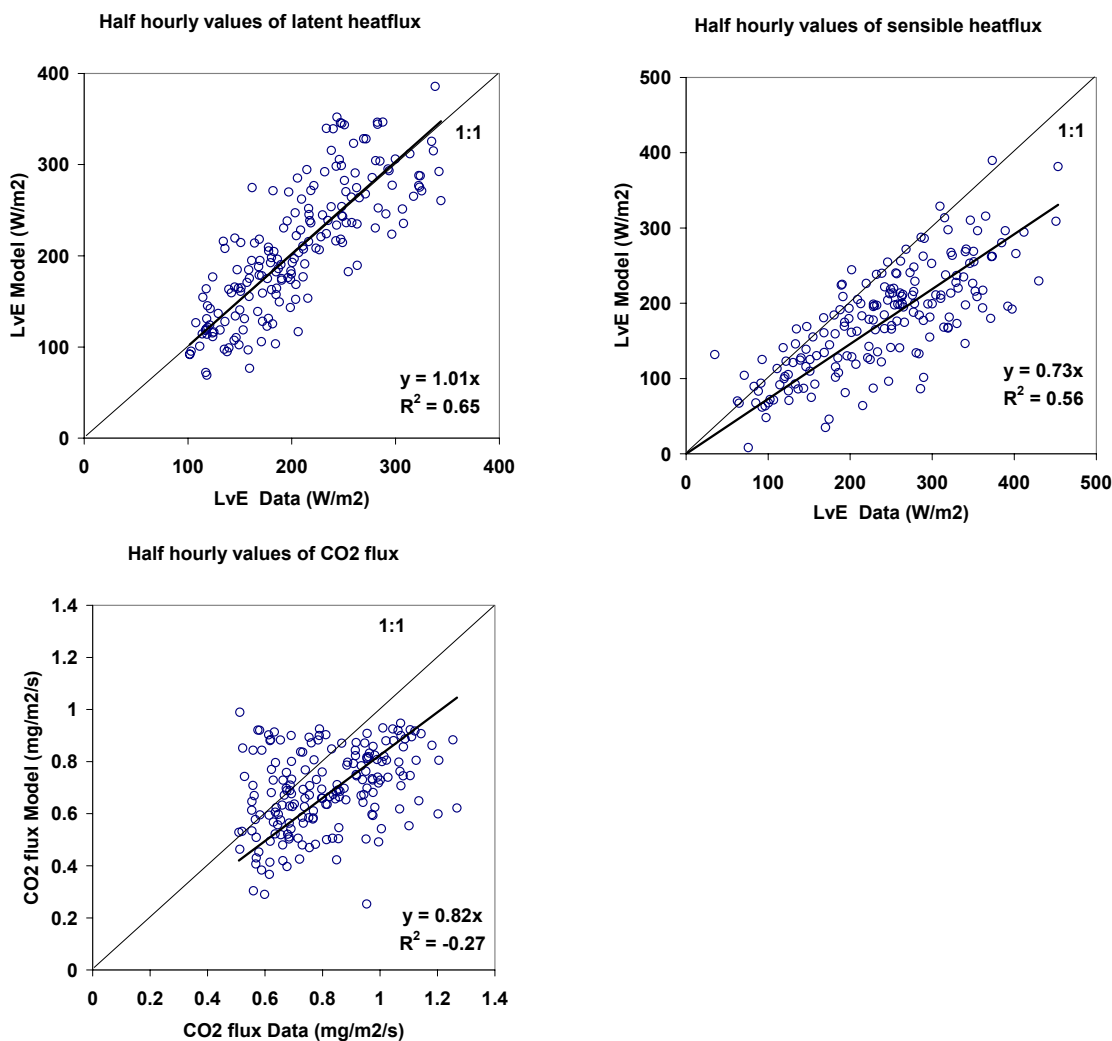
Figure 3.8: Scatter plots of latent- and sensible heat flux and CO_2 flux at leaf level for calibration points for the calibration of $A_{m,max}$ and g_m.

With these values the latent heat flux is predicted quite correctly. On the other hand the sensible heat flux is underestimated. This may be due to too large model values for soil heat stream, and a soil temperature profile that is not in equilibrium with air temperature. The model also underestimates the CO_2 flux density.

3.4 Validation.

After calibration the model must be validated. This is also done with the Loobos data, but now for two whole years round. So calibration and validation with the same dataset seems not to be a problem since only 187 points has been used for the calibration. Validation will be done on the hand of the decadal averaged fluxes and the diurnal cycles of latent and sensible heat. The left panels of figure 3.9 show for 1997 and 1998 the decadal averaged latent heat flux (L_vE) and sensible heat flux (*H*) and CO_2 flux. The averaging (over model and data) took place over the time slots where data were available. This means that model values were ignored when no data

were available. The decades where no data were available are indicated by the dotted line. It appears that the latent heat flux is estimated properly in the summer season. In the non-summer seasons the simulation is worse than in summer. The sensible heat flux is simulated well, except in the winter season. Figure 3.10 depicts scatter plots of both quantities versus data. It appears that there is a good agreement in the latent heat flux and the CO_2 flux and an underestimate (35%) in sensible heat. When negative sensible heat fluxes are ignored this underestimation reduces to 10%.
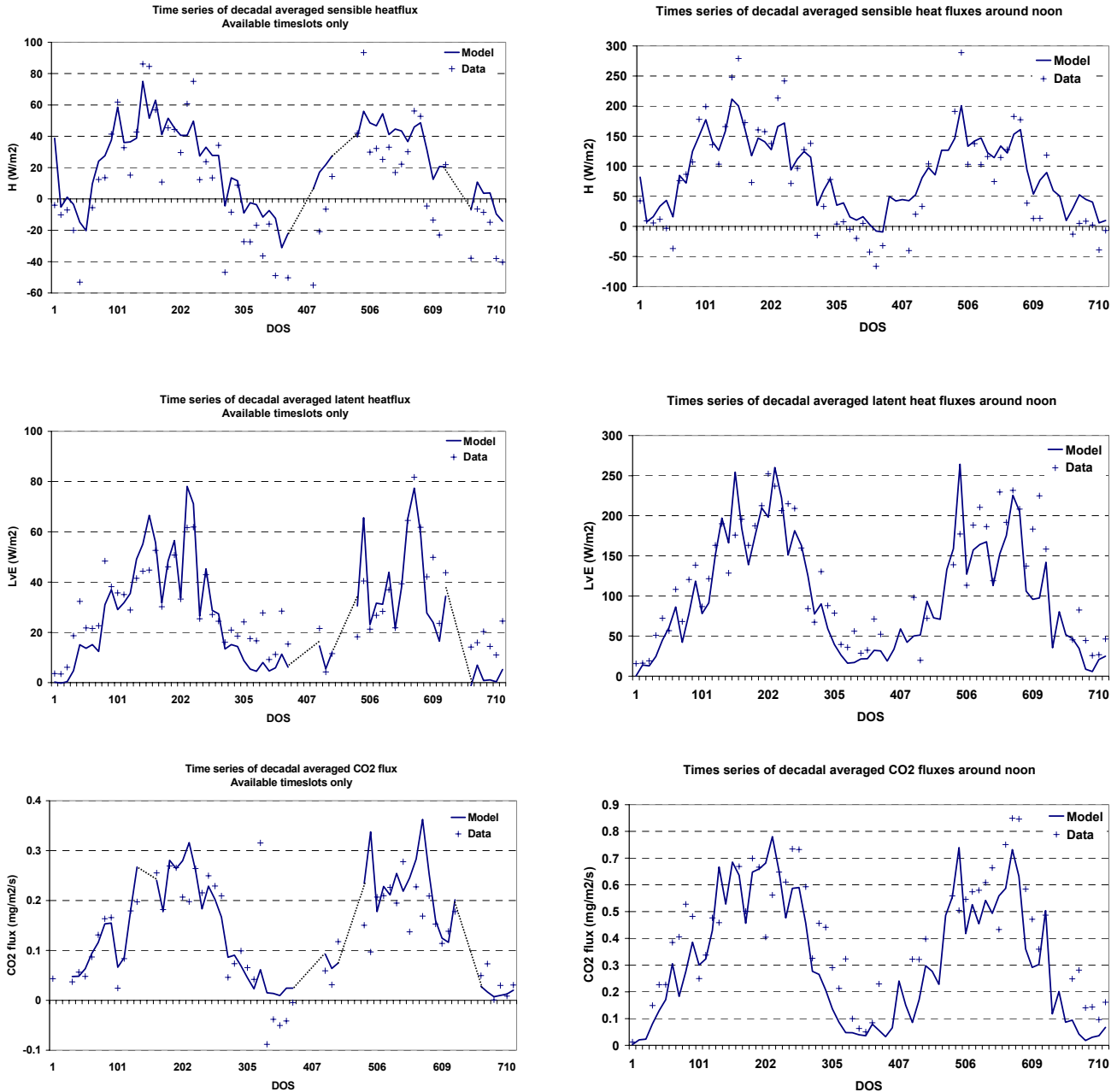
Figure 3.9: Time series of decadal averaged latent and sensible heat flux and CO_2 flux in 1997 and 1998. Left panels: averaged over whole day, right panels: averaged around noon: 10-14 local time.

The right panels in figure 3.9 show decadal averages around noon. Comparing these data it appears that the simulations are quite good. Instead of plotting fluxes in a scatter plot, more information can be obtained from plotting the diurnal cycles of sensible and latent heat flux. This prevents that nighttime errors are included in the comparison. For 1997 and 1998 this is shown in Appendix F. It is seen that especially for the moments where a physiological model is expected to perform well it does so. This is in the growing season and around noon. Figure 3.10 shows scatter plots of decadal averages of the turbulent fluxes for available time slots only, while 3.11 shows these around noon.
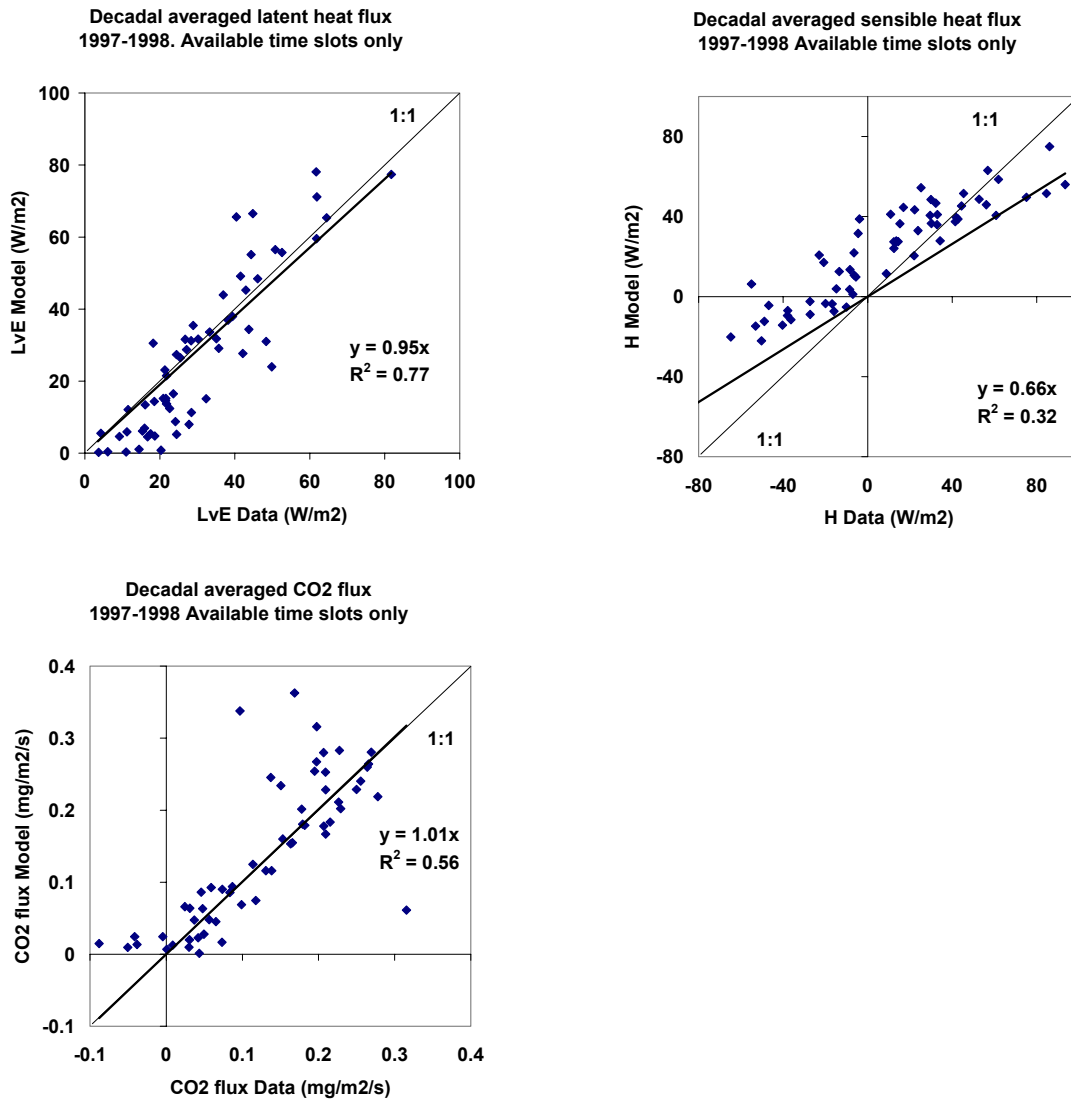
Figure 3.10: Scatter plots comparing model output with measurements for Loobos with $A_{m,max}(@25)=1.0$ mg/m^2/s, $g_m(@25)=3.2$ mm/s, $f_0=0.90$ and $a_d=-0.12$ kPa^{-1}.

Decadal averaged latent heat fluxes around noon (10-14 LT)

Decadal averaged sensible heat fluxes around noon (10-14 LT)

Decadal averaged CO2 flux around noon (10-14 LT)
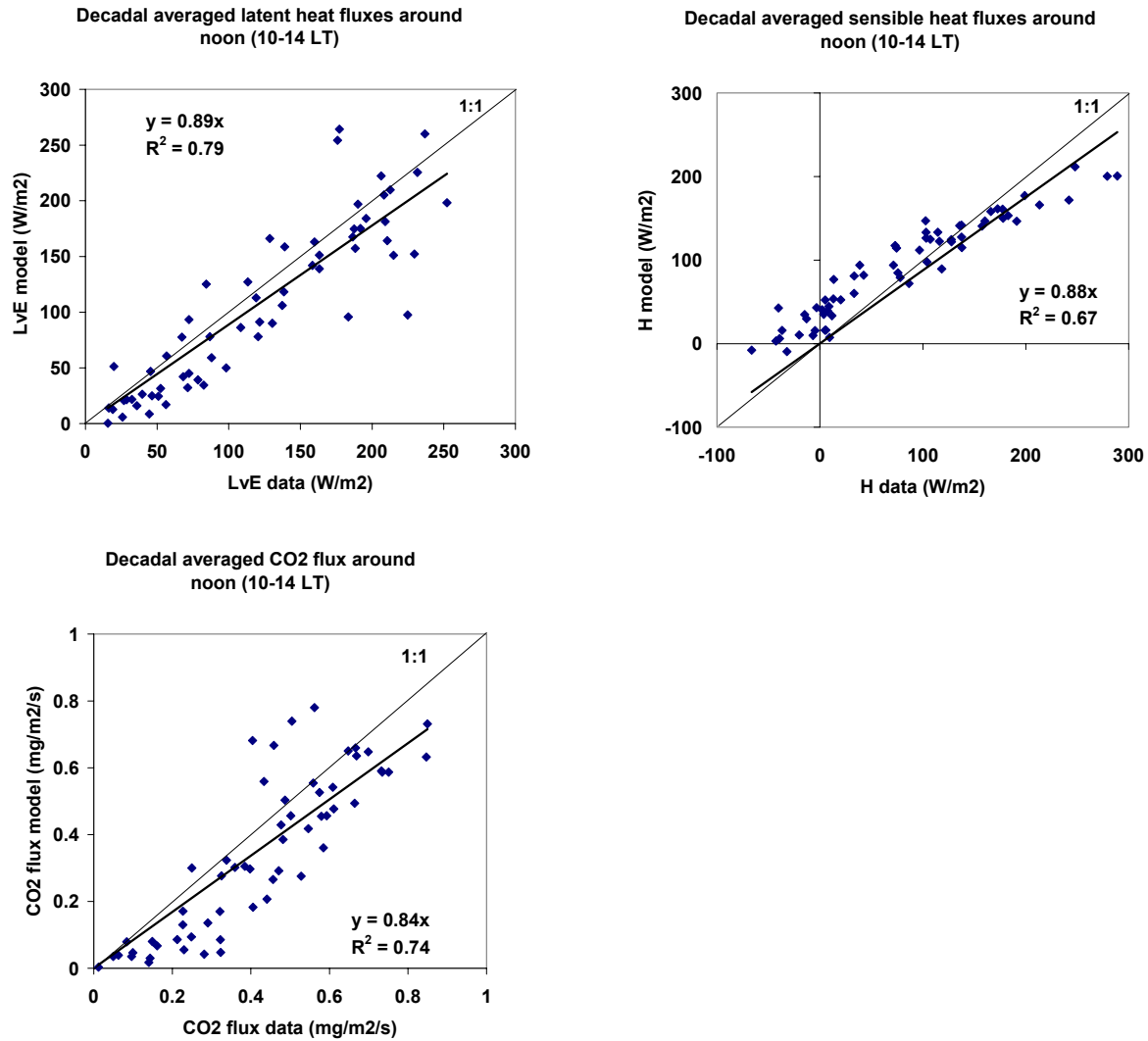
Figure 3.11: Idem as 3.10 but averaging took place only with data around noon (10-14 local time).

Figure 3.12 shows for 199706-199708 the diurnal cycles, including the 'old' A-g_s-scheme, i.e. with photosynthetic parameters like Van de Kassteele (2001). It becomes clear that the new parameters values results in a better performance of the diurnal cycle, especially in simulation of midday peak values. This is confirmed by table 3.4, which summarizes the RMSE of both model runs. For both fluxes in winter the new run shows a slight increase in RMSE, but in the growing season there is a large decrease in RMSE. On the other hand the goal of this study was to find out why the old scheme realised a too large evapotranspiration. In this forest the parameters proposed by Van de Kassteele (2001) *under*estimates this quantity. This can be explained by the low value of f_0 found by Van de Kassteele (2001), calibrated for a boreal forest.
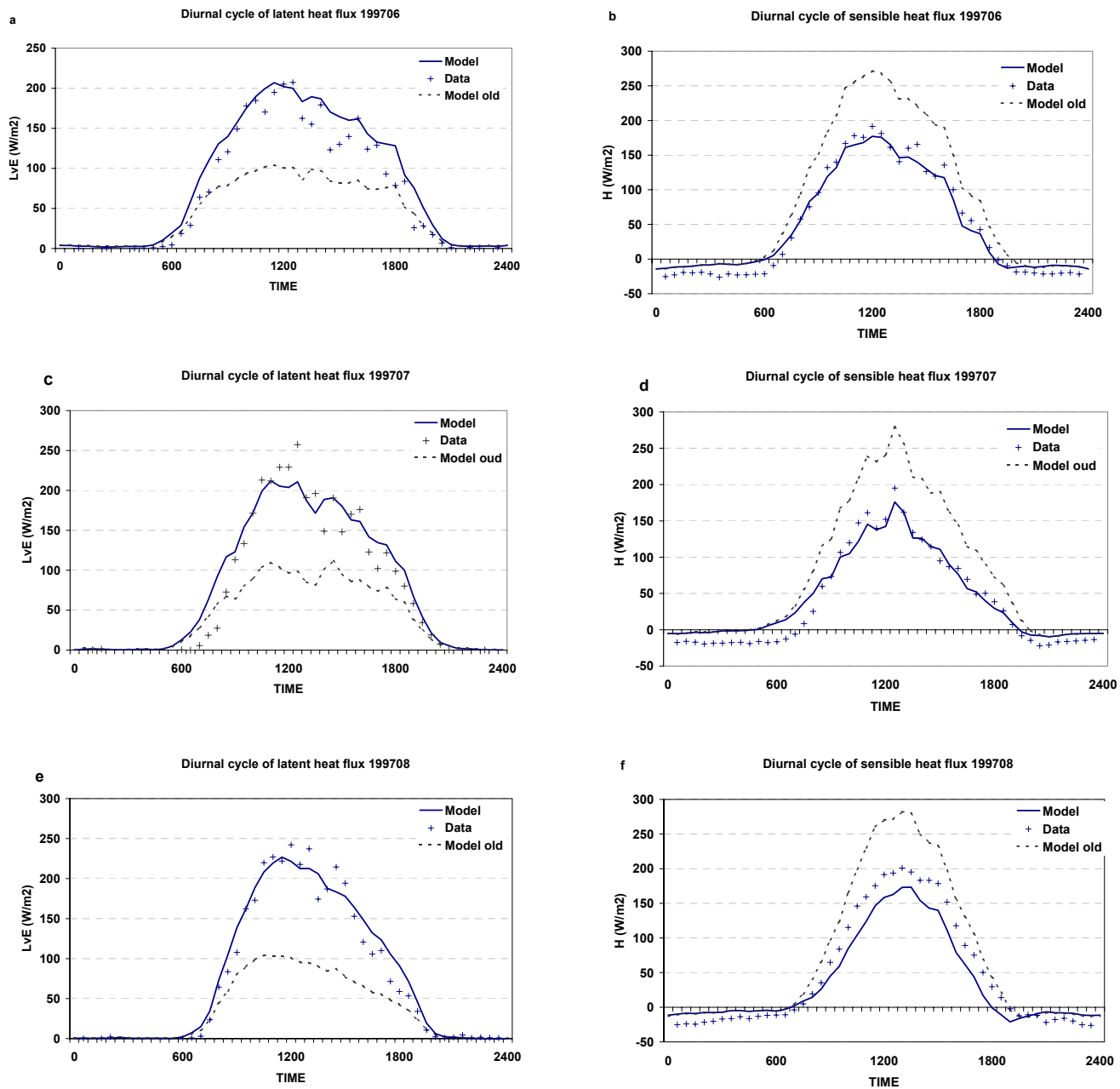
Figure 3.12: Comparison of diurnal cycle of latent and sensible heat flux with observations and the old A-g$_s$ scheme for June 1997 (a & b), July 1997 (c & d) and August 1997(e & f).

Table 3.4: Comparison of RMSE (W/m^2) in the old and new A-gs scheme for the Loobos forest in the growing season.

	A-gs current study		A-gs Van de Kassteele	
	L_vE	H	L_vE	H
199705	18.0	19.7	38.9	41.2
199706	11.6	19.4	46.1	43.6
199707	14.3	20.0	48.5	55.8
199708	22.0	14.4	20.7	20.5
199709	14.0	14.7	34.8	37.4
199805	22.3	34.1	32.7	34.5
199806	18.4	33.9	54.6	54.6
199807	18.6	25.1	53.8	60.9
199808	10.2	12.1	49.1	58.7
199809	22.7	35.7	40.6	60.4

Figure 3.13 shows the performance of the model's three most upper soil layers and the data for soil temperature and soil moisture. For soil moisture deviations from the 2 yr. mean are shown. Data has been interpolated linearly to produce representative values for the model layers. The figure shows that the model makes extremes too extreme for soil temperature. The observations show a smaller annual cycle. Especially in the summer season of 1998 the model performance is quite correct for both soil moisture and soil temperature. Overall this is a proper soil simulation.
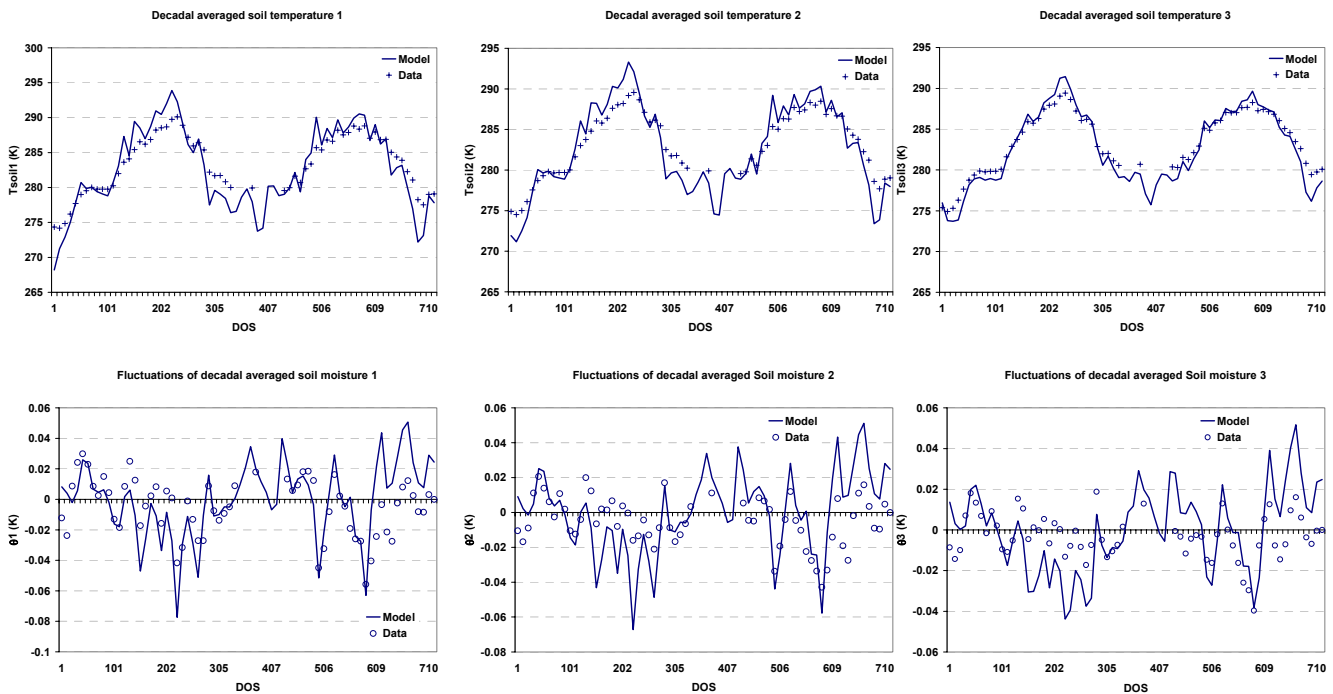
Figure 3.13: Time series for 1997 and 1998 of model results and data for soil variables in three layers: temperature and soil moisture (deviations from the mean value).

For the summer months of 1997 the averaged diurnal cycle of the CO_2 flux into the leaves has been plotted in figure 3.14. In all figures the maximum value of the flux is correct, but the model cycle seems to be shifted to the right compared with the data. This may be due to an error in the calibration of f. In the morning when vapour pressure deficit is small (see picture right below) the modelled flux is too small which means that f is too small. In the afternoon, a too large CO_2 flux is modelled, so f is too large. This means that the dependence of f on vapour pressure deficit must be less steep than determined above. A new model run ($a_d = -0.85$ kPa^{-1}) has been done but this seemed to have no big influence. Another explanation is the time lag has been introduced by the measurement of the CO_2 storage term. When this term was reduced by 50% the time lag disappeared.
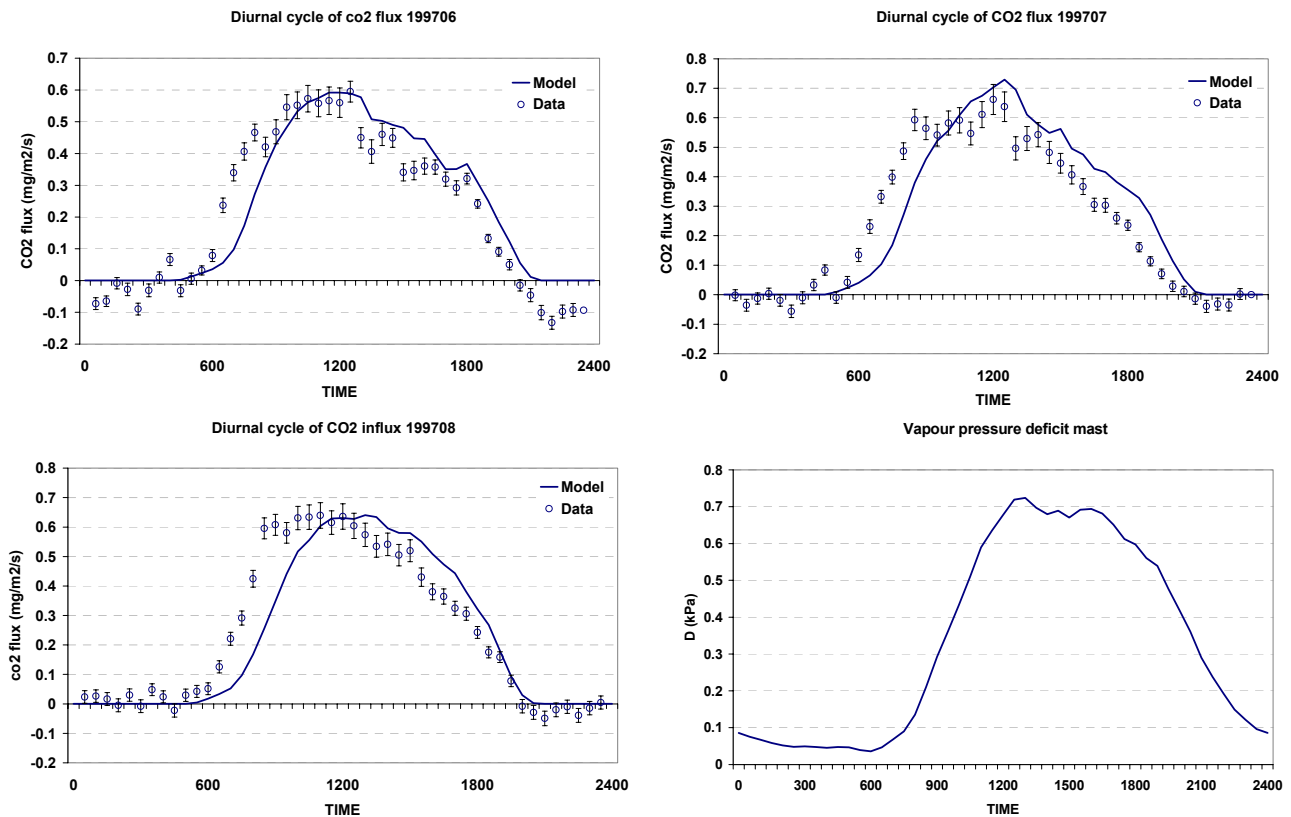
Figure 3.14: Diurnal cycles of modelled and measured CO_2 flux into the big-leaf during three summer months in 1997. The picture right below shows the diurnal cycle of measured vapour pressure deficit during July 1997.

3.5 Conclusions

To use the A-gs model a set of parameters is necessary. We propose the following for the parameters in the A-gs surface scheme. The vegetation can be divided in high and low vegetation and C3 and C4 plants. The high vegetation can be split in deciduous forest and needle leaf forest. It appeared from literature that at least for high vegetation the photosynthesis parameters must be changed compared to Van de Kassteele (2001). This has been confirmed in this study for the Scots pine Loobos data set. The valid set of parameters is summarized in table 3.5. Since there are no indications that deciduous forest behaves different, they can also be applied for this forest

37

type. The new information about C4 forests is that comparison of the A-gs scheme with C99 indicates that $A_{m,max}$(@25) and g_m(@25) must be reduced in the A-gs scheme. The magnitude of decrease is around a factor 2. The result is a set of parameter values that are in line with Calvet (2000) and Carswell *et al.* (2000). See section 2.3.7.

On the other hand this parameter set was found only based on one forest site. We are interested in the performance of this set for BOREAS for which Van de Kassteele (2001) did a calibration. May be the C3 forest should be divided into temperate and boreal forests. In the next section we will examine how robust this parameter set is when it is used in other forests.

Table 3.5: Proposed parameter values in the A-gs scheme.

Parameter	X(@ 298 K) low vegetation	X(@ 298 K) high vegetation	Q_{10}	T1 (K)	T2 (K)
C3					
F_0 (-)	0.89	0.90			
a_d (kPa^{-1})	0.07	0.12			
α_0 (mg J^{-1})	0.017	0.017			
Γ (mg m^{-3})	68.5ρ_a	68.5ρ_a	1.5		
g_m (mm s^{-1})	7.0	3.5	2.0	278	301
$A_{m,max}$ (mg m^{-2} s^{-1})	2.2	1.1	2.0	281	311
$g_{min,c}$	0.25	0.25			
C4					
F_0 (-)	0.85	0.85			
a_d (kPa^{-1})	0.15	0.15			
α_0 (mg J^{-1})	0.015	0.015			
Γ (mg m^{-3})	4.3ρ_a	4.3ρ_a	1.5		
g_m (mm s^{-1})	17.5	8.8	2.0	286	309
$A_{m,max}$ (mg m^{-2} s^{-1})	1.7	0.85	2.0	286	311
$g_{min,c}$	0.25	0.25			

4. A statistical approach to test the robustness of the parameters in the photosynthesis model.

4.1 Introduction

In chapter 3 we presented a new parameter set for the high vegetation type in the A-g_s surface scheme. This resulted in a proper simulation of the turbulent energy fluxes and the CO_2 flux in the Loobos site. On the other hand Van de Kassteele (2001) did a proper simulation with an alternative parameter set on two other data sets (BOREAS and Speuld forest), shown in figure 4.1. So it seems that there is not one unique parameter set that can simulate the turbulent fluxes properly. This has been suggested by Franks *et al.* (1997). They state that most SVAT models are overparameterisized, which means that the data to calibrate these models do not contain enough information to find a unique set of values for all required parameters. Therefore it is hard to find a robust calibration.
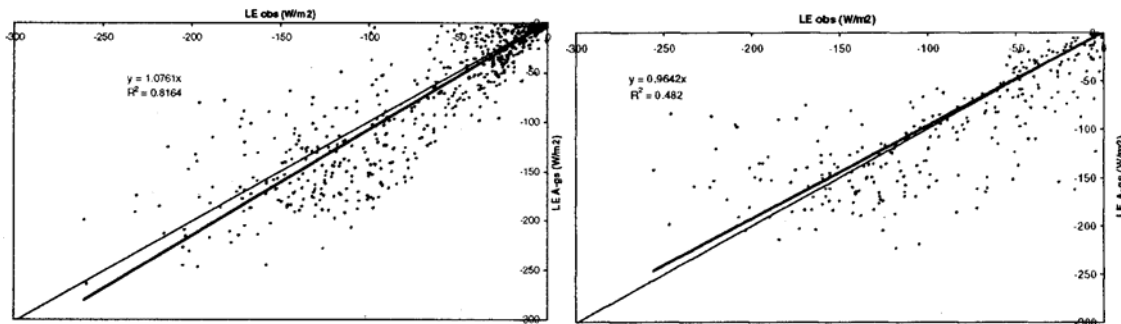
Figure 4.1: Daily averaged simulation of forest evapotranspiration. Left panel: BOREAS, right panel Speuld forest. Taken from Van de Kassteele (2001).

To investigate the uniqueness of the parameter sets we will set up a Monte Carlo approach for four forests. This means that the model is run for the Loobos, BOREAS and the Speuld forest data sets, for several parameter combinations of set $(A_{m,max}(@25), f_0, a_d)$. The purpose is to find whether these forests behave the same for certain parameter combinations.

Four different forest sites of different signature were used for the Monte Carlo approach. The first site used was the Loobos site that was already described in chapter 3. Secondly, BOREAS is a set extracted from a boreal forest from 1994-1996. The dominant vegetation is old black spruce with a LAI around 5. The forest has low assimilation rates and problematic nutrient status. More information can be found in Van den Hurk *et al.* (2000). The Speuld forest (The Netherlands) data set was measured in 1995 and 1996. The forest consists of Douglas fir with a very high leaf area index (LAI=8-10 in 1995) and is situated on a sandy-loam soil. Due to thinning of the forest (cutting of branches) in the winter between these two years, the leaf area index and the albedo show a significant discontinuity. Therefore these two years will be examined separately. In the simulations we used LAI=10 for 1995 and LAI =6.5 in 1996 (pers. com. Bosveld, 2002). A brief description of this forest can be found in Dekker (2000) and Van Wijk (2001). Note that the current Speuld data set is not the same as the one from 1989, used by Van de Kassteele (2001). These data sets contain sufficient information to examine the robustness of the model parameters across a range of forest sites.

4.2 Method

Monte Carlo simulation is a powerful technique to find out the model behaviour for different parameter sets. In the Monte Carlo technique the model is run for several parameter combinations. In this study $A_{m,max}(@25)$ ranges from 0.5-2.4 mg/m^2/s, f_0 from 0.5 - 0.975 and a_d from -0.15- -0.06 kPa^{-1}. The ranges are divided in steps, but these are not always evenly distributed over the range because more resolution was used when a larger sensitivity was expected (e.g. for high f_0 values). Due to indications that at the BOREAS site $A_{m,max}(@25)$ was lower than the mentioned range (Dang *et al.*, 1998), 0.2 mg/m^2/s was taken as lower boundary for that particular site. In addition $g_m(@25)$ has been adjusted relative to $A_{m,max}(@25)$ according to equation (2.19). Note that we assume here that the LAI and the initial light use efficiency are known without uncertainty. For each model run the model sensible (H) and latent heat (L_vE) fluxes have been compared with validation data, i.e. measured turbulent fluxes (eddy correlation) on half hourly basis. Data selection was subject to constraints as in section 3.2.3. These are summarised in table 4.1. In addition all days with precipitation were not used. The RMSE was calculated from these data and the model output. After each run the RMSE for the latent heat flux was kept. Table 4.2 shows the number of runs per forest and the number of data points used in each run to compare model output with measurements. The whole process is illustrated in figure 4.2. In this manner we produced a proper way to verify the sensitivity of the model for its parameters.
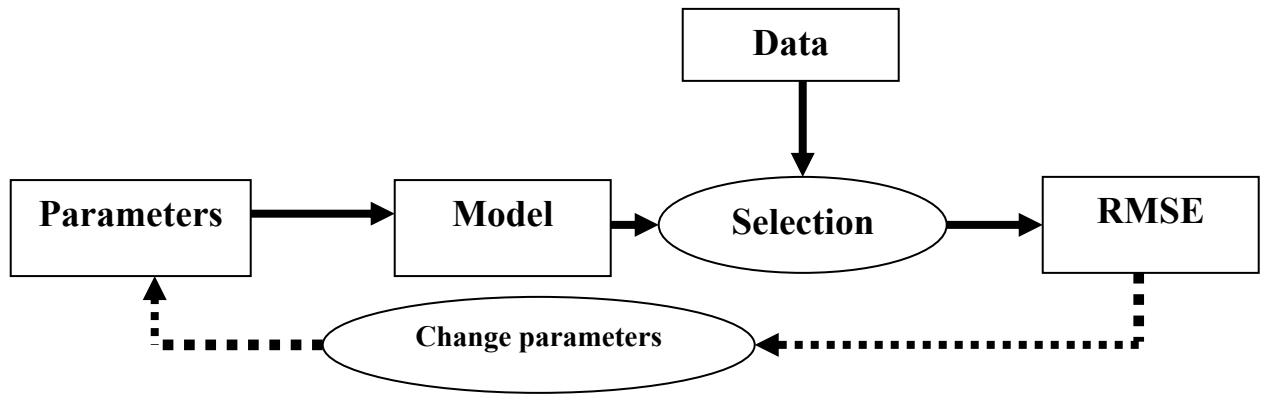
Figure 4.2. Flowchart illustrating the Monte Carlo approach.

To summarize the RMSE results produced in the Monte Carlo simulations a general sensitivity analysis (GSA) was performed. This technique groups the results of all runs in one figure. This works as follows: the Monte Carlo simulations are sorted from low to high values according to the RMSE[1]. The RMSE data are divided in 10 classes from high to low RMSE, and a (relative) cumulative frequency (RCF) distribution is made for each parameter within each class. These are plotted in one figure with the parameter value at the *x*-axis and the RCF at the *y*-axis. When these ten curves are straight lines that are close together, the model output is insensitive to that particular parameter. When the curves of the lowest classes and upper classes are shifted to lower and higher parameter values, the model is sensitive to the parameter (Franks *et al.*, 1997). Thus the GSA technique gives information whether and where the model is sensitive to the parameters. Eventually the parameter sets for all forests are confronted with each other. We made classes of parameters sets: if the RMSE for a certain combination was lower then 1, 2 and 3 times the

---

[1] The technique can also be applied to the turbulent fluxes itself instead of the quality criterion.

standard deviation of the latent heat flux data respectively, the parameter was 'accepted' with that amount of significance. The accepted parameter combinations in each forest are combined: an overlay of accepted parameter combinations was performed for a certain significance level. When all forests have certain parameter sets in common this should be seen in such an overlay.
For some parameter sets the time series of the model simulations will be shown. The constraints applied to determine the RMSE between model and data will be discussed at the end of this chapter.

Table 4.1: Table of constraints applied in each forest for the Monte Carlo simulation runs

Site	Season	Time (LT)	Wind (m/s)	LvE (W/m^2)	F_CO$_2$ (mg/m^2/s)
Loobos	$121 \leq DOY \leq 249$	10.00-14.00	$U > 2$	> 100	< -0.044
Speuld95	$5 \leq month \leq 8$	08.00-14.00	$U > 2$	> 50	Unlimited
Speuld96	$5 \leq month \leq 8$	08.00-14.00	$U > 2$	> 50	Unlimited
BOREAS	$5 \leq month \leq 8$	10.00-14.00	$U > 0.5^*$	> 50	Unlimited

* For BOREAS this lower wind speed was taken to keep enough data points.

Table 4.2: Number of points in the RMSE approach

Forest	Number of selected data points	Number of parameter combinations
Loobos	251	793
Speuld95	879	1620
Speuld96	601	1620
BOREAS	705	1287

4.3 Results.

In this a section a summary of the results of the model simulations for the four forests will be presented.

4.3.1 Loobos.

Figure 4.3 shows a contour plot of the root mean square error (RMSE) for different parameter ranges for the Loobos site. When we start with parameter a_d as a constant and we vary $A_{m,max}$(@25) and f_0 (Fig 4.3a), we can try to find the best set of parameters by requiring a minimum RMSE. But we see a saddle shaped structure that is quite consistent in its form and position when a_d is changed (not shown). So the model is quite insensitive to parameter a_d. Taking $A_{m,max}$(@25) constant at 1.0 mg/m^2/s (Fig. 4.3b), we see a well-defined minimum *range*. This minimum area moves to the left when $A_{m,max}$(@25) is increased (not shown). So more than one parameter set can simulate the same quality value of the criterion. In chapter 3 we determined $a_d = -0.12$ kPa^{-1} and $f_0 = 0.90$ directly from the Loobos and this is consistent with the current result. It is seen that a_d is anticorrelated with f_0. Especially at higher values of f_0 the RMSE increases strongly, which agrees with the large sensitivity of g_c to f_0 shown in Appendix E.

a)

b)

c)
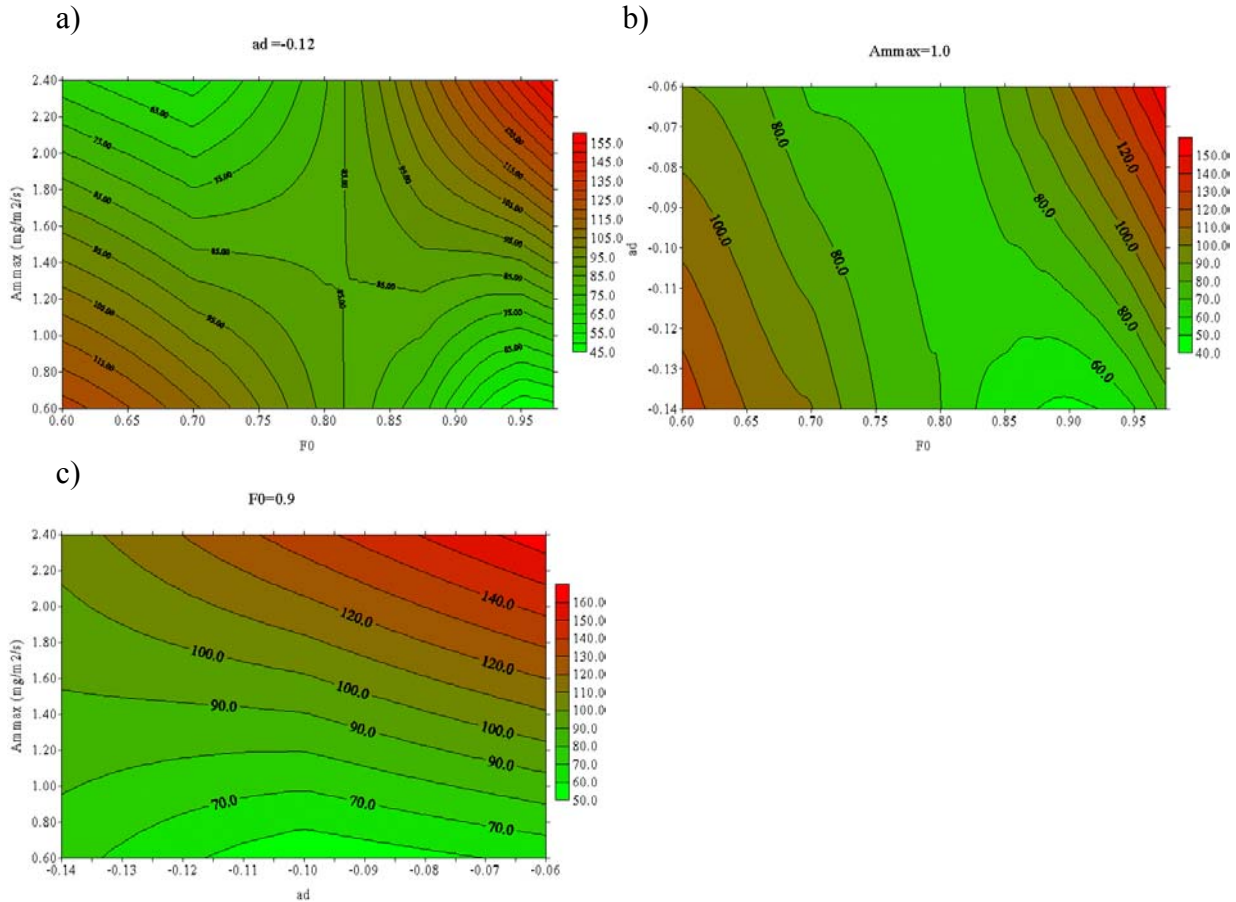
Figure 4.3: Contour plots of root mean square error (RMSE) for latent heat flux (W/m²) for Loobos. a) $A_{m,max}$(@25) vs. f_0 with a_d=-0.12 kPa⁻¹, b) a_d vs. f_0 with $A_{m,max}$(@25)= 1.0 mg/m²/s, c) $A_{m,max}$(@25) vs. a_d with f_0=0.90. These plots were made with the software package Surfer6.

When f_0 is held constant (Fig 4.3.c) we see that the RMSE is not sensitive to parameter a_d in the lower range. The green band of low RMSE is situated quite horizontally.

The whole exercise is also shown for all parameter combinations as a GSA in figure 4.4. In these figures the relative cumulative frequency distribution is shown per class. Class 1 contains the model realisations with the lowest RMSE and class 10 contains the worst performances. The picture is confirmed here: significant sensitivity of RMSE to f_0 and $A_{m,max}$(@25), while the model is insensitive to a_d. Note that the first f_0 class behaves quite different than the other classes; an S-shaped curve is seen while the other classes show convex or concave shapes. The largest sensitivity in class 1 is found at f_0=0.90 and relative cumulative frequency (RCF) =0.5. In general we conclude that no clear minimum in RMSE can be found, and thus no single parameter set. The model is sensitive to $A_{m,max}$(@25) and f_0 and less to a_d.
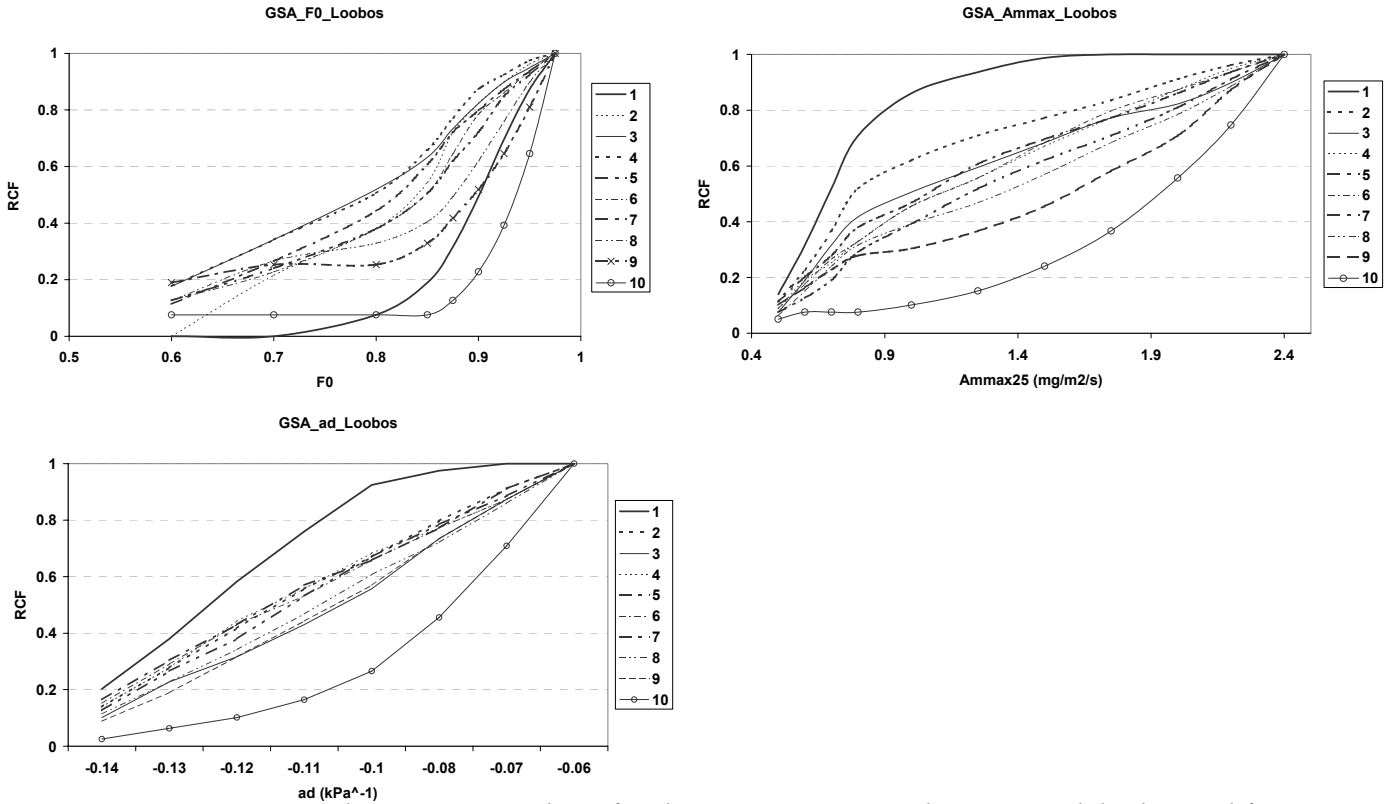
Figure 4.4: General sensitivity analysis for three parameters in the A-gs model, obtained from Loobos. The parameter is on the horizontal axis, the RCF on the vertical axis. Classes are shown with line appearances as indicated in the legend. Class 1 has the lowest RMSE and class 10 the largest RMSE

4.3.2 BOREAS

For BOREAS the parameter set a_d =-0.15 kPa^{-1}, f_0 =0.8 and $A_{m,max}$(@25) =0.3 mg/m^2/s resulted in the lowest RMSE (and bias). Note that this $A_{m,max}$(@25) value is nearly 10 times lower than the standard value for C3 ($A_{m,max}$(@25) =2.2 mg/m^2/s) proposed by Jacobs (1994) and Ronda (2001)! Results of Dang *et al.* (1998) confirm the low photosynthetic capacity. For old black spruce they found $A_{m,max}$(@25) = 0.2 mg/m^2/s in the field, although the less representative laboratory tests indicate $A_{m,max}$(@25) = 0.3 mg/m^2/s. Low available nutrient status may explain these low parameter values, which indicates again that nutrient status must be included in the model.
The BOREAS surface plots also show a saddle area, although it is less pronounced and present at lower values of $A_{m,max}$(@25) than in Loobos (Fig. 4.5a). When a_d is varied we see the same pictures each time: the result is not sensitive to a_d. From these plots the optimal combination of the other two parameters can be found. For a_d = -0.15 kPa^{-1} two areas of optimal values are seen. The above-mentioned set (f_0=0.8; $A_{m,max}$(@25)=0.2 mg/m^2/s) is in one of these areas, but combinations of lower f_0 and higher $A_{m,max}$(@25) also seem also to be valid, although f_0 =0.4 is physiologically not a likely value.
When $A_{m,max}$(@25) is taken constant (Fig 4.5b) it is found that a wide band of parameter values has a low RMSE. Increasing f_0 increases the RMSE. Note that the depicted minimum in the

figure for $A_{m,max}$(@25) = 0.3 mg/m^2/s is a plot artefact because no values lower than RMSE = 65 W/m^2 were in the model data set.

a)

b)

c)
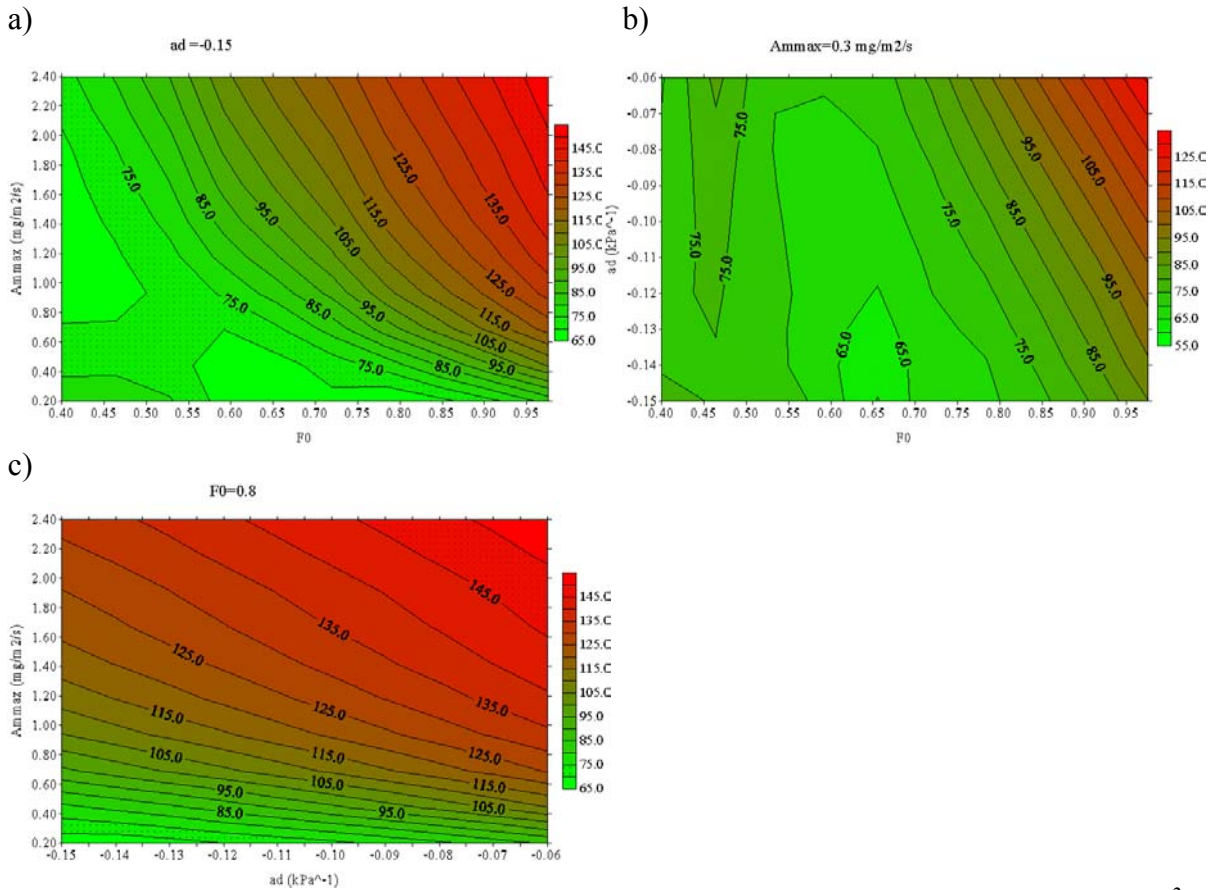
Figure 4.5: Contour plots of root mean square error (RMSE) for latent heat flux (W/m^2) for BOREAS. a) $A_{m,max}$(@25) vs. f_0 with a_d=-0.15 kPa^{-1}, b) a_d vs. f_0 with $A_{m,max}$(@25)= 0.3 mg/m^2/s, c) $A_{m,max}$(@25) vs. a_d with f_0=0.80.

With f_0 as a constant parameter (Fig. 4.5c) the sharp dependence on $A_{m,max}$(@25) is seen; a steep gradient between $A_{m,max}$(@25) = 0.2 and 0.6 mg/m^2/s is recognised.

The GSA for BOREAS is depicted in figure 4.6. In the best performing class (1) f_0 and $A_{m,max}$(@25) have preference to take lower values. The model's low sensitivity to a_d is confirmed here.

In summary: BOREAS has a significantly lower $A_{m,max}$(@25) than Loobos, but sensitivities are in agreement with Loobos.

GSA_F0_BOREAS

GSA_Ammax_BOREAS

GSA_ad_BOREAS
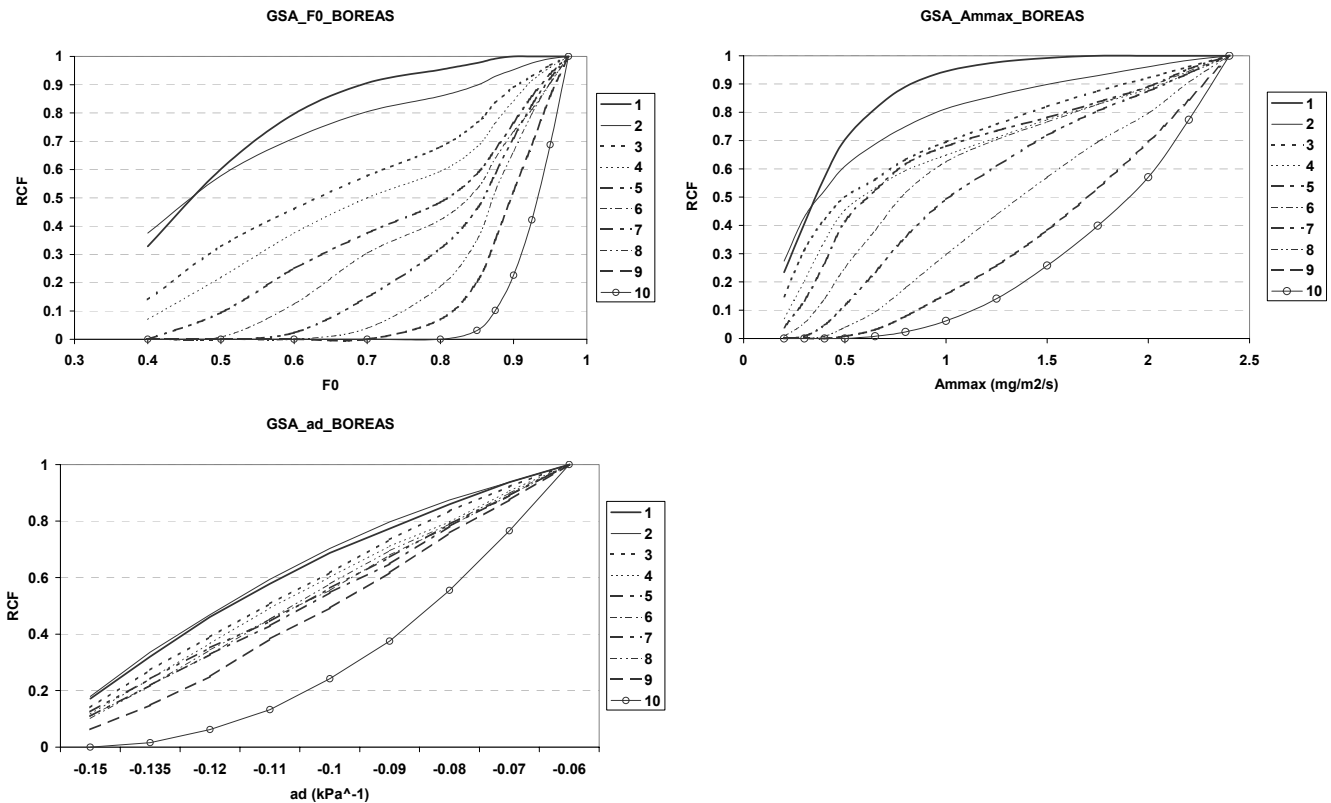
Figure 4.6: As in figure 4.4 for BOREAS.

4.3.3 Speuld95

Figures 4.7a-c give an overview of the sensitivities in this forest. With a_d constant (Fig. 4.7a) an area of minimum RMSE is shown. Increasing f_0 and $A_{m,max}(@25)$ results in a sharp increase of RMSE. This is in agreement with the previous forests. Strange is the minimum in RMSE at a relatively low value of $A_{m,max}(@25)$ =0.2 mg/m^2/s because there is no clear indication that this forest suffers from low nutrient status. When $A_{m,max}(@25)$ is supposed to be higher, this forest will have a relative low f_0. Dekker (2000) found $A_{m,max}(@25)$=1.0 mg/m^2/s for this forest. An other possible explanation is that the chosen LAI=10 was too high which is compensated by the model by reducing $A_{m,max}(@25)$. When the RMSE is determined from CO_2 then a higher estimate of the maximum assimilation rate is found ($A_{m,max}(@25)$=0.6 mg/m^2/s). When $A_{m,max}(@25)$ is held constant (Fig 4.7b) we recognise the area of low RMSE as in the other two forests. The large sensitivity of f_0 in the highest range is again present. Figure 4.7c consolidates the low sensitivity to a_d.

The GSA of this forest is shown in figure 4.8. The model was sensitive again to f_0 and $A_{m,max}(@25)$ but less to a_d. We see a large sensitivity for $A_{m,max}(@25)$ below 1.0 mg/m^2/s. In class 1 nearly all parameter values are below this value. Class one in the plot for f_0 is nearly a straight line indicating that in that particular class f_0 is evenly distributed.
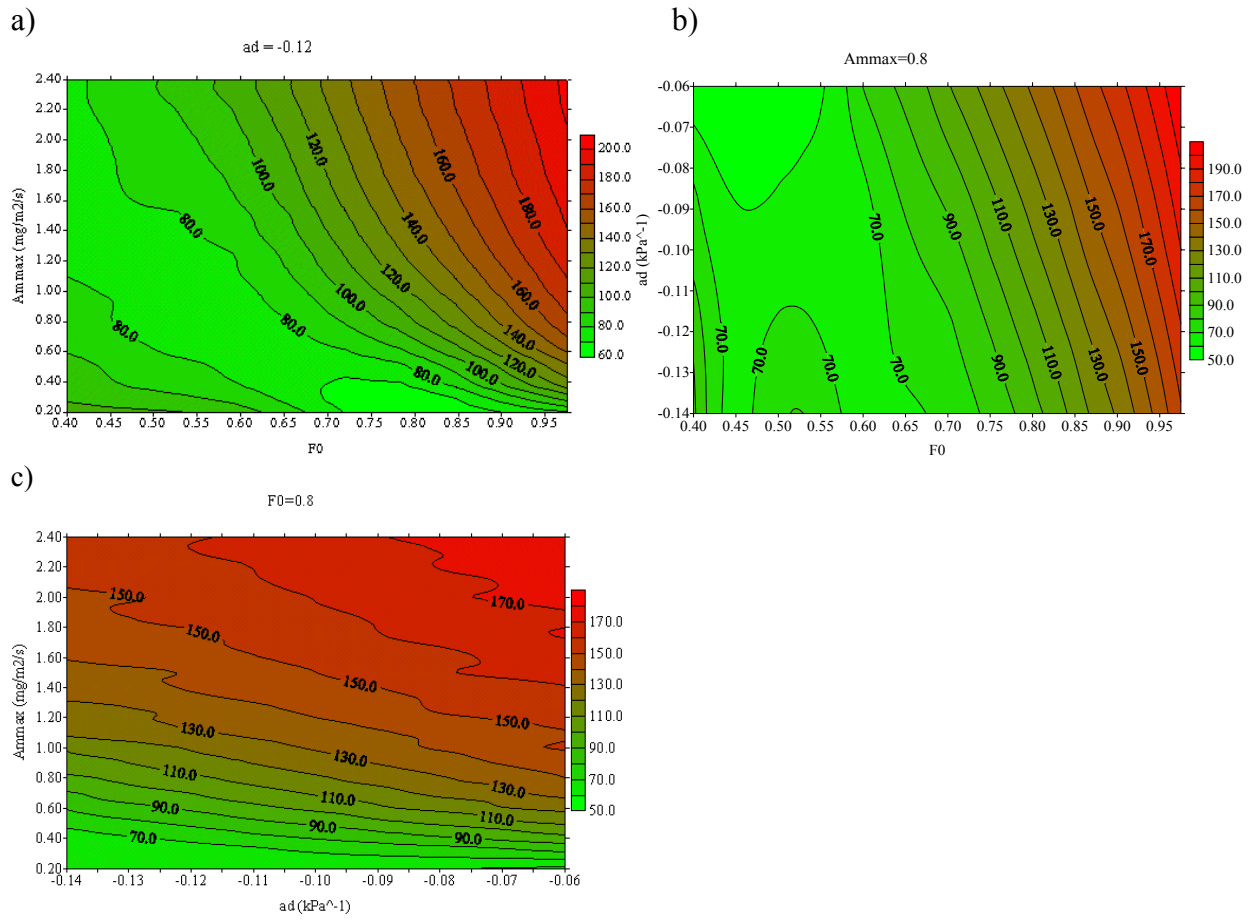
Figure 4.7: Contour plots of root mean square error (RMSE) for latent heat flux (W/m²) for Speuld95. a) $A_{m,max}(@25)$ vs. f_0 with ad=-0.12 kPa⁻¹, b) a_d vs. f_0 with $A_{m,max}$= 0.8 mg/m²/s, c) $A_{m,max}(@25)$ vs. a_d with f_0=0.80.
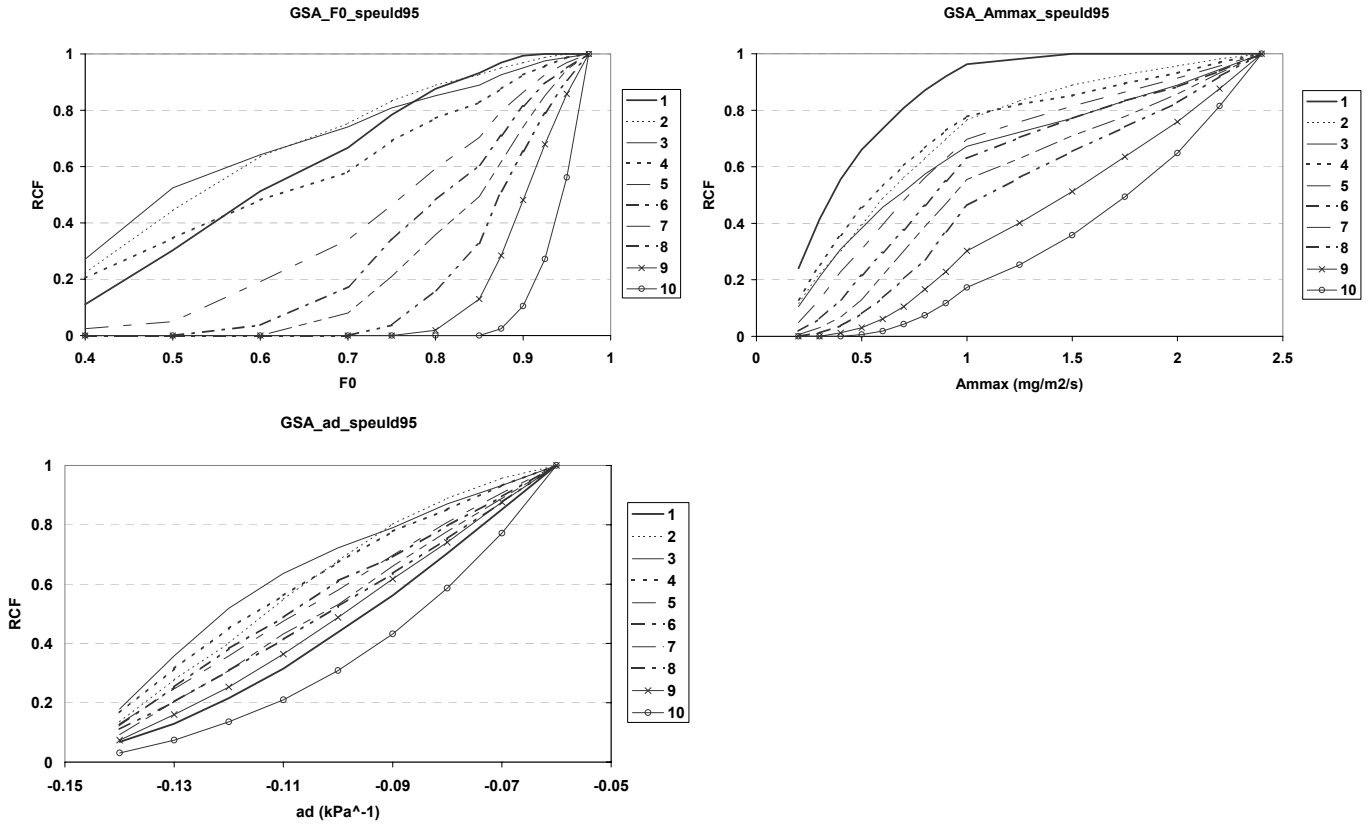
Figure 4.8: As in figure 4.4 for Speuld95.

4.3.4 Speuld96

The contour plots for this forest are depicted in figure 4.9. When a_d is constant (Fig 4.9a) an earlier seen picture returns: an area of low RMSE together with high RMSE at large f_0 and $A_{m,max}(@25)$. Figure 4.9b is different from the other forests because no minimum is seen. This is seen at other levels of $A_{m,max}(@25)$ too (not shown). If a minimum is present then it should be at the left edge, but the required f_0 value is not very likely. Figure 4.9c does not differ a lot from the other plots where f_0 is held constant.

The GSA of this forest (Fig 4.10) is in agreement with the one for Speuld95. Again the model is sensitive to f_0 and $A_{m,max}(@25)$ and less sensitive to a_d. Class 1 for f_0 is a nearly straight line, which indicates that the sensitivity in this class is evenly distributed over the domain of f_0. In the best performing class (1) for $A_{m,max}(@25)$ the majority of the members lie below $A_{m,max}(@25)$ =1.0 mg/m^2/s. The largest sensitivity for $A_{m,max}(@25)$ lies between 0.2 and 1.0 mg/m^2/s and it decreases for class one when $A_{m,max}(@25)$ increases.

a)

b)

c)
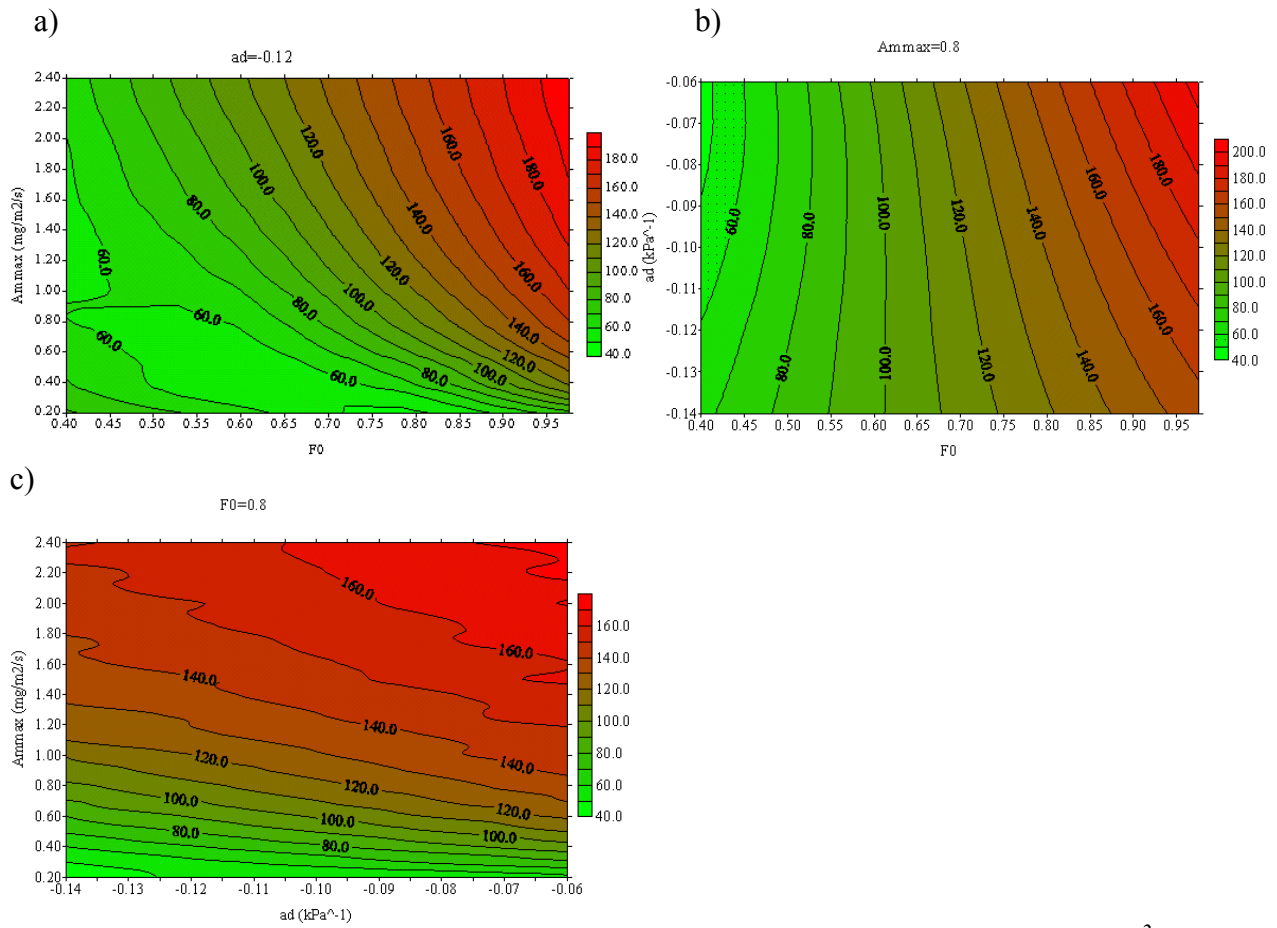
Figure 4.9: Contour plots of root mean square error (RMSE) for latent heat flux (W/m²) for Speuld96. a) $A_{m,max}(@25)$ vs. f_0 with a_d=-0.12 kPa⁻¹, b) a_d vs. f_0 with $A_{m,max}(@25)$= 0.8 mg/m²/s, c) $A_{m,max}(@25)$ vs. a_d with f_0=0.80.
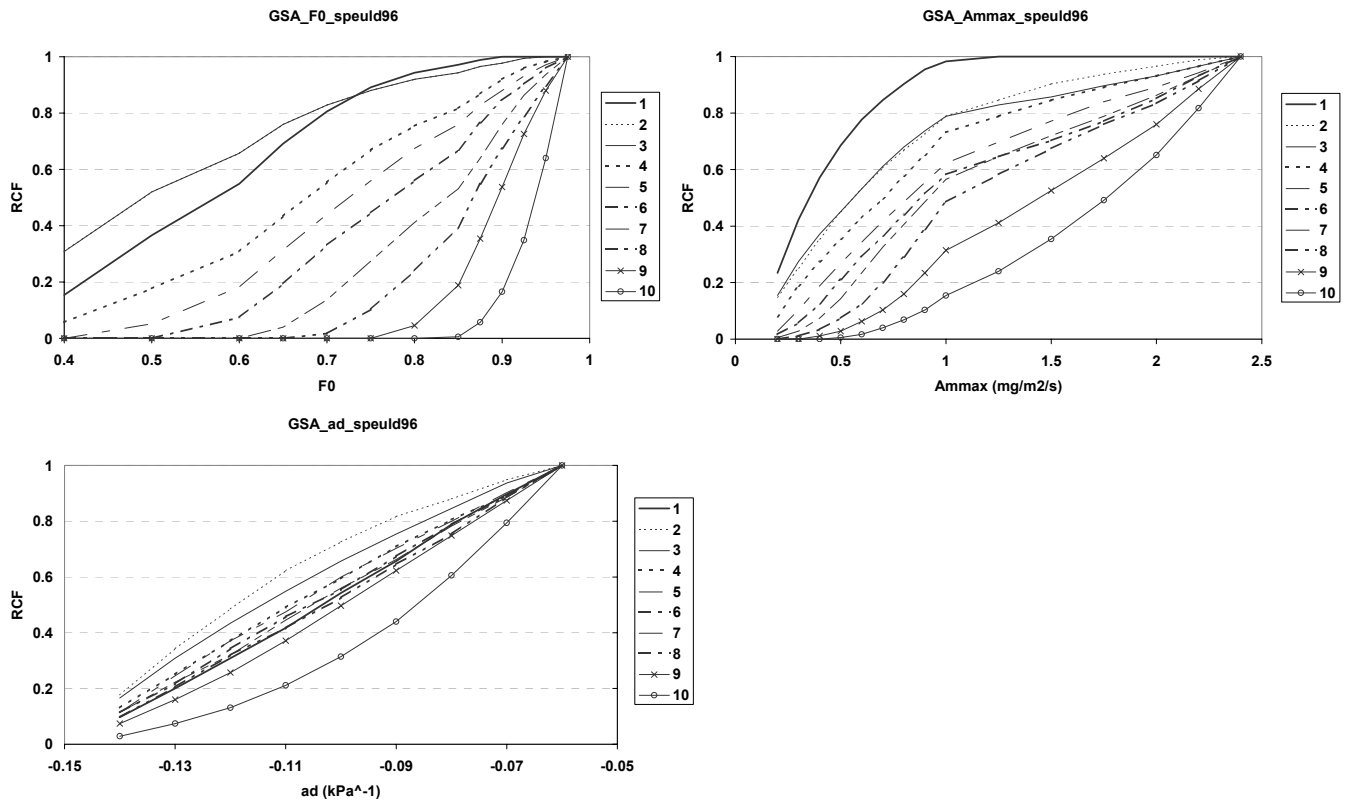
Figure 4.10: As in figure 4.4 for Speuld96.

4.4 Acceptable parameter combinations.

The Monte Carlo simulations of the previous sections produced lots of RMSE values. The contour plots show that a clear minimum cannot be found, but that an area of 'acceptable' parameter combinations is present. To find out whether (and with what significance) a certain parameter set is acceptable, the RMSE of the latent heat fluxes is scaled with the standard deviation of the measured latent heat fluxes. This gives a measure of the significance of the obtained parameter sets. This approach can also be found in Van Wijk (2001). Table 4.3 shows for the standard deviation of $L_v E$ per forest. Figure 4.11 shows the accepted sets per significance level. Red dots (RMSE$<\sigma_{LvE}$) denote a set with more significance than the green (RMSE$<2\sigma_{LvE}$) and the blue (RMSE$<3\sigma_{LvE}$) dots, respectively. For Speuld95 no sets with *RMSE*$<\sigma_{LvE}$ are present so $1.5\sigma_{LvE}$ is plotted in figure 4.11. For BOREAS even this significance level is not present, which is due to the low σ_{LvE}.

Table 4.3: Standard deviation of latent heat flux of the selected data points.

Site	Standard deviation σ_{LvE} (W/m^2)
Loobos	60.57
Speuld95	55.45
Speuld96	49.81
BOREAS	42.90
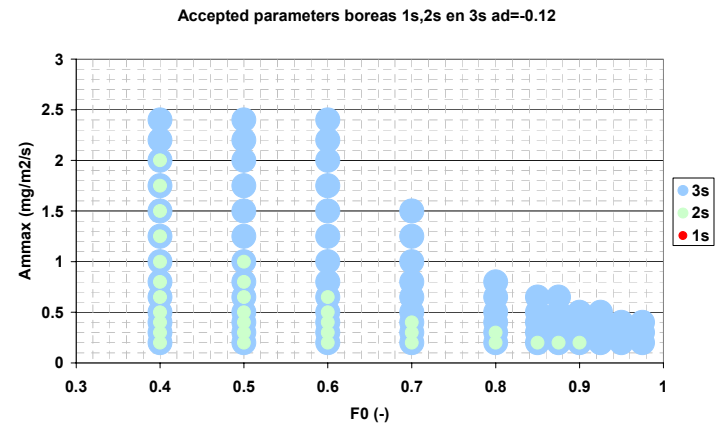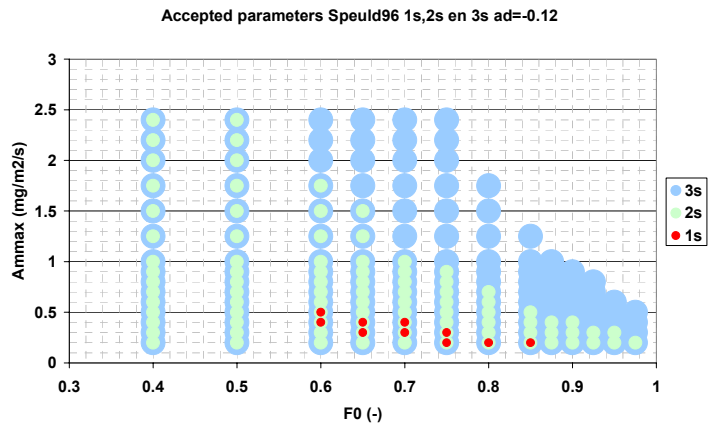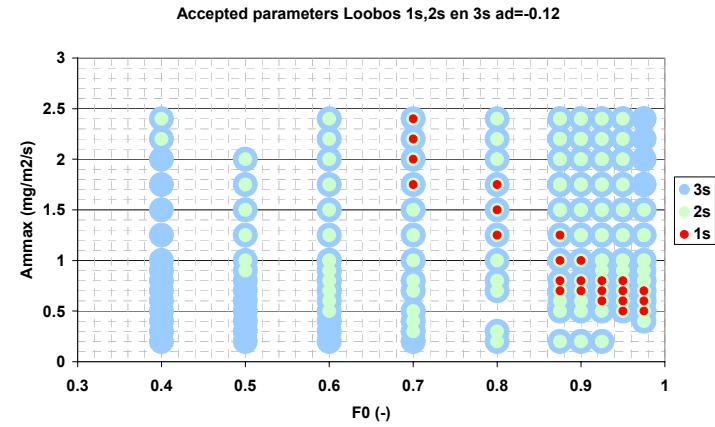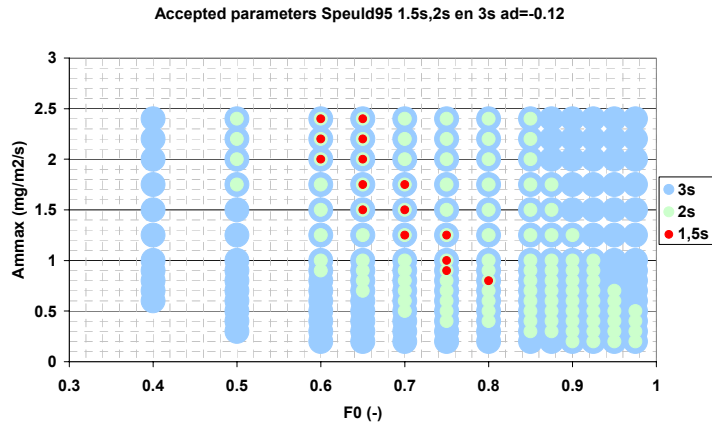
Figure 4.11: Accepted parameter values for Loobos, Speuld95, Speuld96 and BOREAS for varying significance levels. Red means that RMSE<σ_{LvE} (1.5σ_{LvE} for Speuld95), green that RMSE<2σ_{LvE} and blue that RMSE<3σ_{LvE}. Note that for BOREAS no red points are present.
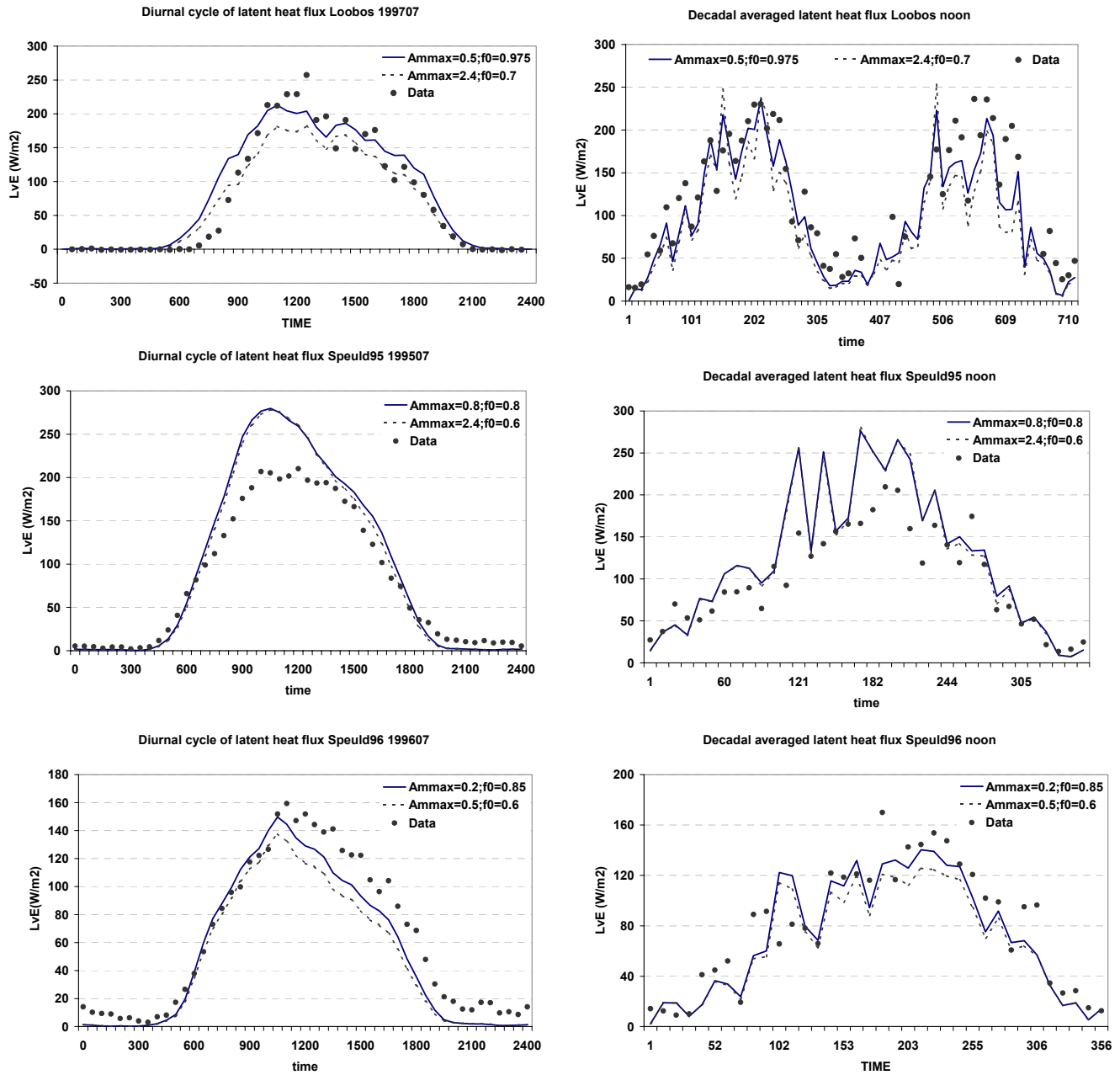
Figure 4.12 Time series (left panel diurnal cycle July, right panel decadal averages of time slots around noon) of latent heat flux for different parameter sets ($a_d = -0.12$ kPa^{-1}) within the area of σ_{LvE} for Loobos, Speuld95 and Speuld96.

The much lower $A_{m,max}$(@25) values in 1996 for Speuld than in 1995 was also recognised by Van Wijk (2001). This decrease of maximum assimilation is due to management activities that affected the foliage. Thinning resulted on average in a younger canopy because the older branches will be removed. Immature foliage has a lower photosynthetic capacity which is seen in figure 4.11.

To examine the model variability within the group of the highest significance in figure 4.11, time series for each forest are shown for two extreme locations within this high significance area.

51

Figure 4.12 shows these time series of latent heat flux taken from parameter value combination giving RMSE $<\sigma_{LvE}$. The diurnal cycle for Loobos indicates that the first parameter set with $A_{m,max}(@25) =0.5$ mg/m^2/s and $f_0= 0.975$ is more driven by light regulation. Its performance is better during high light intensities. The second set ($A_{m,max}(@25) =2.4$ mg/m^2/s and $f_0= 0.7$) is driven by humidity stress and performs better during low light intensities. This is confirmed in the seasonal cycle: the first set performs better during the summer months than the second set. The model output for Speuld95 shows no significant difference between both runs. In the case of Speuld96 we see that the morning simulations are quite correct for both runs, while in the afternoon both model runs underestimate the latent heat flux. Even the difference between both model runs is substantial, while they have the same RMSE in the Monte Carlo calculations. This may indicates that this month is not representative for the conditions where the RMSE was calculated for. Thus even within the class where RMSE $<\sigma_{LvE}$ substantial differences in model output can occur. The wide range of acceptable parameter combinations is due to the scatter in the data.

When the pictures in figure 4.11 in the last section are combined in an overlay, it becomes clear whether those four forests behave the same in the sense of acceptable parameter values. The overlay is shown in figure 4.13a using $2\sigma_{LvE}$ as a quality criterion. Since the model is not so sensitive to a_d we choose a_d constant at -0.12 kPa^{-1}, which is a reasonable value for forests as shown in chapter 3 and in Van de Kassteele (2001). Common parameter combinations could be recognised when four colours are present at the same set.
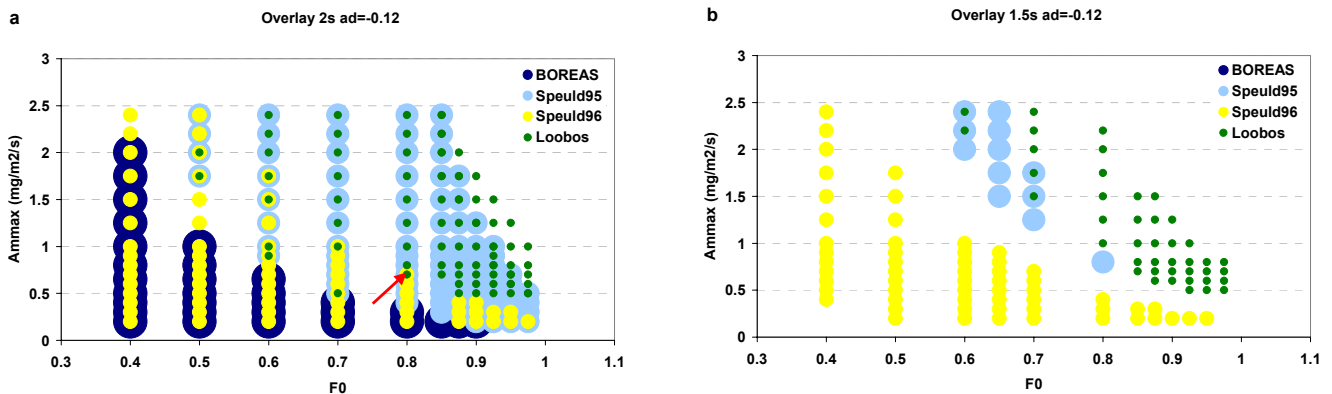
Figure 4.13: Overlay of the accepted parameter sets [f$_0$, A$_{m,max}$(@25)] for a$_d$=-0.12 kPa^{-1} within a) 2σ_{LvE} and b) 1.5σ_{LvE} in the four forests.

In figure 4.13a it is clearly seen that the 4 forests do not have a parameter set in common. On the other hand many sets are possible for each forest. There is no match between the BOREAS forest site on the one hand and the other ones. There are a few points where the remaining forests seem to have parameters in common. Those are summarised in table 4.4. Many of them are in the range where they are not expected physiologically ($f_0 = 0.4$-0.7). When the required significance is increased (Fig 4.13b) the division between the forests is emphasised. Speuld96 is totally apart and BOREAS disappeared from the picture.

Table 4.4: Common parameter sets for Loobos, Speuld95 and Speuld96 with $2\sigma_{LvE}$ as criterion.

Set	$A_{m,max}(@25)$	f_0	Set	$A_{m,max}(@25)$	f_0
1	2.0	0.5	6	0.9	0.6
2	1.75	0.5	7	0.5	0.7
3	1.75	0.6	8	1.0	0.7
4	1.5	0.6	9	0.7	0.8
5	1.0	0.6			
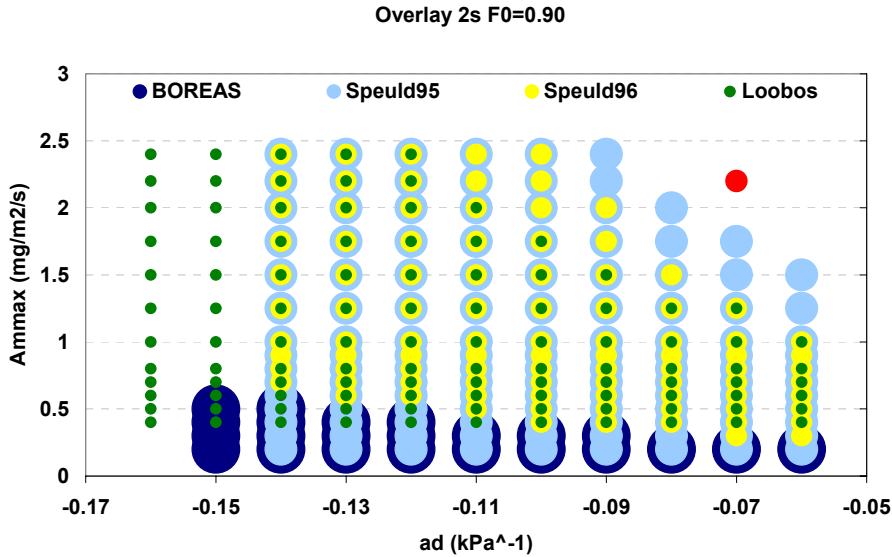
Figure 4.14: Overlay of the accepted parameter sets [$A_{m,max}(@25), a_d$] for f_0=0.90 within $2\sigma_{LvE}$ in the four forests. The red dot indicates the standard parameter values in the A-gs scheme.

Figure 4.14 shows an overlay with f_0 being constant instead of a_d. Still a wide range of parameter values is valid, but the standard values in Jacobs *et al.* (1994) ($A_{m,max}(@25) = 2.2$ mg/m^2/s and a_d = -0.07 kPa^{-1}) is not accepted with the lowest significance (RMSE< $3\sigma_{LvE}$) for all forests. The figure indeed confirms the idea postulated in chapter 2 that both $A_{m,max}(@25)$ and a_d must be lower for forests than for low vegetation.

To examine whether the dissent parameter values for BOREAS result in proper simulation time series of latent heat flux are shown. Figure 4.15 depicts the latent heat flux with parameter set $A_{m,max}(@25)$=0.3 mg/m^2/s, f_0=0.8 and a_d=-0.06 kPa^{-1}, which had the lowest RMSE and bias in the Monte Carlo series. The picture shows that the dissent behaviour of BOREAS in Fig 4.13a is confirmed and results in a proper simulation of the latent heat flux. This supports the suggestion that the model set up is valid, but the parameters differ per biome.
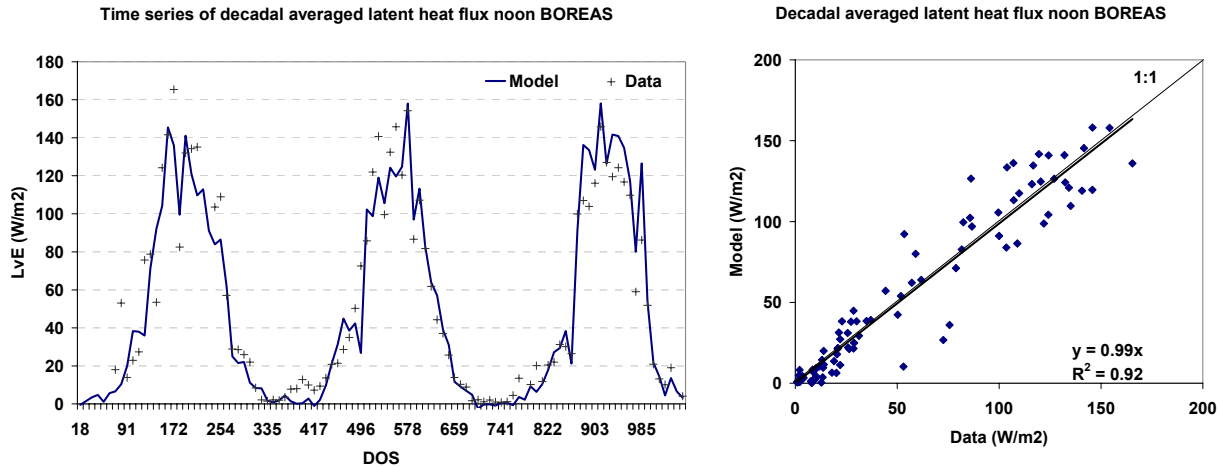
Figure 4.15: Time series of decadal averaged latent heat flux for BOREAS with parameter set: $A_{m,max}(@25)=0.3$ mg/m^2/s, $f_0=0.8$ and $a_d=-0.06$ kPa^{-1}.

4.5 Time series of the overlay results

In the overlays we saw that three of the four forests may have in common the parameter combination $A_{m,max}(@25)=0.7$ mg/m^2/s with $f_0=0.8$ and $a_d=-0.12$ kPa^{-1}. The red arrow in figure 4.13a highlights this one. Here we examine time series to consider the model performance for this parameter combination. Note in advance that this point lies on the left edge of Speuld95 and on the right edge of Speuld96. In this section the time series of latent heat flux, sensible heat flux and CO_2 flux (when available) will be shown. The month July will be used to evaluate the diurnal cycles in summer. Shown are daily averaged fluxes during daytime (10-14 local time).

4.5.1 Loobos

Figure 4.16 shows that for the current parameter set the evapotranspiration is underestimated in the diurnal cycle of July 1997. This is confirmed by the daily averages shown in figure 4.17. The underestimation amounts 40%. This underestimation can also be seen in figure 4.13 where the current parameter set is on the left edge of the area of acceptable parameter sets for Loobos. It turns out that this result is still within two times the standard deviation. This is due to a large standard deviation in Loobos, compared to the other forests. On the other hand it is seen that the CO_2 flux is simulated quite correctly, although there is a considerable amount of scatter, which indicates that the model stomatal conductance was calculated properly. The time shift in figure 4.16 is again caused by the CO_2 storage term. The sensible heat flux was simulated correctly, and since we know that the energy balance was closed in the data, there is apparently a (too) large soil heat stream (not shown).
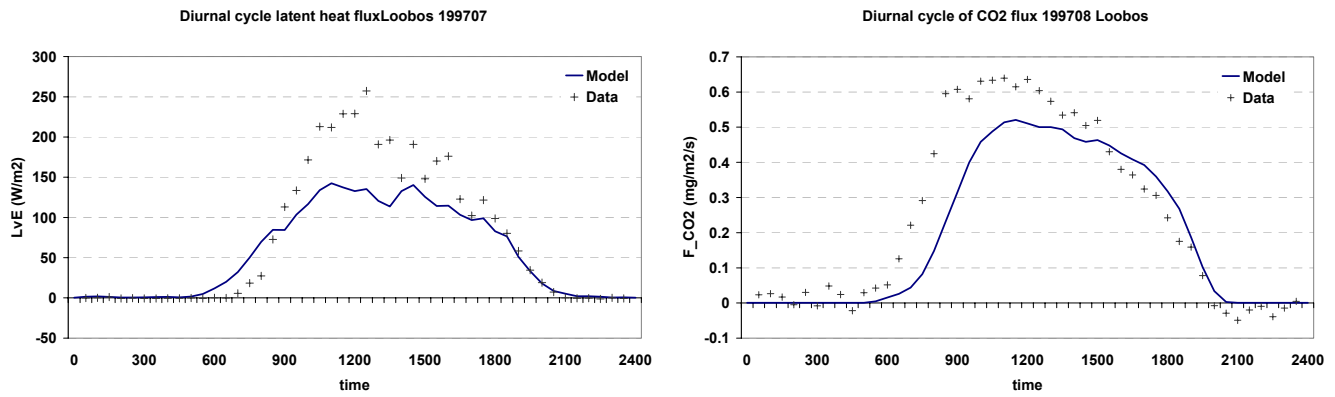
Figure 4.16: Diurnal cycle of fluxes of latent heat (left panel) and CO$_2$ (right panel) in Loobos.
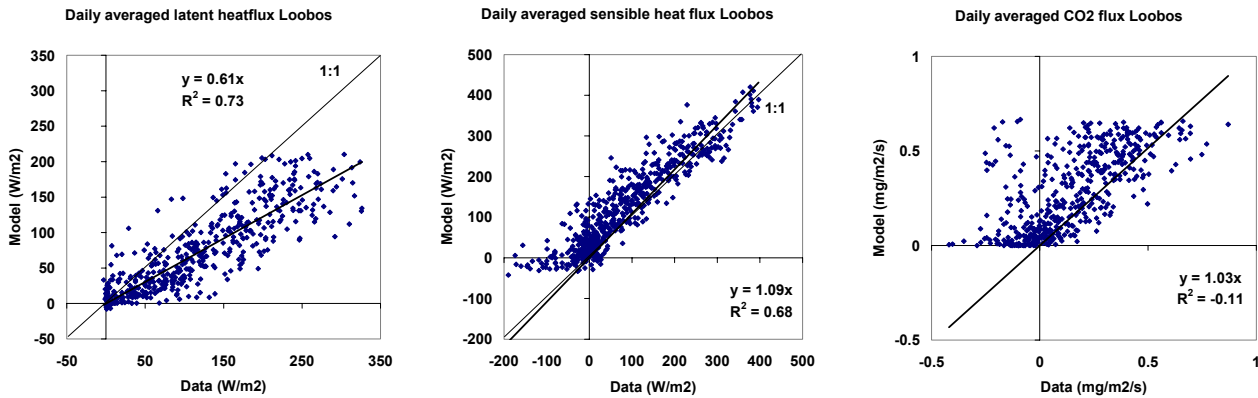
Figure 4.17: Daily averaged daytime fluxes of latent heat (left panel), sensible heat (middle panel) and CO$_2$ (right panel) for Loobos.

4.5.2 Speuld95

Contrary to Loobos, in Speuld95 (Figs 4.18-4.20) the latent heat flux is overestimated by 16% with this parameter combination although the bias is lower than in Loobos. Again the CO$_2$ flux seems to be represented correctly. Especially the times series (Fig.4.20) give confidence, also because of the relatively low amount of scatter. Note that only CO$_2$ measurements of DOY>180 are used here, because no data were available before DOY 180 (Van Wijk, 2001). The sensible heat flux is underestimated by 40%, which again indicates a systematic mismatch in the soil heat flux.
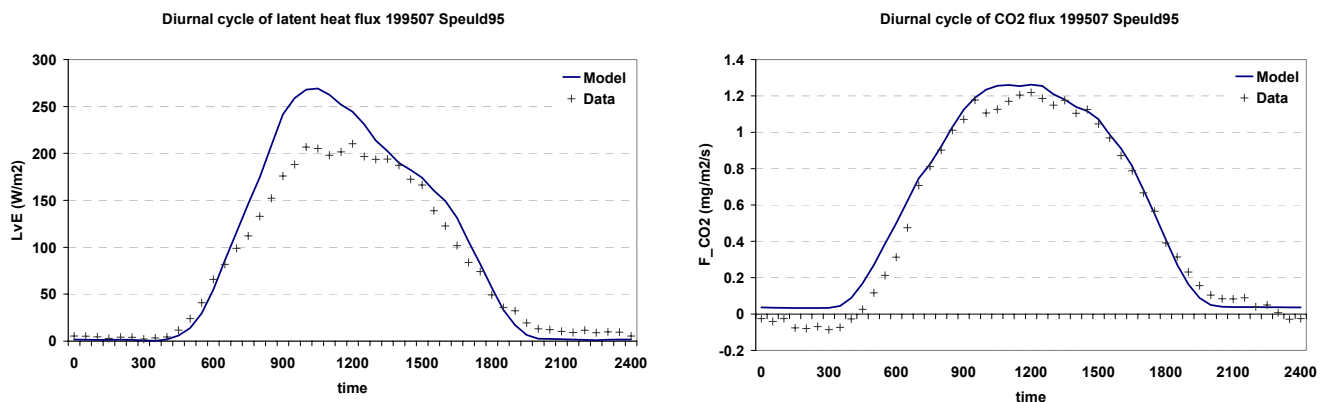
Figure 4.18: Diurnal cycle of fluxes of latent heat (left panel) and CO$_2$ (right panel) in Speuld95.
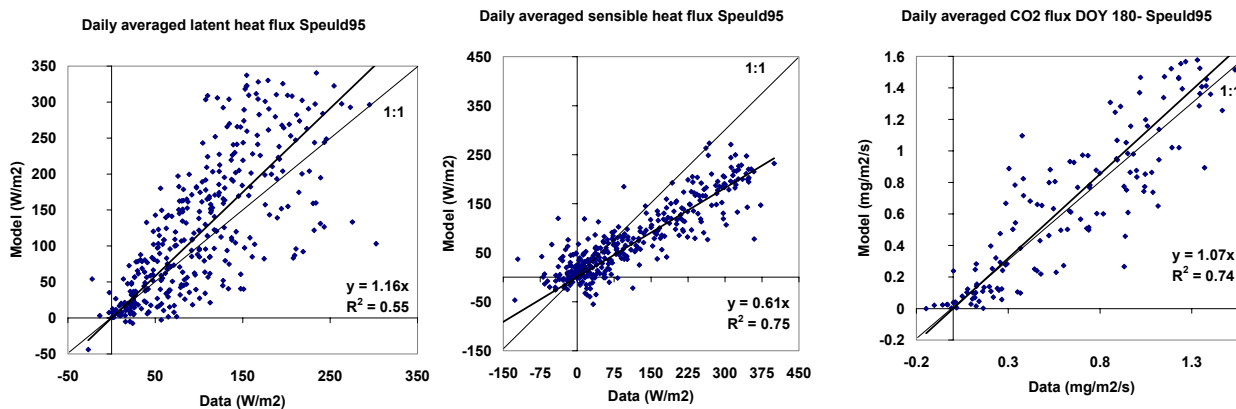
Figure 4.19: *Daily averaged daytime fluxes of latent heat (left panel), sensible heat (middle panel) and CO_2 (right panel) for Speuld95.*
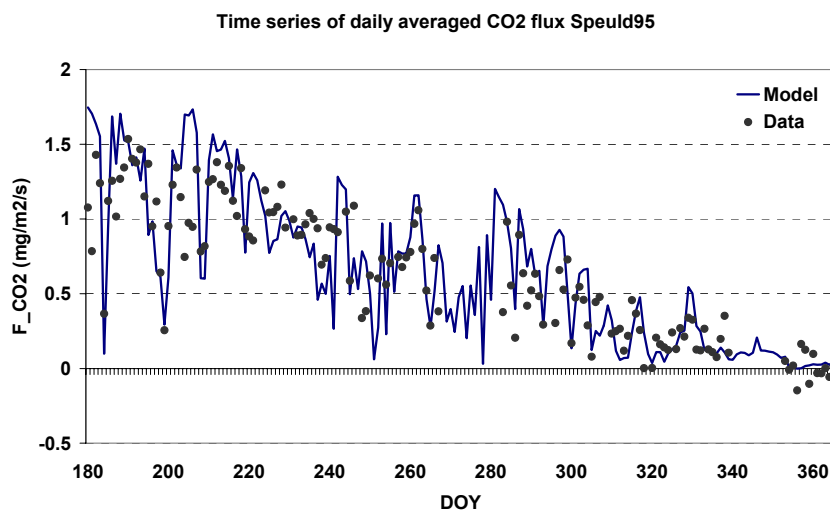
Figure 4.20: *Time series of daily averaged daytime CO_2 flux for Speuld95.*

4.5.3 Speuld96

In Speuld96 both L_vE and F_CO_2 are overestimated by 40 W/m^2 and 0.2 mg/m^2/s respectively (Fig 4.22). Figure 4.23 shows that this is mainly the case in spring (DOY 100-160), and still present in summer (see diurnal cycle). The underestimation of sensible heat flux is confirmed here, again by 40%. So these results are in agreement with those of Speuld95.

56
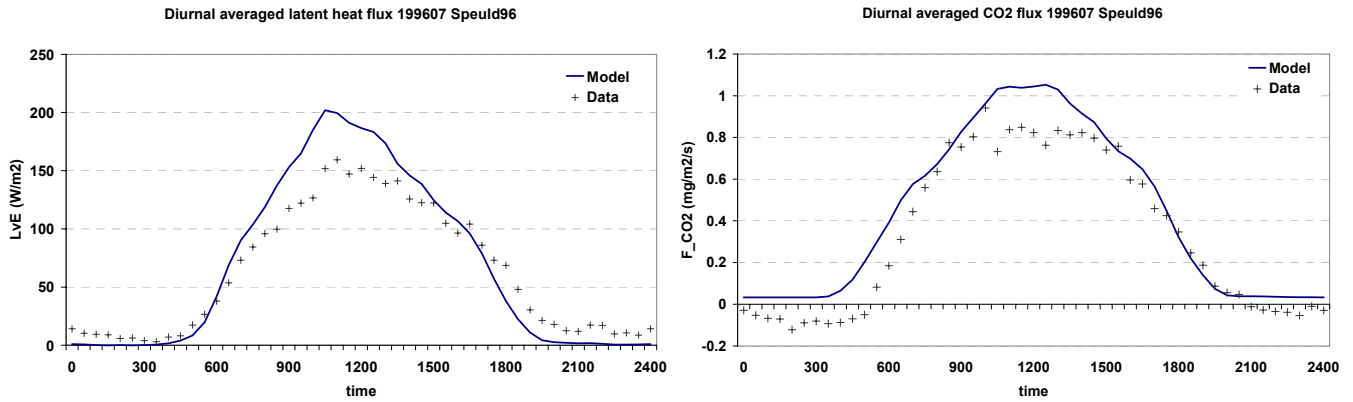
Figure 4.21: Diurnal cycle of fluxes of latent heat (left panel) and CO_2 (right panel) in Speuld96.
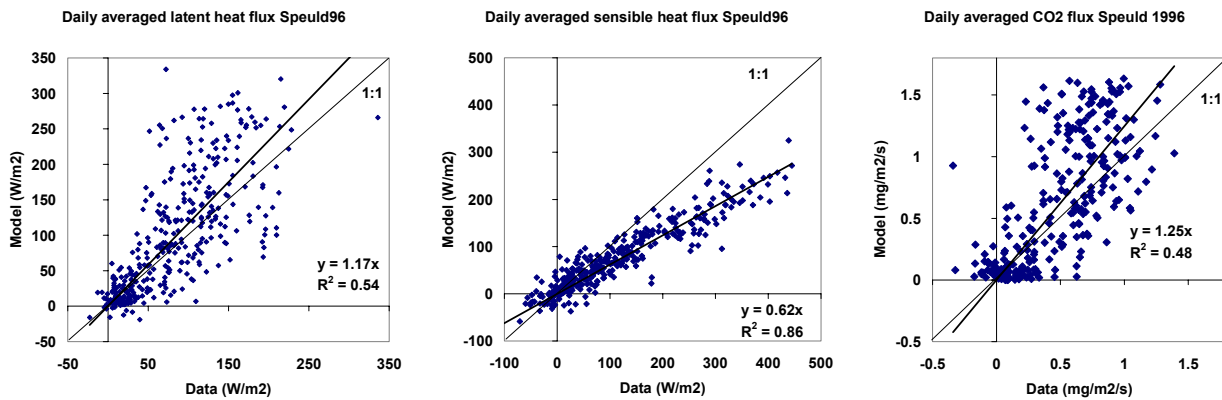
Figure 4.22: Daily averaged daytime fluxes of latent heat (left panel), sensible heat (middle panel) and CO_2 (right panel) for Speuld96.
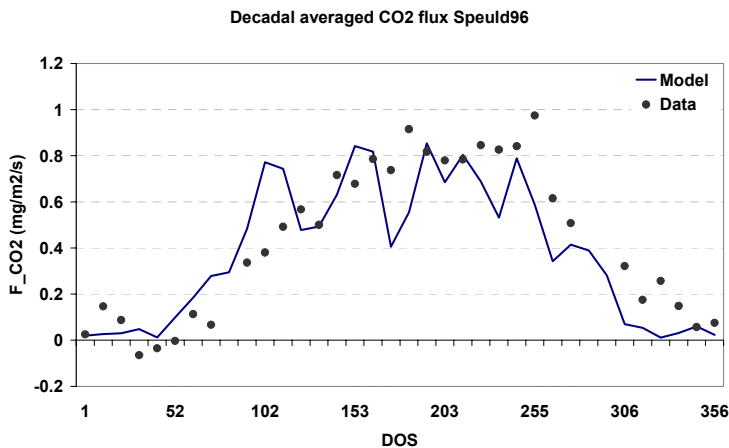
Figure 4.23: Time series of decadal averaged daytime CO_2 flux for Speuld96.

4.5.4 BOREAS

From Figs 4.24-4.25 it is very clear that the current parameter set is not a proper one for BOREAS, so the time series confirms our results of the statistical exercise. The latent heat flux is

overestimated by more than 30%, shown in figures 4.24 and 4.25. The sensible heat flux is underestimated by 27%. No CO_2 flux measurements were available in this data set. It is clear that the current maximum assimilation value is too large for this forest.

Daily averaged latent heat flux boreas

$y = 1.32x$
$R^2 = 0.83$

Daily averaged sensible heat flux boreas

$y = 0.73x$
$R^2 = 0.70$
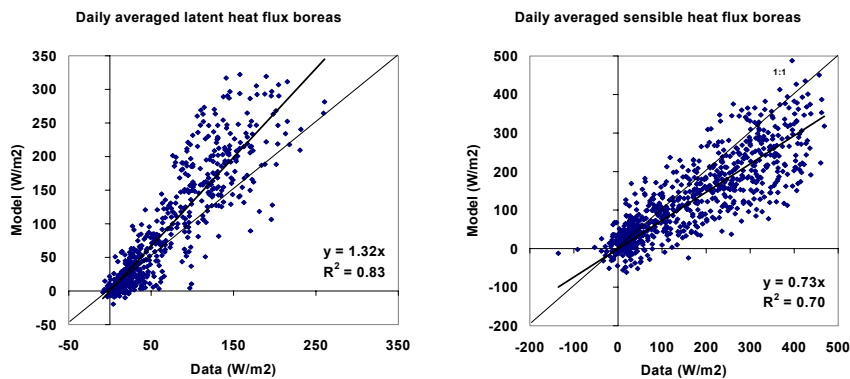
Figure 4.24: Daily averaged daytime fluxes of latent heat (left panel) and sensible heat (right panel) for BOREAS.

Diurnal cycle of latent heat flux 199407 boreas
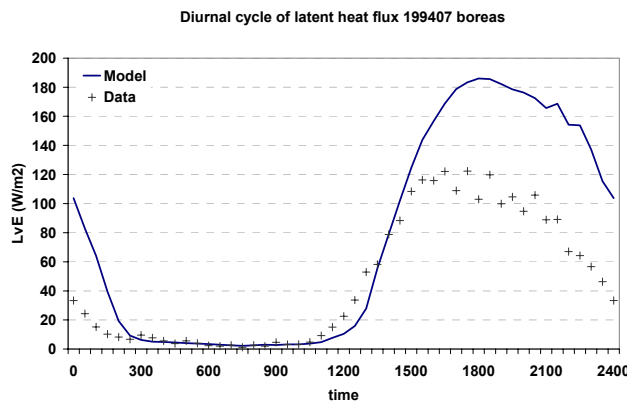
Figure 4.25: Diurnal cycle of latent heat flux for BOREAS.

4.6 Conclusions and discussion.

The latent heat fluxes of these forests cannot be simulated by one unique parameter set even when this set is chosen as an optimum compromise for all forest sites simultaneously. For BOREAS this was already clear from figure 4.13. For the other forests it appears that the standard deviation in the data is so large that a common parameter set passes the selection criterion, but the times series show that this set does not simulate the latent heat flux properly. The CO_2 flux is modelled quite well, indicating that the stomatal conductance is represented properly. The misfit in the latent heat flux may be due to incorrect simulation of the surface skin temperature and/or a problem in the heat storage term and soil heat flux. This may be due to the big-leaf approach that may not be valid in forests. Another possible reason for the mismatch may be the leaf nitrogen (or other nutrients) concentration influencing the maximum assimilation rate. Since the carbon dioxide exchange is simulated quite well, this argument seems not to be valid.

There may be discussion about the selection criteria applied in this study (Table 4.1). This is an optimalisation between getting enough data points in the statistical sample on the one hand and neglecting time slots that are not representative for testing the photosynthesis part of the model

on the other hand. For example when rain interception water on the vegetation is present, data are excluded. We chose the time slots in which we expected the vegetation to be active. Those are the ones where the model performance is most powerful, thus without stresses. The danger in this approach is that the model calibration is carried out under unstressed conditions, which leads to overestimation of the latent heat flux and the CO_2 fluxes under stressed conditions.

This study used the RMSE of the latent heat flux to obtain acceptable parameters. It may be better to take the RMSE in the CO_2 flux. Of course the uncertainty in measured CO_2 fluxes will be larger than in the latent heat flux, see table 3.3. But on the other hand the model seems to have problems with the energy partitioning: the sensible heat flux is underestimated systematically. This will have its influence on simulated latent heat fluxes. To overcome this problem it is recommended to calibrate with CO_2 fluxes and evaluate the latent heat flux as a secondary quantity.

5 Recommendations for further research

It is now time the consider the implementation of the parameter values of the A-g_s scheme for each grid box in the three dimensional version of RACMO.

This study has shown that a division of plants in C3 and C4 is not enough to result in proper simulation of the turbulent fluxes of heat and humidity. The standard value of $A_{m,max}$(@25) (2.2 mg/m^2/s, Jacobs, 1994)is too large for forest biomes. Consequently the mesophyll conductance should be decreased too for forests. This adjustment is important because a substantial part of earth's surface is covered with forests.

Due to the clear dissent behaviour of the parameter values for BOREAS compared to the temperate coniferous forests as shown in this study, we can think of subdivision of the C3 species in 'low vegetation', 'boreal forest' and 'not boreal forest'. On the other hand we tested only one boreal forest, so our results may not be valid for other boreal forests too. Within the group of 'not boreal' forests we saw that no single set of parameter values was present to simulate the fluxes well. This implies that the physical reasons are for the differences have to be explored. This may be due to nutrient status (see below). A possibility to get a parameter set for each grid box in RACMO is to aim at a geographical distribution of leaf nutrient status. This can be retrieved from regional data sets or from advanced remote sensing techniques to monitor leaf chlorophyll. See for example the study of Endo *et al*. (2000). This could form the base of a quantification of the maximum photosynthetic capacity. In this manner it is also possible to introduce a seasonal cycle in $A_{m,max}$(@25) which is currently not implemented. For f_0 and a_d values of 0.90 and –0.12 kPa^{-1} can be taken for all forest types. For 'low vegetation' the parameter values do not need adaptation.

Beyond this, there are some points for future research that are worth mentioning:

- The maximum rate of carboxylation $V_{c,max}$ can be related to the leaf nitrogen content in the future. It is recommended to implement this dependence in the A-gs scheme, because this mechanism may be able to explain a part of the non-uniqueness of the parameters. C99 and Dickinson *et al* (2002) already implemented this in their climate models. A disadvantage of implementation of nitrogen sensitivity is that only limited data sets are available where all meteorological parameters and plant nitrogen are present. This reduces the possibility to test the model. Measurement campaigns in the future should include the measurement of leaf nitrogen concentration, both on mass and area basis. Because nitrogen content is not constant during the growing season and variable with canopy height, nitrogen should be measured once a week at several levels. In addition it is recommended to measure phosphorus status too.

  If this implementation of this nitrogen dependency is successful in the off line mode, a 3D RACMO run on European scale could be applied.

  There is some uncertainty whether the V_{cmax}-N-relationship will hold under elevated CO$_2$ and temperature. At first sight $V_{c,max}$ tends to stay constant (Wang *et al*., 1996; Takeuchi *et al*., 2001), but on the other hand the N concentration shows a decrease under these conditions. This indicate that the $V_{c,max}$-N-relationship is not stationary in time. Thus this must be examined to understand plant behaviour under enhanced greenhouse conditions.

- Off line evaluation of the MOSES scheme for the forests data sets is necessary. The MOSES scheme was only rudimentary tested on forest sites. The above mentioned nitrogen sensitivity is already included in MOSES. Both properties are reason to evaluate this model off line as was done for the A-gs scheme in Van de Kassteele (2001).

Quantities to test are the turbulent heat and CO_2 fluxes and soil temperatures and moisture. This can give enhanced confidence to the MOSES scheme.

- Because we found that the model is unable to represent sensible heat flux when latent heat flux and CO_2 are simulated well, it should be evaluated whether the model representation of soil heat flux, heat storage and surface temperature is also valid for forests. There may be a problem with the representation of the stable air stratification in the forest during daytime. Adjustment of the soil conductivity or adjustment of the current implemented heat reservoir that represents forest heat storage are ideas to get a better performance.

- As mentioned in section 3.2, hydraulic lift may affect the transport of soil moisture significantly in forests. Current models overlook this redistribution process. This is a mechanism that should be tested whether to increase the model performance quality. As a first step the model of Reyl *et al*. (2002) can be used. For some days they found hydraulic redistribution responsible for 20% increase in transpiration.

- The original motivation for this study was the overestimation of the latent heat flux in forests in Eastern Europe. The land use characterisation may have a large impact on the exchange processes of heat, humidity and CO_2. So it is worth to do experiments with other land use classification charts.

Acknowledgements

References

Baldocchi, D.D, J.D. Fuentes, D.R. Bowling, A.A. Turnispeed, R.K. Monson, 1999: Scaling Isoprene Fluxes from leaves to Canopies: Test Cases over boreal Aspen and a Mixed species temperate forest, *J. Appl. Meteor.*, **38**, 885-898.

Begon M., J.L. Harper and C.R. Townsend, 1996: *Ecology: individuals, populations and communities*, 3rd edition, Blackwell Science Ltd, Oxford, 1068 pp.

Berger, B. W., Davis, K. J., Bakwin, P. S., Yi, C., Zhao, C., 2001: Long-term carbon dioxide fluxes from a very tall tower in a northern forest: Flux measurement methodology, *J. Atmospheric and Oceanic Technology*, **18,** 529-542.

Bosveld, F.C., A.A.M. Holtslag and B.J.J.M. van den Hurk,1999: Nighttime convection in the interior of a dense Douglas fir forest, *Bound. Layer. Meteor.*, **93**,171-195.

Calvet, J.C., 2000: Investigating soil and atmospheric plant water stress using physiological and micrometeorological data, *Agric. For. Meteor.*, **103**, 229-247.

Calvet, J.C, J. Noilham, J.L. Roujean, P. Bessemoulin, M. Cabelguenne, A. Olioso and J.P. Wigneron, 1998: An interactive vegetation SVAT model tested against data from six contrasting sites, *Agric. For. Meteor.*, **92**,73-95.

Carswell, F.E., P. Meir, E.V. Wandelli, L.C.M. Nonates, B. Kruijt, E.M. Barbosa, A.D. Nobre, J. Grace and P.G. Jarvis, 2000: Photosynthetic capacity in a central Amazonian forest, *Tree physiology*, **20**, 179-186.

Collatz, G.J., J.T. Ball, C. Grivet and J.A. Berry, 1991: Physiological and environmental regulation of stomatal conductance, photosynthesis and transpiration: A model that includes a laminar boundary layer, *Agric. For. Meteor.*, **54**, 107-136.

Cox, P.M., C. Huntingford and R.J. Harding, 1998: A canopy conductance and photosynthesis model for use in a GCM land surface scheme, *J. Hydrol*, **212-213**, 79-94.

Cox P.M., R.A. Betts, C.B. Bunton, R.L.H Essery, P.R. Rowntree and J. Smith,1999:, The impact of a new land surface physics on the GCM simulation of climate and climate sensitivity, *Clim. Dyn.*, **15**, 183-203.

Dang, Q.L., H.A. Margolis and G.J. Collatz, 1998: Parametrization and testing of a coupled photosynthesis –stomatal conductance model for boreal trees, *Tree physiology*, **18**, 141-153.

Davidson, E.A., E. Belk and R. Boone,1998: Soil water content and temperature as independent or confounded factors controlling soil respiration in a temperate mixed hardwood forest, *Global Change Biology*, **4**, 217-227.

Dekker S.C., 2000: *Modelling and Monitoring Forest Evapotranspiration*, PhD thesis, University of Amsterdam, Amsterdam, 120p.

Dreyer, E., X. Le Roux, P. Montpied, F. A. Daudet and F. Masson, 2001: Temperature response of leaf photosynthetic capacity in seedlings from seven temperate tree species, *Tree physiology*, **21**, 223-232.

Endo, T., T. Okuda, M. Tamura and Y. Yasuoka, 2000: Estimation of Photosynthetic Rate of Plant from Hyper-spectral Remote Sensing of Biochemical Content, http://www.gisdevelopment.net/aars/acrs/2000/ts16/hype0003.shtml

Farquhar, G.D., S. von Caemmerer and J.A. Berry, 1980: A biochemical model of photosynthetic CO2 assimilation in leaves of C3 species, *Planta*, **149**, 78-90.

Feddes, R.A. and Coauthors, 2001: Modeling Root Water Uptake in Hydrological and Climate models, *Bull. Am. Met. Soc*, **82**, 2797-2809.

Foster, D. and J. Hadley, 1998: CO_2 exchange by hemlock forests in central New England, Annual Progress Report for FY 97/98, Harvard University. http://nigec.ucdavis.edu/publications/annual98/northeast/project70.html.

Franks, S.W., K.J. Beven, P.F. Quinn and I.R. Wright, 1997: On the sensitivity of soil-vegetation-atmosphere transfer (SVAT) schemes: equifinality and the problem of robust calibration, *Agric. For. Meteor.*, **86**, 63-75.

Givnish, T.J.,1983: *On the economy of plant form and function*, Cambridge University press, Camebridge,717 p.

Goudriaan, J., H.H. van Laar, H. van Keulen and W. Louwerse, 1985: Photosynthesis, CO_2 and plant production. In: W. Day and R.K. Atkin (eds), *Wheat growth and modelling*, NATO ASI series, Series A, Vol 86, Plenum Press, New York, 107-122.

Harding, R.J., C. Huntingford and P.M. Cox, 2000: Modelling long-term transpiration measurements from grassland in southern England, *Agric. For. Meteor.*, **100**, 309-322.

Hikosaka, K. and T. Hirose, 1998: Leaf and Canopy photosynthesis of C3 plants at elevated CO2 in relation to optimal partitioning of nitrogen among photosynthetic components: theoretical prediction.

Hurk, B.J.J.M. van den, P. Viterbo, A.C.M. Beljaars and A.K. Betts, 2000: *Off Line validation of the ERA40 surface scheme*, Technical Memorandum 295, ECMWF, Reading.

Hurk, B.J.J.M van den, A.J. Dolman, A.A.M. Holtslag, R. Hutjes, J. van de Kassteele, R. Ronda and R.J.M. IJpelaar, 2001: The land-component in the climate system, in: J. Berdowski, R. Guicherit and B.J. Heij (eds.), *The climate system*, Balkema, Lisse, 178 p.

Jacobs, C.J.M, 1994: *Direct impact of atmospheric CO_2 enrichment on regional transpiration, PhD thesis*, Agricultural University Wageningen, Wageningen.

Jacobs, A.F.G and B.G. Heusinkveld, 1999: Meteorologische meetinstrumenten, Wageningen Agricultural University, Wageningen, 103pp. Lecture notes (in Dutch) CM 06254612.

Jarvis, P.G., 1976: *The interpretation of the variations in leaf water potential and stomatal conductance found in canopies in the field*, Phil. Trans. R. Soc. Lond. Ser. B. 273, 593-610.

Jong de, T.M. and J.F. Doyle, 1985: Seasonal relationships between leaf nitrogen content (photosynthetic capacity) and leaf canopy light exposure in peach (*Prunus persica*), *Plant, Cell and Environment*, **8**, 701-706.

Kassteele, J. van de, 2001: *Evaluation of a plant physiological canopy conductance model in the ECMWF land surface scheme*, KNMI TR-234, De Bilt, 55pp.

Kellomäki, S. and K.Y. Wang, 1997: Photosynthetic responses of Scots pine to elevated CO_2 and nitrogen supply: results of a branch-in-bag experiment, *Tree physiology*, **17**, 231-240.

Künz, R.P., R.E. Schulze and R.J. Scholes, 1995: An approach to modelling spatial changes of plant carbon: nitrogen ratios in southern Africa in relation to anticipated global climate change, *J. of Biogeography*, **22**, 401-408.

Leuning, R., 1995: A critical appraisal of a stomatal-photosynthesis model for C3 plants, *Plant, Cell and Environment*, **18**, 339-355.

Lövenstein, H., E.A. Lantinga, R. Rabbinge, and H. van Keulen, 1995: *Principles of Production Ecology*, Wageningen Agricultural University, Wageningen, 121pp. CM 06380101.

Morison, J.I.L. and R.M. Gifford, 1983: Stomatal sensitivity to Carbon dioxide and Humidity, a comparison of two C3 and C4 grass species, *Plant Physiology*, **71**, 789-796.

Niyogi, D.S. and S. Raman, 1997: Comparison of four different resistance schemes using FIFE observations, *J. Appl. Meteor.*, **36**, 903-917.

Niyogi, D.S., S. Raman and K. Alapaty, 1998: Comparison of four resistance schemes using FIFE data. Part II: Analysis of terrestrial biospheric-atmospheric interactions, *J. Appl. Meteor.*, **37**, 1301-1320.

Pope, V.D., M.L. Gallani, P.R. Rowntree and R.A. Stratton, 2000: The impact of new physical parametrizations in the Hadley Centre climate model: HadAM3, *Clim. Dyn.*, **16**,123-146.

Porté, A. and D. Loustau, 1998: Variability of photosynthetic characteristics of mature needles within the crown of a 25-year-old *Pinus pinaster*, *Tree Physiology*, **18**, 223-232.

Reich, P.B., M.B. Walters and D.S. Ellsworth, 1997: From tropics to tundra: Global convergence in plant functioning, *Proc. Natl. Acad. Sci.*, **94**, 13370-13734.

Reyl, R.J., M.M. Caldwell, C.K. Yoder, D. Or and A.J. Leffler, 2002: Hydraulic redistribution in a stand of *Artemisia tridentate*: evaluation of benefits to transpiration assessed with a simulation model, *Oecologia*, **130**, 173-184.

Ronda, R.J, H.A.R. de Bruin and A.A.M. Holtslag, 2001: Representation of the Canopy Conductance in Modeling the Surface Energy Budget for Low Vegetation, *J. Appl. Meteor.*, **40**, 1431-1444.

Schulz, K., A. Jarvis, K. Beven and H. Soegaard, 2001: The predictive uncertainty of Land Surface Fluxes in response to Increasing Ambient Carbon dioxide, *J. Climate*, **14**, 2551-2562.

Schulze, E.D., F.M. Kelliher, C. Körner, J. Lloyd and R. Leuning, 1994: Relations among maximal stomatal conductance, ecosystem surface conductance, carbon assimilation rate, and plant nitrogen nutrition: A Global Ecology Scaling Exercise, *Annu. Rev. Ecol. Syst.*, **25**, 629-660.

Shuttleworth W.J., 1989: *Micrometeorology of a temperate and tropical forest*, Phil.Trans, R. Soc, Lond., B 324-334.

Soet, M, R.J. Ronda, J.N.M. Stricker and A.J. Dolman, 2000: Land surface scheme conceptualisation and parameter values for three sites with contrasting soils and climate, *Hydr. Earth Syst. Sci.*, **4**, 283-294.

Stewart J.B., 1988: Modelling surface conductance of pine forest, *Agric. For. Meteor.*, **30**, 111-127.

Takeuchi, Y., M.E. Kubiske, J.G. Isebrands, K.S. Pregtizer, G. Hendrey and D.F. Karnosky, 2001: Photosynthesis, light and nitrogen relationships in a young deciduous forest canopy under open-air CO_2 enrichment, *Plant, Cell and Environment*, **24**, 1257-1268.

Wang, K.Y, S. Kellomäki and K. Laitinen, 1996: Acclimatisation of photosynthetic parameters in Scots pine after three years exposure to elevated temperature and CO_2, *Agr. For. Meteor*., **82**,195-217.

Wilson M.F. and A. Henderson-Sellers, 1985: Cover and soil datasets for use in general circulation models, *J. of Climatology*, **20**, 119-143.

Wilson, K.B., D.D. Balldocchi and P.J. Hanson, 2000: Spatial and seasonal variability of photosynthetic parameters and their relationship to leaf nitrogen in a deciduous forest, *Tree physiology*, **20**, 565-578.

Wijk, M.T. van, 2001: *Quantification of the mutual relationships between forest growth and forest water use*, University of Amsterdam, Amsterdam, PhD thesis,192p.

Wong, S.C., I.R. Cowan and G.D. Farquhar,1979: Stomatal conductance correlates with photosynthetic capacity, *Nature*, **282**, 424-426.

Wullschleger, S.D., 1993: Biochemical limitations to carbon assimilation in C3 species- a retrospective analysis of the A/C_i curves from 109 species, *J. Exp. Bot*., **44**, 907-920.

Zhang, H. and P.S. Nobel, 1996: Dependency of c_i/c_a and leaf transpiration efficiency on the vapour pressure deficit, *Aust. J. Plant. Physiol*., **23**, 561-568.

For measurement of long wave radiation, beyond 3micron m, EKO, 30-10-2001, http://eko.co.jp/eko/english/03/4.html.

Monocots and dicots, 21-2-2002, Museum of paleontology Berkeley, http://www.ucmp.berkeley.edu/glossary/gloss8/monocotdicot.html

Appendix A. Leaf photosynthesis model in the A-gs model

Here a brief presentation of the leaf photosynthesis model used in A-gs follows. Constants are summarized in Table A1.

Gross assimilation A_g is calculated with:

$$A_g = (A_m + R_d)\left(1 - e^{-[\alpha PAR/(A_m + R_d)]}\right) \tag{A1}$$

with

$$A_m = A_{m,\max}\left(1 - e^{-[g_m((C_i - \Gamma)/A_{m,\max}]}\right) \tag{A2}$$

and α being the initial light use efficiency: $\alpha = \alpha_0 \dfrac{C_s - \Gamma}{C_s + 2\Gamma}$. $\qquad$ (A3)

Note that C_i instead C_s of should be used in (A3), but because (A3) applies at PAR ~ 0 then $C_i = C_s$ (Jacobs, 1994).
Γ is the compensation point, which is temperature dependent:

$$\Gamma(T_{sk}) = \Gamma(@\,298)Q_{10}^{(T_{sk}-298)/10} \tag{A4}$$

like g_m and $A_{m,\max}$:

$$X(T_{sk}) = \frac{X(@\,298)Q_{10}^{(T_{sk}-298)/10}}{\{1 + \exp(0.3[T1 - T_{sk}])\}\{1 + \exp(0.3[T_{sk} - T2])\}} \tag{A5}$$

where X denotes g_m (mesophyll conductance) or $A_{m,\max}$, the maximum photosynthetic rate under high CO_2 and light conditions.
The dark respiration R_d is derived as a fraction of A_m:

$$R_d = 0.11 A_m \tag{A6}$$

Table A1: Overview of leaf photosynthesis parameters for C3 and C4 plants (Ronda, 2001).

Plant type	Parameter	$X(@\,298)$	Q_{10}	T1 (K)	T2 (K)
C3	f_0 (-)	0.89			
	a_d (kPa^{-1})	0.07			
	α_0 (mg J^{-1})	0.017			
	Γ (mg m^{-3})	68.5ρ_a	1.5		
	g_m (mm s^{-1})	7.0	2.0	278	301
	$A_{m,\max}$ (mg m^{-2} s^{-1})	2.2	2.0	281	311
C4	f_0 (-)	0.85			
	a_d (kPa^{-1})	0.15			
	α_0 (mg J^{-1})	0.017			
	Γ (mg m^{-3})	4.3ρ_a	1.5		
	g_m (mm s^{-1})	17.5	2.0	286	309
	$A_{m,\max}$ (mg m^{-2} s^{-1})	1.7	2.0	286	311

Appendix B: FORTRAN program for calibration of f_0 and a_d

```
       PROGRAM IJKING LOOBOS
       IMPLICIT NONE
       INTEGER J
       LOGICAL LO
       REAL DAT(20)
       REAL RESP,GC2,Pres
       REAL RD,RV,f,GAMMA,DMAST
       PARAMETER(RD=287,RV=462.,PRES=1013E2)
       REAL TS,ES,EA,GA,QC,GC,QSAT,QA,DS,DS2
       REAL CO2FLUX,COUT,CIN
       PARAMETER (LO=.TRUE.)
       Kx=0.7
       LAI =1.9
       OPEN(1,FILE='bron.txt',STATUS='old')
       READ(1,*)
       DO WHILE (LO)
       READ(1,*,END=1000)(DAT(J),J=1,20)
        DO J=1,20
          IF (DAT(J).LT.-800.) GOTO 2000
       ENDDO
       RESP=(.037*exp(0.094*DAT(17)))*1000/44
        IF(DAT(4).GT.0.and.DAT(8).GT.100) THEN
        IF(DAT(12).LT.-1.and.DAT(20).GT.2) then
      IF (DAT(3).GE.1000.AND.DAT(3).LE.1400.AND.DAT(15).EQ.0) THEN
           TS=(DAT(6)/(.98*5.67E-8))**(.25)
           TS=TS-273.15
c Ts is nu in Celsius
           ES=610.7*10.**(7.5*TS/(237.3+TS))
           QSAT=RD/RV*ES/PRES
c QSAT is dus in kg/kg en dus specifieke vochtigheid aan het bladoppervlak
           EA=610.7*10.**(7.5*DAT(4)/(237.3+DAT(4)))
           QA=DAT(5)/100.*RD/RV*EA/PRES
c QA is dus specifieke vochtigheid op meetnivo
           DMAST=EA*(1-DAT(5)/100)/1000
c DMAST is in kPa
           GA=DAT(7)/(1.2*1005.*(TS-DAT(4)))
           QC=QA+DAT(8)/(1.2*2.5E6*GA)
c is de specifieke vochtigheid op leaf level (kg/kg)
           GC=DAT(8)/(1.2*2.5E6*(QSAT-QC))
           GS=GC*Kx/(1-Kx*LAI)
           GC2=GA/(GA*(QSAT-QA)/(DAT(8)/(1.2*2.5E6))-1.)
           CO2FLUX=(DAT(12)-RESP-DAT(13))*44/1000
c RESP, DAT(12) en DAT(13) zijn gegeven is umolCO2/m2/s
c CO2FLUX is in mgCO2/m2/s
           DS=(QSAT-QC)*1000
c DS is dus in g/kg
           DS2=DS/1000000*PRES/0.622
c DS2 is in kPa
           COUT=640.+CO2FLUX/GA
c 640 mg/m3 is ca. 350 ppm
           CIN=COUT+CO2FLUX/(GS/1.6)
           GAMMA=68.5*PRES/(287*(dat(4)+273))
c GAMMA,CIN en COUT zijn in mg/m3
           f=(CIN-GAMMA)/(COUT-GAMMA)
       IF(GC.GT.0.and.CO2FLUX.LT.-0.5) then
       write(2,'(8(1x,F16.4))')DAT(2),DAT(3),f,DS2,DAT(8),CO2FLUX
       end if
       end if
       end if
       ENDIF
2000   ENDDO
1000   CLOSE(1)

       END
```

Appendix C: Derivation of equation 3.1

$$\frac{E}{\rho_a} = g_c\left(q_{sat} - q_{leaf}\right) = g_a\left(q_{leaf} - q_a\right) \Rightarrow \tag{C1}$$

$$g_c q_{sat} - g_c q_{leaf} = g_a q_{leaf} - g_a q_a \Rightarrow$$

$$\left(g_a + g_c\right) q_{leaf} = g_c q_{sat} + g_a q_a \Rightarrow$$

$$q_{leaf} = \frac{1}{g_a + g_c}\left(g_c q_{sat} + g_a q_a\right) \Rightarrow \quad \text{Insert in (C1)}$$

$$\frac{E}{\rho_a} = g_c q_{sat} - \frac{g_c^2 q_{sat}}{g_a + g_c} - \frac{g_a g_c q_a}{g_a + g_c} = \frac{g_c\left(g_a + g_c\right) - g_c^2}{g_a + g_c} q_{sat} - \frac{g_a g_c}{g_a + g_c} q_a =$$

$$\left(\frac{g_a g_c}{g_a + g_c}\right)\left(q_{sat} - q_a\right)$$

Appendix D: Statistics

Many statistical quantities are used in literature to determine model quality. A short overview will be presented here.

1. Bias or mean error (ME). This is the mean deviation of the model to the data:

    $$ME = \frac{1}{N}\sum_{i=1}^{N} MOD_i - OBS_i$$

    A low ME indicates that a good model, but may be large positive and negative errors are compensating each other.

2. Chi-quadrate (χ^2) or sum of squares of residuals (SS)

    $$SS = \chi^2 = \sum_{i=1}^{N}\left(MOD_i - OBS_i\right)^2$$

    A of SS = 0.25 indicates a good model performance.

3. Mean square error (MSE):

    $$MSE = \frac{1}{N}\sum_{i=1}^{N}\left(MOD_i - OBS_i\right)^2$$

    MSE avoids the problem of compensating errors as in ME.

4. The root mean square error (*RMSE*) is defined by $RMSE = \sqrt{\frac{1}{N}\sum_{i=1}^{N}\left(MOD_i - OBS_i\right)^2}$

    This is a common used quality indicator. It has the benefit that its unit is the same as the observations and the model values.

5. The unbiased root mean square error (*URMSE*) is defined by

    $$URMSE = \sqrt{\frac{1}{N}\sum_{i=1}^{N}\left(MOD_i - OBS_i\right)^2 - \left[\frac{1}{N}\sum_{i=1}^{N} MOD_i - OBS_i\right]^2}$$

    This indicator corrects the *RMSE* for the bias, so this is a better indicator than *RMSE*.

Appendix E: Sensitivity for g_s to f_0 in the A-g_s model.

The main equation in the A-gs scheme is (Leuning,1995, Ronda, 2001):

$$g_{l,c} = g_{min,c} + \frac{a_1 A_g}{(C_s - \Gamma)\left(1 + \dfrac{D_s}{D_*}\right)}$$

with the closure of Jacobs (1994)

$$C_s - \Gamma = \frac{C_i - \Gamma}{f_0\left(1 - \dfrac{D_s}{D_0}\right) + f_{min}\dfrac{D_s}{D_0}}$$

with $D_* = D_0/(a_1-1)$ and $a_1 = 1/(1-f_0)$ this results in:

$$g_{l,c} = g_{min,c} + \frac{a_1 A_g\left(f_0\left(1 - \dfrac{D_s}{D_0}\right) + f_{min}\dfrac{D_s}{D_0}\right)}{(C_s - \Gamma)\left(1 + \dfrac{D_s}{D_*}\right)}$$

$$g_{l,c} = g_{min,c} + \frac{A_g\left(f_0\left(1 - \dfrac{D_s}{D_0}\right) + f_{min}\dfrac{D_s}{D_0}\right)}{(1 - f_0)(C_s - \Gamma)\left(1 + \dfrac{D_s(a_1 - 1)}{D_0}\right)}$$

After some re-arranging it follows that:

$$g_{l,c} = g_{min,c} + \frac{A_g\left(f_0\left(1 - \dfrac{D_s}{D_0}\right) + f_{min}\dfrac{D_s}{D_0}\right)}{(C_s - \Gamma)\left((1 - f_0) + f_0\dfrac{D_s}{D_0}\right)}$$

Using the quotient rule for differentiating it follows that:

$$\frac{\partial g_{l,c}}{\partial f_0} = \frac{A_g(C_i - \Gamma)\left(1 - \dfrac{D_s}{D_0}\right)\left(f_0\left(\dfrac{D_s}{D_0} - 1\right) + 1\right) + A_g(C_i - \Gamma)\left(1 - \dfrac{D_s}{D_0}\right)\left(f_0\left(1 - \dfrac{D_s}{D_0}\right) + f_{min}\dfrac{D_s}{D_0}\right)}{(C_i - \Gamma)^2\left(f_0\left(\dfrac{D_s}{D_0} - 1\right) + 1\right)^2}$$

Re-arranging results in:

$$\frac{\partial g_{l,c}}{\partial f_0} = \frac{A_g}{C_i - \Gamma} \frac{f_{min}\dfrac{D_s}{D_0} - 1}{f_0^2 \left(\dfrac{D_s}{D_0} - 1\right) + 2f_0 + 1 / \left(\dfrac{D_s}{D_0} - 1\right)}$$

This equation is illustrated in figure E.1 for $D_s/D_0 = 0.20$ and $A_g/(C_i\text{-}\Gamma) = 3.6.10^{-4}$ m/s.

Sensitivity of g_c to f_0 increases with increasing f_0
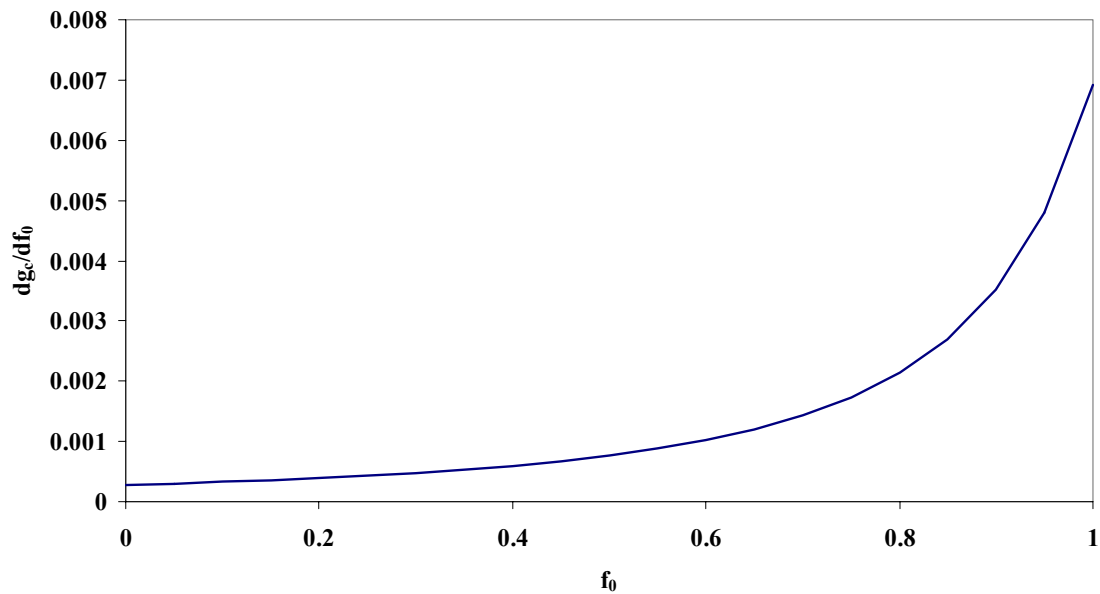
Figure E.1: The sensitivity of $g_{l,c}$ for f_0 as function of f_0. At large values of f_0 a larger sensitivity is obtained.

Appendix F: Diurnal cycles of latent and sensible heat flux per month in Loobos.
The year and months are given as yyyymm: so 199708 is August 1997.

Diurnal cycle of latent heat flux 199701

Diurnal cycle of sensible heat flux 199701

Diurnal cycle of latent heat flux 199702

Diurnal cycle of sensible heat flux 199702

Diurnal cylce of latent heat flux 199703

Diurnal cylce of sensible heat flux 199703

Diurnal cylce of latent heat 199704

Diurnal cylce of sensible heat 199704

72
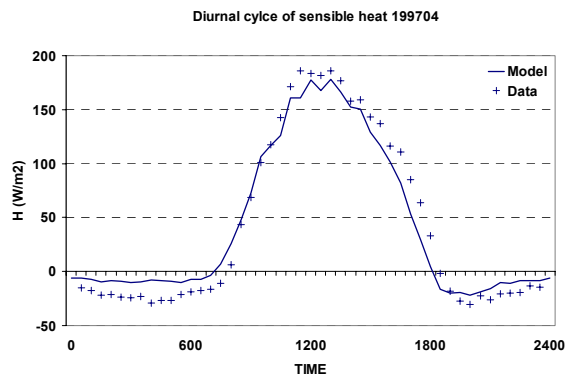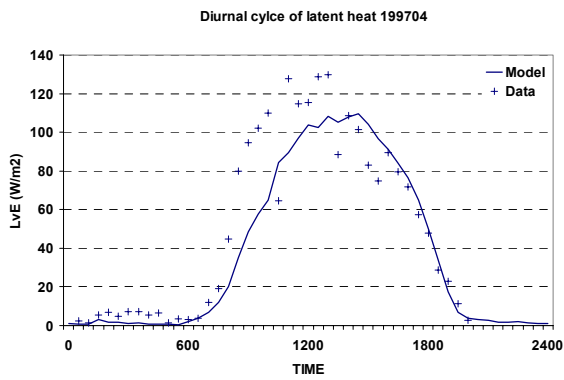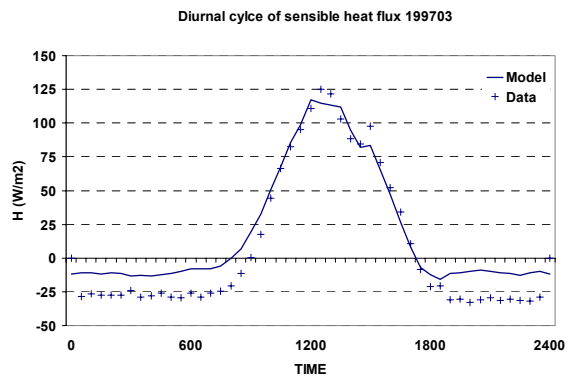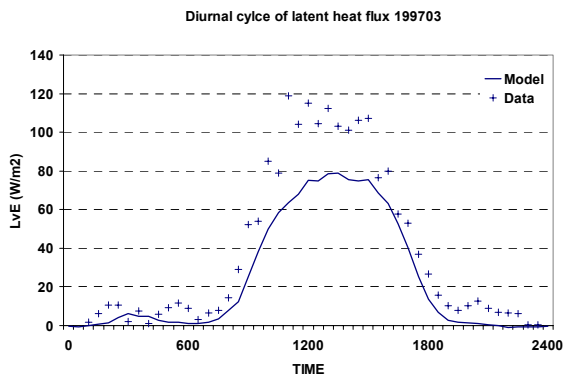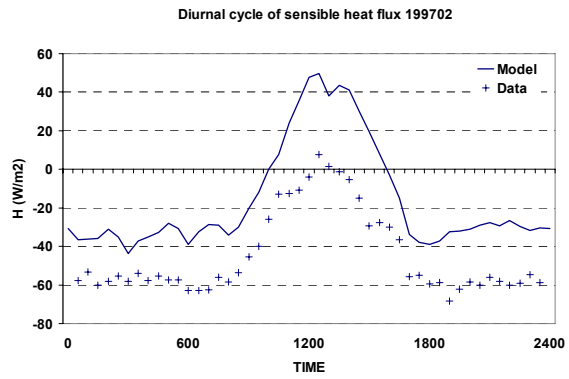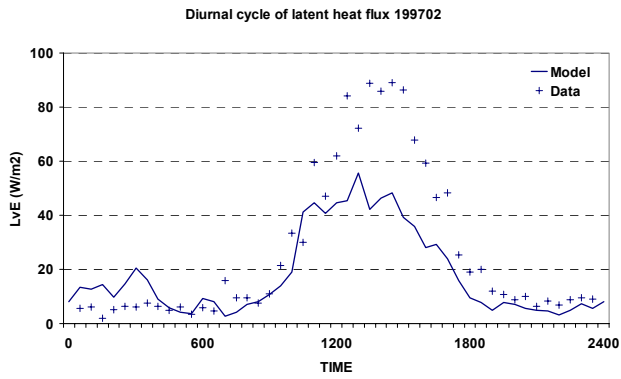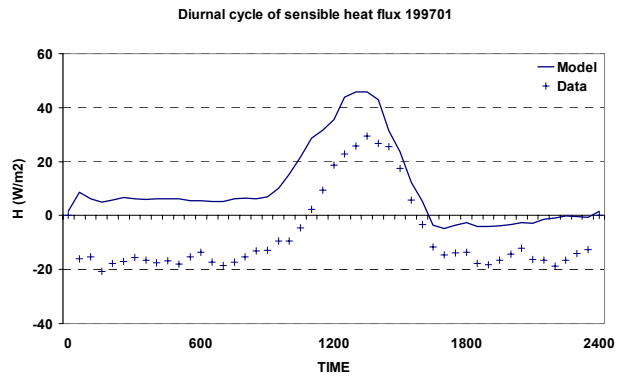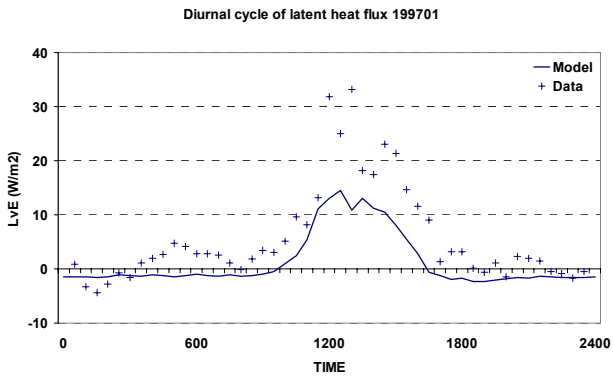
Diurnal cycle of latent heatflux 199705
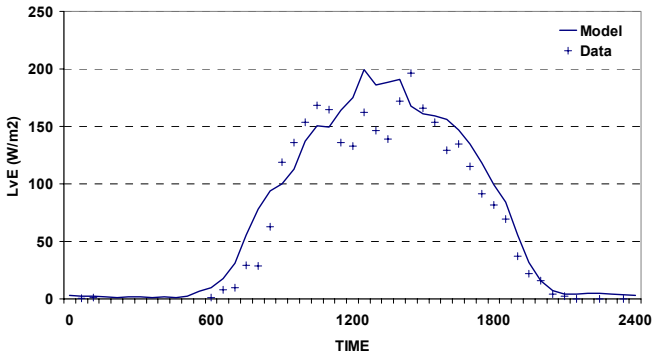
Diurnal cycle of sensible heatflux May 1997
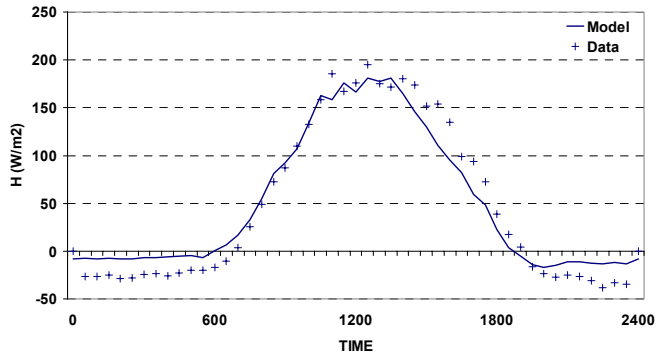
Diurnal cycle of latent heat flux 199706
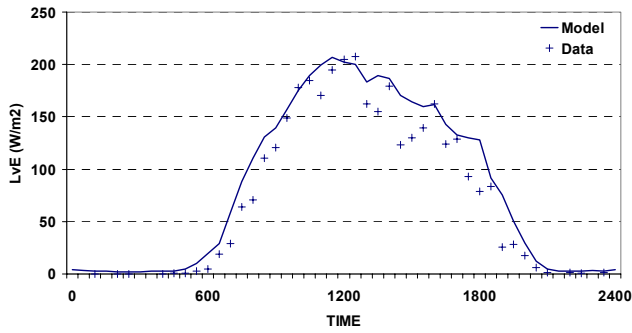
Diurnal cycle of sensible heat flux 199706
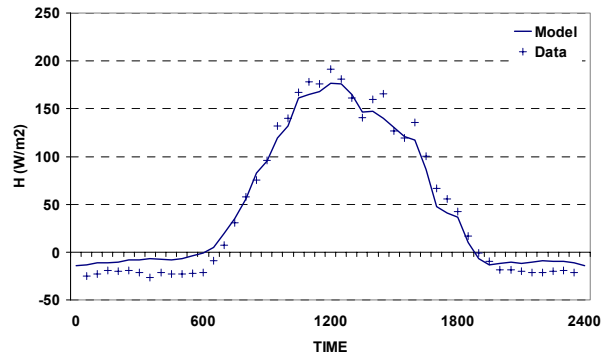
Diurnal cycle of latent heat flux 199707
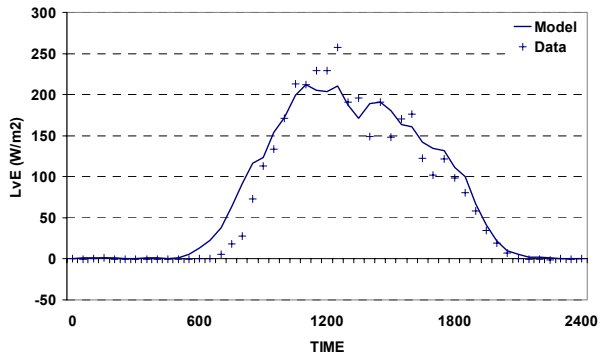
Diurnal cycle of sensible heat flux 199707
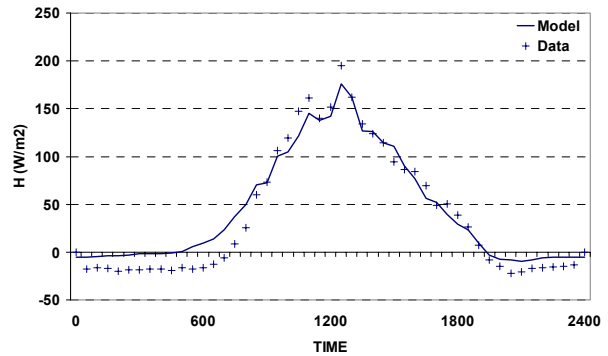
Diurnal cycle of latent heat flux 199708
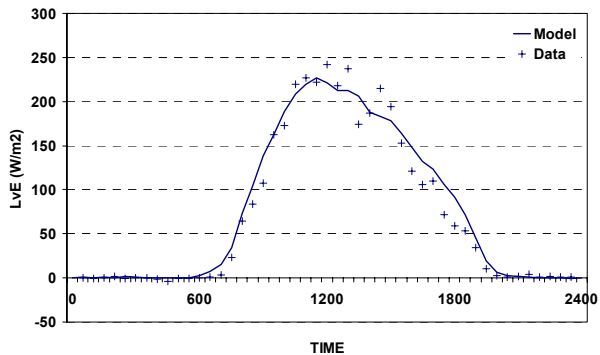
Diurnal cycle of sensible heat flux 199708
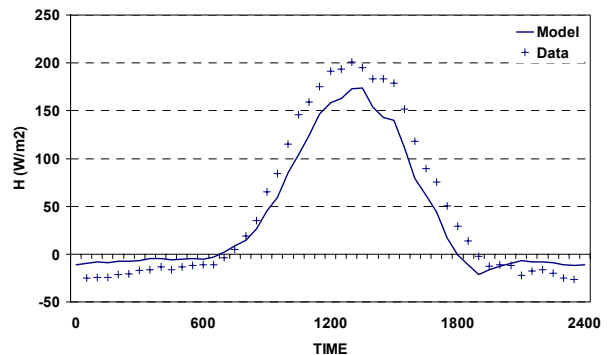
Diurnal cycle of latent heat flux 199709
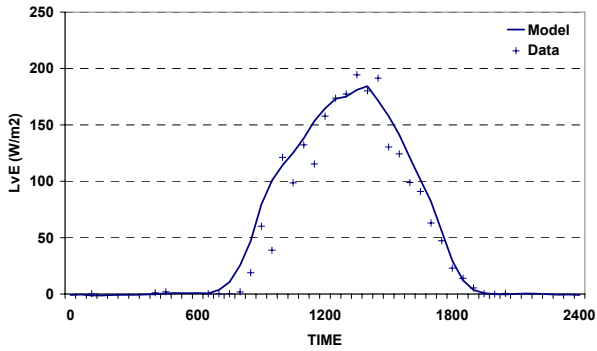
Diurnal cycle of sensible heat flux 199709
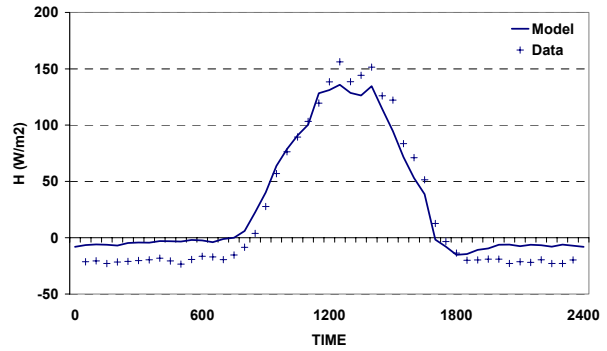
Diurnal cycle of latent heat flux 199710
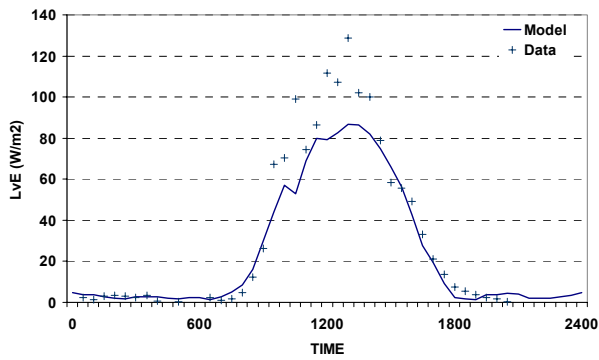
Diurnal cycle of sensible heat flux 199710
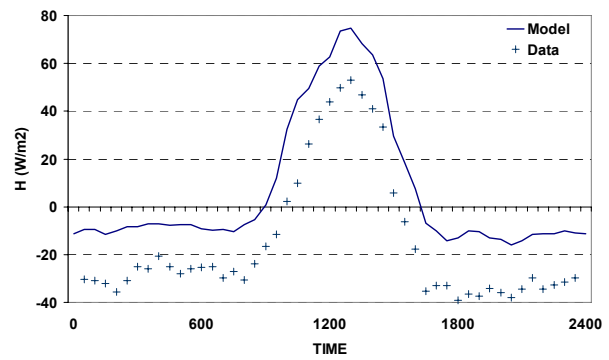
Diurnal cycle of latent heat flux 199711
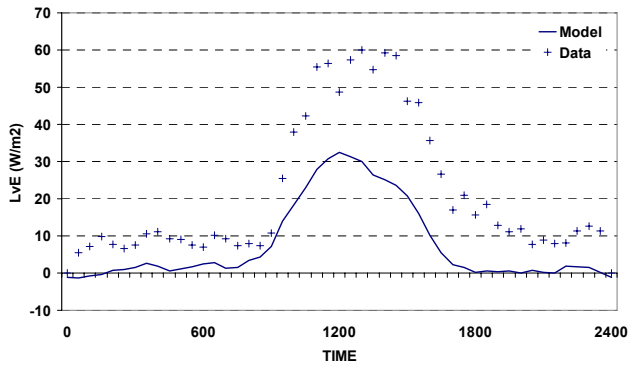
Diurnal cycle of sensible heat flux 199711
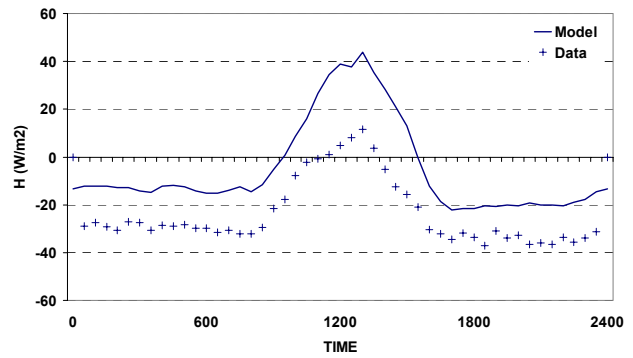
Diurnal cucle of latent heat flux 199712
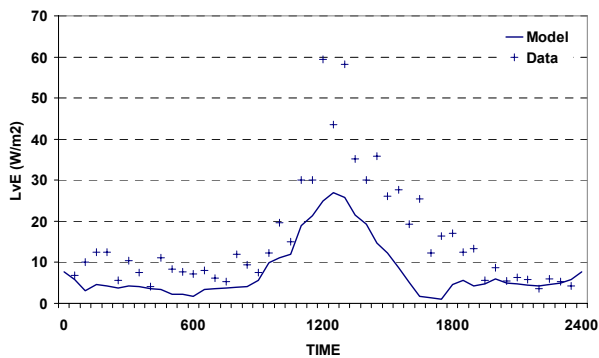
Diurnal cycle of sensible heat flux 199712

74
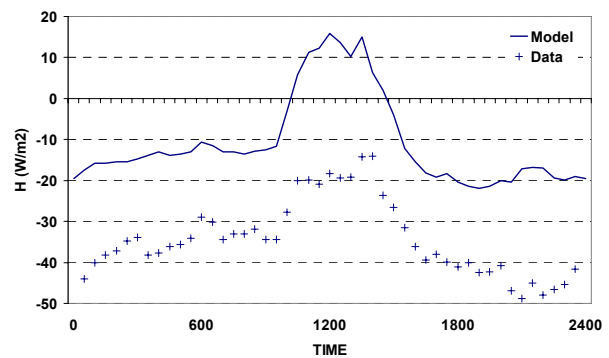
Diurnal cycle of latent heat flux 199801
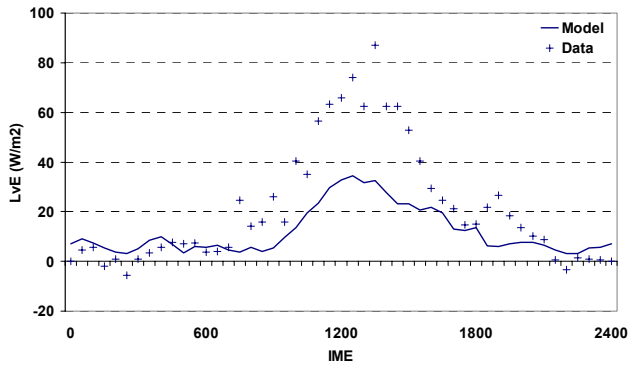
Diurnal cycle of sensible heat flux 199801
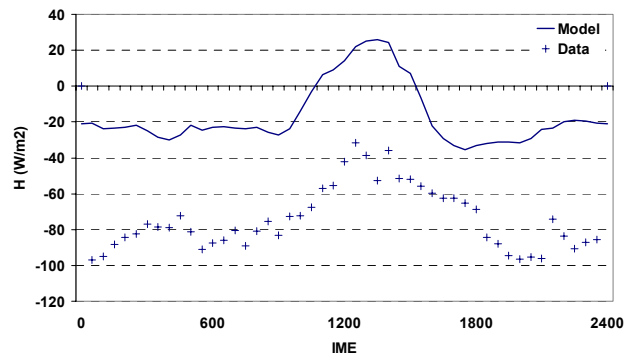
199802: No latent heat flux data

Diurnal cycle of sensible heat flux 199802
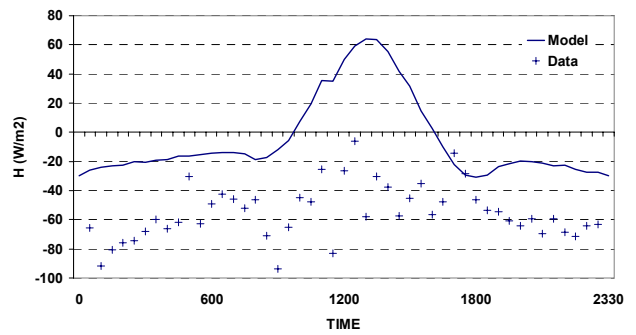
Diurnal cycle of latent heat flux 199803
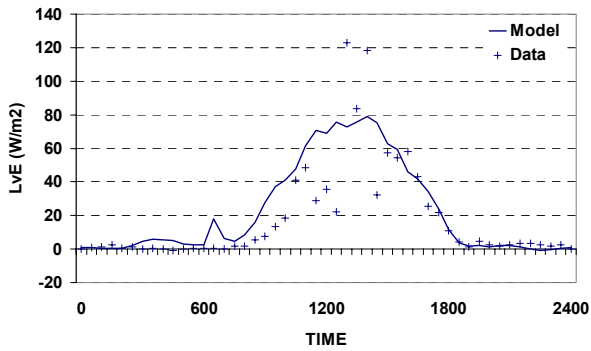
Diurnal cycle of sensible heat flux 199803
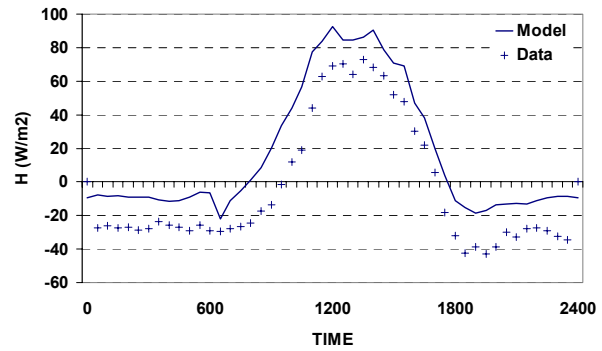
199804: No data latent and sensible heat

Diurnal cycle of latent heat flux 199805
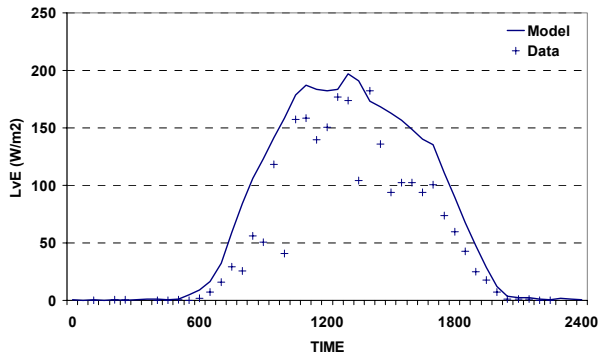
Diurnal cycle of sensible heat flux 199805
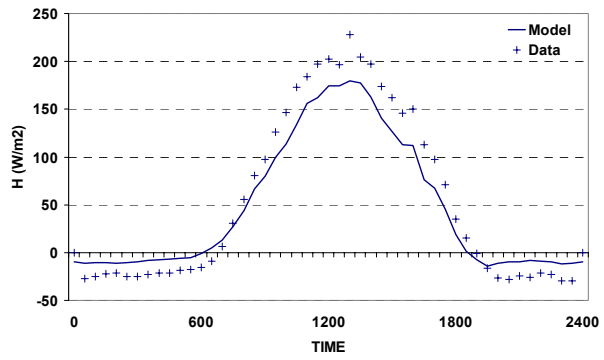
Diurnal cycle of latent heat flux 199806
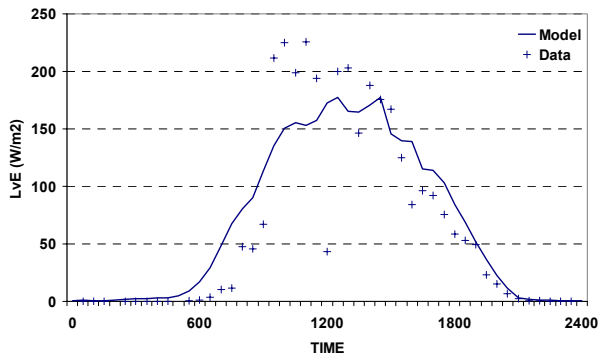
Diurnal cycle of sensible heat flux 199806
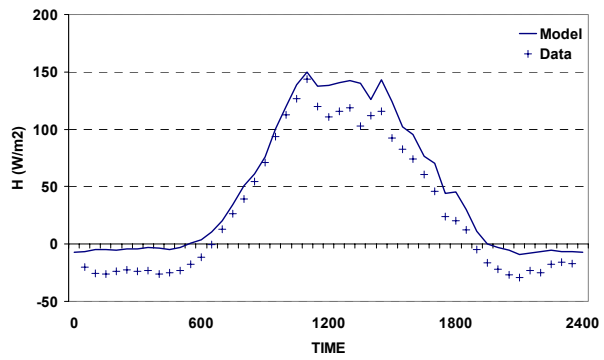
Diurnal cycle of latent heat flux 199807
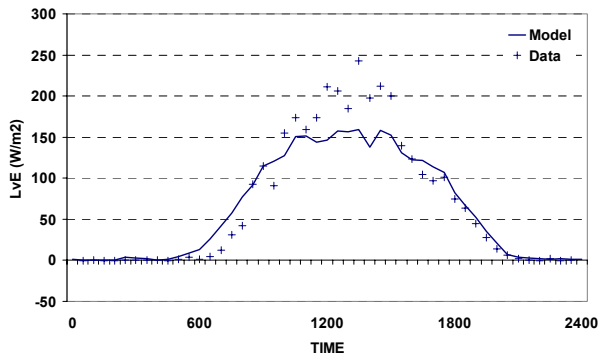
Diurnal cycle of sensible heat flux 199807
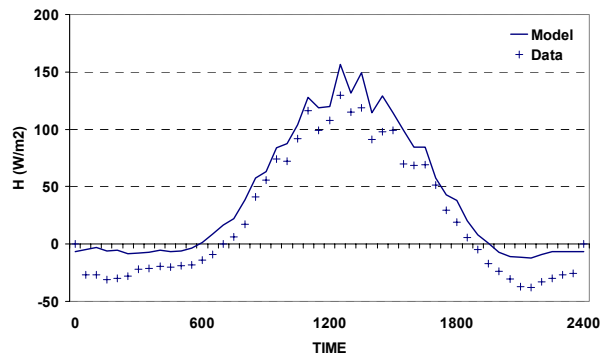
Diurnal cycle of latent heat flux 199808
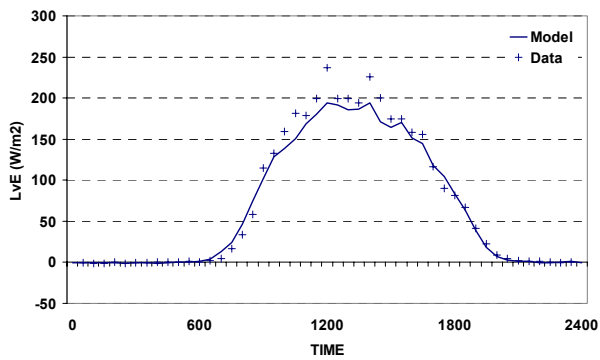
Diurnal cycle of sensible heat flux 199808
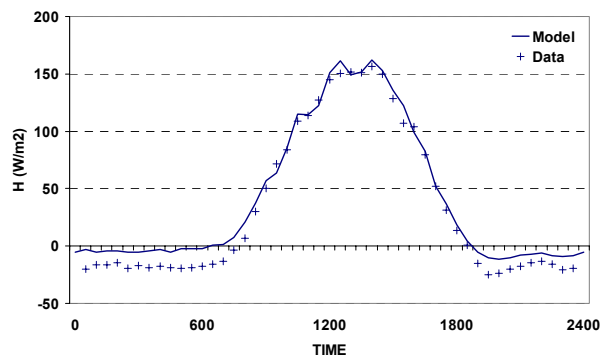
Diurnal cycle of latent heat flux 199809
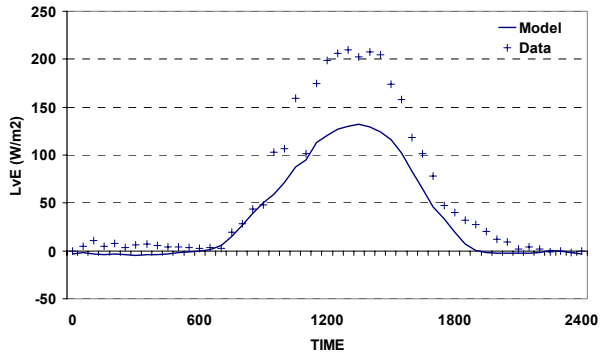
Diurnal cycle of sensible heat flux 199809
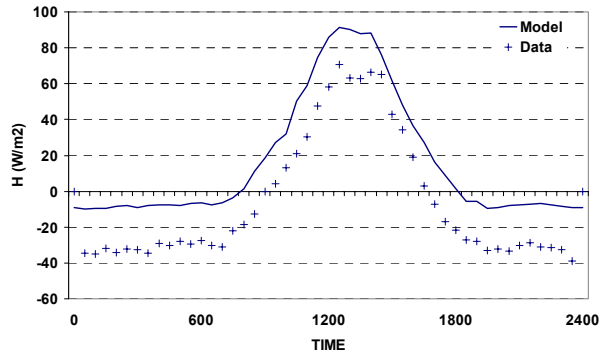
199810: No data latent and sensible heat flux

Diurnal cycle of latent heat flux 199811
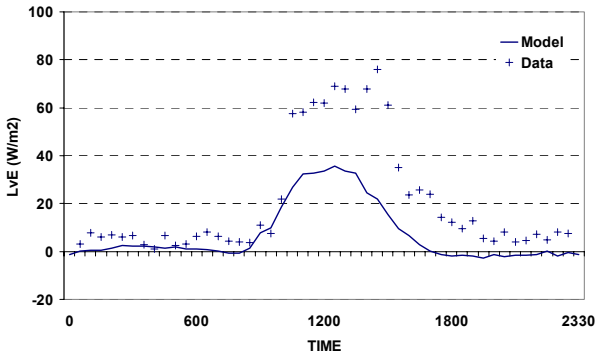
Diurnal cycle of sensible heat flux 199811
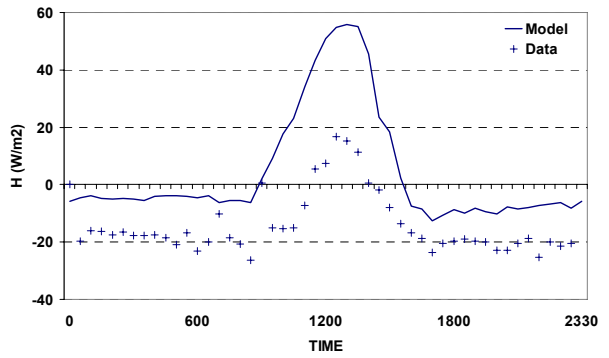
Diurnal cycle of latent heat flux 199812
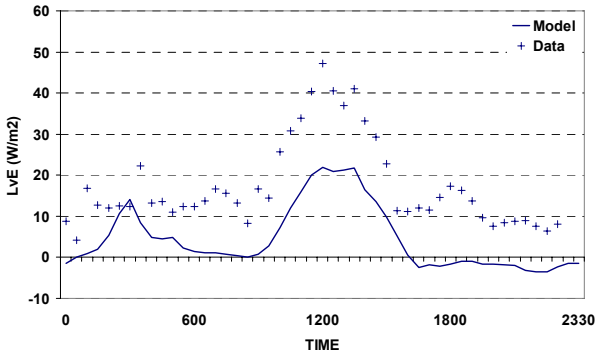
Diurnal cycle of sensible heat flux 199812
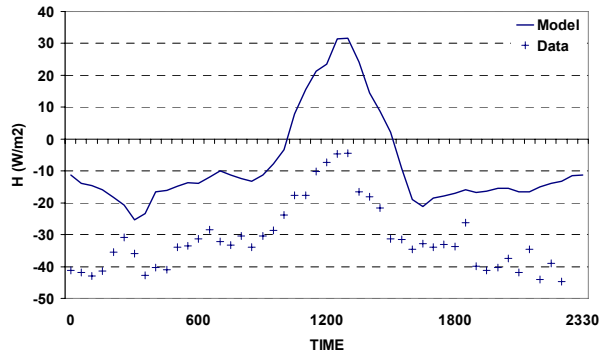
Appendix G: General Sensitivity Analysis in FORTRAN.

```
      program gsa
c Dit FORTRAN programma berekent de GSA volgens Franks 1997

      implicit none
      integer i,j,k,teller
      real Dat(15)
      integer aantalperklasse
      integer dim_F0,dim_ad,dim_Ammax,klasse
      real F0(12),F0_teller(12)
      real Ammax(15),Ammax_teller(15)
      real ad(9),ad_teller(9)
      real AmmaxCum,F0Cum,adCum
      character*100 chead


      OPEN(1,FILE='/usr/people/steeneve/surf1d/work/s1dags_control/GSA/r
     &mse_speuld95.txt',STATUS='old')
      OPEN(3,FILE='GSA_F0',STATUS='unknown')
      write(3,'(a)')'klasse F0  N  RCF'
      OPEN(4,FILE='GSA_ad',STATUS='unknown')
      write(4,'(a)')'klasse ad  N  RCF'
      OPEN(5,FILE='GSA_Ammax',STATUS='unknown')
      write(5,'(a)')'klasse Ammax  N  RCF'

      aantalperklasse =162
      klasse=0
      dim_ad =9
      dim_Ammax=15
      dim_F0=12
C vergeet niet bij de declaraties deze dimensies aan te geven.

      Ammax(1)=0.2
      Ammax(2)=0.3
      Ammax(3)=0.4
      Ammax(4)=0.5
      Ammax(5)=0.6
      Ammax(6)=0.7
      Ammax(7)=0.8
      Ammax(8)=0.9
      Ammax(9)=1.0
      Ammax(10)=1.25
      Ammax(11)=1.5
      Ammax(12)=1.75
      Ammax(13)=2.0
      Ammax(14)=2.2
      Ammax(15)=2.4

      F0(1)=0.4
      F0(2)=0.5
      F0(3)=0.6
      F0(4)=0.7
      F0(5)=0.75
      F0(6)=0.8
      F0(7)=0.85
      F0(8)=0.875
      F0(9)=0.9
      F0(10)=0.925
      F0(11)=0.95
      F0(12)=0.975

      ad(1)=-0.14
      ad(2)=-0.13
```

```
      ad(3)=-0.12
      ad(4)=-0.11
      ad(5)=-0.10
      ad(6)=-0.09
      ad(7)=-0.08
      ad(8)=-0.07
      ad(9)=-0.06


c headers inlezen
      read(1,*) chead

      do while (1.eq.1)
        READ(1,*,end=1000)(DAT(i),i=1,15)
        teller=teller+1
        do 100 i=1,dim_F0
          if (dat(1).eq.F0(i)) then
          F0_teller(i)=F0_teller(i)+1
          end if
100     continue
        do 200 j=1,dim_Ammax
          if (dat(3).eq.Ammax(j)) then
          Ammax_teller(j)=Ammax_teller(j)+1
          end if
200     continue
        do 300 k=1,dim_ad
          if (dat(2).eq.ad(k)) then
          ad_teller(k)=ad_teller(k)+1
          end if
300     continue

        if (teller.eq.aantalperklasse) then
         klasse=klasse+1
        do 400 i=1,dim_F0
        F0Cum=F0Cum+F0_teller(i)
          write(3,'(I3,3(1x,f12.4))') klasse,F0(i),F0_teller(i),F0Cum/
     &aantalperklasse
          F0_teller(i)=0
400     continue
        do 500 j=1,dim_ad
        adCum=adCum+ad_teller(j)
          write(4,'(I3,3(1x,f12.4))') klasse,ad(j),ad_teller(j),adCum/
     &aantalperklasse
        ad_teller(j)=0
500     continue
        do 600 k=1,dim_Ammax
          AmmaxCum=AmmaxCum+Ammax_teller(k)
          write(5,'(I3,3(1x,f12.4))') klasse,Ammax(k),Ammax_teller(k),
     &AmmaxCum/aantalperklasse
          Ammax_teller(k)=0
600     continue
          teller=0
        end if
       F0Cum=0
       adCum=0
       AmmaxCum=0

      enddo

1000  close(1)
      close(3)
      close(4)
      close(5)
      end
```